SENSOR AND SIMULATION NOTES

Note 315

On the Thin Toroidal and Elliptical Antennas

C. Zuffada
F.C. Yang
I. Wong

Kaman Sciences Corporation
Dikewood Division/Santa Monica
2800 28th Street, Suite 370
Santa Monica, California 90405

January 1989

Abstract

The current along the thin toroidal and elliptical antennas and the electromagnetic fields at and around their center have been derived using the asymptotic antenna theory. Frequency and time domain calculations are presented. Both cases of a δ-gap generator and of a distributed source with the field configuration of a biconical wave launcher have been considered. The field uniformity in the working volume has been calculated as a function of frequency, for different geometrical configurations. For the case of the elliptical geometry, parametric studies to analyze the dependence of the field behavior on source location and value of the loading resistance, eccentricity and wire thickness have been performed.

Acknowledgement

Work performed for AIR FORCE WEAPONS LABORATORY, NTAAT, under contract F29601-88-C-0027. The authors wish to thank C.E. Baum, Capt. T. Smith and Mr. W. Prather for their interest and many helpful discussions.

SENSOR AND SIMULATION NOTES

Note 315

On the Thin Toroidal and Elliptical Antennas

C. Zuffada
F.C. Yang
I. Wong

Kaman Sciences Corporation
Dikewood Division/Santa Monica
2800 28th Street, Suite 370
Santa Monica, California 90405

January 1989

Abstract

The current along the thin toroidal and elliptical antennas and the electromagnetic fields at and around their center have been derived using the asymptotic antenna theory. Frequency and time domain calculations are presented. Both cases of a δ-gap generator and of a distributed source with the field configuration of a biconical wave launcher have been considered. The field uniformity in the working volume has been calculated as a function of frequency, for different geometrical configurations. For the case of the elliptical geometry, parametric studies to analyze the dependence of the field behavior on source location and value of the loading resistance, eccentricity and wire thickness have been performed.

Acknowledgement

Work performed for AIR FORCE WEAPONS LABORATORY, NTAAT, under contract F29601-88-C-0027. The authors wish to thank C.E. Baum, Capt. T. Smith and Mr. W. Prather for their interest and many helpful discussions.

INTRODUCTION

In the recent past attention has been given to the problem of calculating the fields produced by a toroidal antenna at and around its center (Refs. 1 and 2). Specifically, for a δ-gap generator it was determined that a low frequency E/H ratio at the center equal to the free-space intrinsic impedance can be achieved with a particular uniform loading resistance. The results obtained in the above papers have been revisited here with a much simpler approach, based on the asymptotic antenna theory, for the case of a thin Torus. The fields have been calculated at and around the center, in the frequency and time domains. The cases of one and of two δ-gap generators (one source plus its image) were investigated. The current was calculated in the time domain at three different locations along the wire. A "uniformity error" based on the root-mean-square variation of the principal field component around its average value in a certain domain of interest has been computed also. In addition, other properties of toroidal antennas, such as the input impedance have been derived. The case of a finite-gap source with the field configuration at the gap produced by a biconical wave launcher has also been investigated. The approach has been extended to the elliptical geometry and the same electromagnetic quantities were derived. In addition, parametric studies to analyze the field behavior as a function of the loading resistance, the location of the source, the eccentricity and the thickness of the wire relative to the major semiaxis were also conducted. In Part I the circular geometry is discussed, whereas Part II is concerned with the elliptical one. This approach is particularly appealing since the analytical results can be cast in closed forms.

1.0 PART I: THIN TOROIDAL ANTENNA

1.1 SINGLE δ-GAP GENERATOR

1.1.1 Current Along A Thin Circular Loop Antenna

Figure 1 illustrates the geometry of the antenna being analyzed, together with the cylindrical coordinate system used in the calculations. It is shown that the radius of the antenna is a and the radius of the wire is b. We shall indicate with $\bar{a}_\rho$, $\bar{a}_\phi$ and $\bar{a}_z$ the unit vectors normal to the surfaces ρ = const, ϕ = const, and z = const, respectively, and forming a right handed system. In the case of a single δ-gap source, which is dealt with first, it is assumed that its location is coincident with the origin of the ϕ coordinate. The same approach is applicable also in the case of multiple δ-gap generators located along the antenna, as will be discussed in Section 1.2. The particular case of a

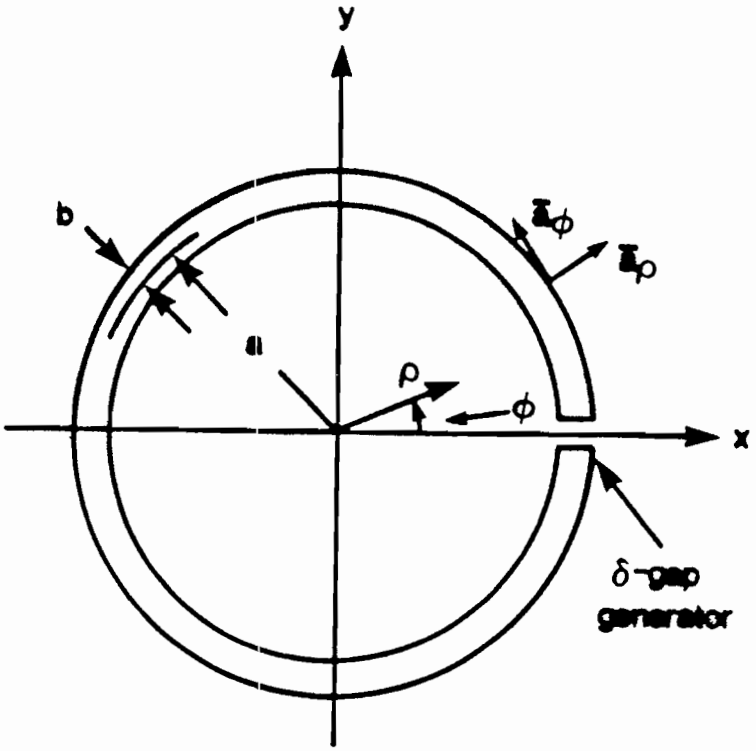

Figure 1. Geometry of TORUS antenna with δ-gap generator located at $\phi = 0^o$.

half circle with single or multiple δ-gaps above a perfectly conducting ground, with the plane of the antenna perpendicular to the ground, can be treated within this last category.

It is noted that with the approximation of a thin antenna, i.e., $a >> b$, $kb << 1$, one can ignore the current flow along the circumference of the wire and consider only that along the antenna loop, i.e. along ϕ. That is to say that the current has only one component in the ϕ direction. One can see, from Maxwell equations and the equations for the vector potential in cylindrical coordinates (Ref. 3) that, associated with $I_\phi(\phi)$ along the loop are two components of the vector potential, A_ϕ and A_ρ. On the antenna surface the potential can be represented, in terms of the currents, by

$$A_\phi(\phi) = \frac{\mu_o}{4\pi}\int_o^{2\pi} \frac{I_\phi(\phi')e^{ik\sqrt{a^2[2-2\cos(\phi-\phi')]+b^2}}}{\sqrt{a^2[2-2\cos(\phi-\phi')]+b^2}}\, a\cos(\phi-\phi')\,d\phi' \tag{1}$$

and

$$A_\rho(\phi) = \frac{\mu_o}{4\pi}\int_o^{2\pi} \frac{I_\phi(\phi')e^{ik\sqrt{a^2[2-2\cos(\phi-\phi')]+b^2}}}{\sqrt{a^2[2-2\cos(\phi-\phi')]+b^2}}\, a\sin(\phi-\phi')\,d\phi' \tag{2}$$

where, in the integrand, use has been made of the approximate kernel discussed in Ref. 4. These integrals can be evaluated approximately when ka is large. In fact, in such case, due to the oscillatory nature of the exponential terms in Eqs. 1 and 2 and the assumption that $b << a$, only the values of ϕ' close to ϕ are going to contribute significantly to the integral. By using this approximation, Eqs. 1 and 2 become

$$A_\phi(\phi) \simeq \frac{\mu_o}{4\pi} I_\phi(\phi)\int_o^{2\pi} \frac{e^{ik\sqrt{4a^2\sin^2(\phi'/2)+b^2}}}{\sqrt{4a^2\sin^2(\phi'/2)+b^2}}\, a\,d\phi' \tag{1.a}$$

$$A_\rho(\phi) \simeq 0 \tag{2.a}$$

Since, for $\phi \sim \phi'$, $\cos(\phi-\phi') \sim 1$ and $\sin(\phi-\phi') \sim 0$. By making the change of variable $\zeta = 2a\sin(\phi'/2)$, $d\zeta = a\cos(\phi'/2)d\phi' \simeq a\,d\phi'$, because most of the contribution to Eq. 1.a is coming from ϕ' close to 0^o, it is obtained

$$A_\phi(\phi) \simeq \frac{\mu_o}{2\pi} I_\phi(\phi) \int_0^{2a} \frac{e^{ik\sqrt{\zeta^2+b^2}}}{\sqrt{\zeta^2+b^2}}\, d\zeta \qquad (1.b)$$

$$= \frac{\mu_o}{4\pi} I_\phi(\phi) \left\{ \int_{-\infty}^{\infty} \frac{e^{ik\sqrt{\zeta^2+b^2}}}{\sqrt{\zeta^2+b^2}}\, d\zeta - 2 \int_{2a}^{\infty} \frac{e^{ik\sqrt{\zeta^2+b^2}}}{\sqrt{\zeta^2+b^2}}\, d\zeta \right\}$$

In writing Eq. 1.b one must exclude the point $\phi = 0°$. In fact, because of the δ-gap generator, the current is infinite at the gap location. The nature of the singularity of the current has been investigated by T.T. Wu and R.W. P. King in Ref. 5 who found it to be of logarithmic type, therefore integrable. Hence Eq. 1.b does not represent correctly, at $\phi = 0°$, the relationship between the potential, which is finite, and the current which diverges. However, for the purpose of calculating the current everywhere else and consequently, the fields, Eq. 1.b and its approximate forms are adequate.

The contribution to $A_\phi(\phi)$ from the second integral is negligible compared to that of the first integral for large ka. Therefore one obtains

$$A_\phi(\phi) \simeq \frac{\mu_o}{4\pi} I_\phi(\phi) \times \left\{ i\pi H_o^{(1)}(kb) \right\} \qquad (1.c)$$

where $H_o^{(1)}$ is the Hankel function of the first kind and order 0. Eq. 1.c for small kb, can be written as

$$A_\phi(\phi) \simeq \frac{\mu_o}{4\pi} I_\phi(\phi) \times \left\{ -2\ln(kb) \right\} \qquad (1.d)$$

Furthermore, Eqs. 1 and 2 can be evaluated approximately at low frequencies also, i.e. when $ka << 1$ and the exponential factor in Eqs.1 and 2 is taken equal to 1. In this case the same argument used before to justify neglecting A_ρ compared to A_ϕ can be invoked again. In fact, the integrand $1/\{k^2(a^2[\,2-2\cos(\phi-\phi')] + b^2)\}$ is very large when $\phi \simeq \phi'$ and decays rapidly to much smaller values elsewhere since $a >> b$. Then, one is left with the evaluation of the integral

$$A_\phi(\phi) \simeq \frac{\mu_o}{4\pi} I_\phi(\phi) \int_o^{2\pi} \frac{a\cos\theta}{\sqrt{4a^2\sin^2(\theta/2) + b^2}}\, d\theta \qquad (1.e)$$

which yields

$$A_\phi(\phi) = \frac{\mu_o}{4\pi} I_\phi(\phi)\left\{2[\ln(8a/b) - \ln(2) - 3/4]\right\} \qquad (1.f)$$

which is the result obtained within the Ω-theory, as described in Ref. 6. It is interesting to notice that for frequencies $f(=c/\lambda)$ such that $2\pi a \simeq \lambda$, Eq. 1.d can be written as

$$A_\phi(\phi) \simeq \frac{\mu_o}{4\pi} I_\phi(\phi) 2 \ln(a/b) \qquad (1.g)$$

which is quite close to Eq. 1.f since $\ln 8 \sim 2 \sim (\ln 2 + 3/4)$. This approximation is legitimate particularly when $a >> b$, which is the case of interest here. Since the approximation (Eqs. 1.c and 1.d) used to evaluate the integrals is also known as ψ-theory (Ref. 7), the derivations illustrated above show that the two theories can be reconciled. It will be shown shortly that choosing Eq. (1.g) for the potential is also equivalent to the approach used in Ref. 1, i.e. the same results for the electromagnetic fields at the center of the antenna are found. This is to say that the more complicated approach of Ref. 1 when taking the thin wire approximation can also be obtained from a much simpler asymptotic antenna theory. Again it is stressed that the key approximations involved in Eqs. 1.b through 1.g are that $kb << 1$, $a >> b$. Therefore, in the following, the reader should exercise care when interpreting the results in the frequency range in which kb approaches 1.

The surface of the toroid is loaded with an impedance per unit length Z^i. The choice of the value of Z^i depends upon the radiated fields' properties that the designer intends to achieve. Ample discussion of this issue is presented in Ref. 1 where a value for Z^i had been obtained such that $E/H = 377\ \Omega$ at the center of the loop. In this note it will be shown that when this Z^i_o is chosen, there is complete agreement between the results for the fields at the center, both in the high and low frequency limits, obtained with the method presented in Ref. 1 and with the asymptotic antenna theory described in the following. Therefore this same value Z^i_o is retained throughout most of Part I.

Because the antenna internal impedance is negligible, one has

$$E_\phi(\phi,\omega) = I_\phi(\phi,\omega) Z^i \qquad (3)$$

everywhere along the antenna except at the source location. For the case of a δ-gap generator, at the source location $E_\phi = -V_o\delta(\phi)/a$.

From Maxwell equations and the equations for the potential one obtains

$$E_\phi = -(\nabla\phi)_\phi + i\omega A_\phi \tag{4}$$

with

$$\nabla \cdot \overline{A} - ik^2/\omega\,\phi = 0 \tag{5}$$

By combining Eqs. 3, 4, and 5, neglecting the contribution of A_ρ since it is much smaller than A_ϕ, as shown by Eqs. 2 and 2.a, one can write,

$$\frac{1}{a^2}\frac{\partial^2 A_\phi}{\partial\phi^2} + k^2 A_\phi = \frac{ik^2}{\omega}\left[Z^i I_\phi - \frac{V_o}{a}\delta(\phi)\right] \tag{6}$$

which can be rewritten in terms of the current as

$$\frac{1}{a^2}\frac{\partial^2 I_\phi}{\partial\phi^2} + k^2\left[1 + i\,\frac{2\pi Z^i}{\omega\mu_o \ln(kb)}\right]I_\phi = \frac{i2\pi k^2}{\omega\mu_o \ln(kb)}\,\frac{V_o}{a}\,\delta(\phi) \tag{7}$$

to be solved together with the boundary conditions

$$I_\phi(0) = I_\phi(2\pi) \tag{8}$$

and

$$\frac{1}{a^2}\int_{\text{across gap}} \frac{\partial^2}{\partial\phi^2} I_\phi\, a\, d\phi = PV_o \tag{9}$$

where $P = \dfrac{2\pi i k^2}{\omega\mu_o \ln(kb)}$.

Equation 7 is also interpreted formally as a transmission line equation. The "characteristic impedance" of such line is defined as $-\sqrt{\mu_o/\varepsilon_o}\,\ln(kb)/2\pi$. However, this does not imply that the solution for the current represents the lowest order mode of propagation in a transmission line and

that, therefore, should be valid only when ka is small. In fact the term "transmission line model" is used improperly and the more correct term "asymptotic antenna theory" should be used instead.

At frequencies at which $2\pi a = \lambda$ and below, ln(kb) is replaced by $-\ln(a/b)$, since Eq. 1.d is replaced by Eq. 1.g. Furthermore, at frequencies at which $kb > 0.1$ ln (kb) must be replaced with $(-i\pi/2)\,H_0^{(1)}(kb)$ since the approximation of Eq. 1.e by Eq. 1.d is not very accurate.

By defining

$$\gamma^2 = -k^2\left[1 + \frac{Z^i P}{k^2}\right] \tag{10}$$

the solution to Eq. 7 with Eqs. 8 and 9 can be written as

$$I_\phi(\phi,\omega) = Ae^{\gamma a\phi} + Be^{-\gamma a\phi} \tag{11}$$

where

$$A = \frac{PV_o}{2\gamma(1 - e^{2\gamma a\pi})}, \quad B = \frac{-PV_o}{2\gamma(1 - e^{-2\gamma a\pi})} \tag{12}$$

In Eq. 11 the explicit dependence of I_ϕ on ω as well as ϕ has been emphasized. It is noted that this approximation does not exhibit the divergent behavior at $\phi = 0°$. However for the purpose of calculating the fields this approximation is adequate, because the effect of the singular term is very localized. One could always add this singular term according to Ref. 5.

When Z^i is assumed equal to $Z_o^i = R_o/2\pi a = \eta_o[\ln(8a/b) - 2]/2\pi a \simeq \eta_o \ln(a/b)/2\pi a$ derived in Ref. 1, Eq. 10 it is obtained

$$\gamma/\gamma_o = \sqrt[4]{1 + \frac{\ln^2(a/b)}{k^2a^2[\ln(ka) + \ln(b/a)]^2}} \times \exp\left\{i\frac{1}{2}\arctan\left[\frac{\ln(a/b)}{ka\,[\ln(ka) + \ln(b/a)]}\right]\right\} \tag{13}$$

where $\gamma_o a = +ika$ and $\eta_o = 377\ \Omega$ is the vacuum intrinsic impedance. Again, at frequencies at which $2\pi a = \lambda$ and below, the term ln (ka) is neglected. The normalized wave number γ/γ_o is plotted in Fig. 2, as a function of ka, while b/a acts as a parameter. It appears that at high frequency the propagation along the antenna tends to resemble that in free space, i.e. $\gamma = \gamma_o = ik$, whereas at relatively low frequency it is characterized by the dispersive behavior illustrated by the two curves. Note that for $a/b = 10^2$ both real and imaginary part of γ/γ_o become infinite at $ka = 100$. This is

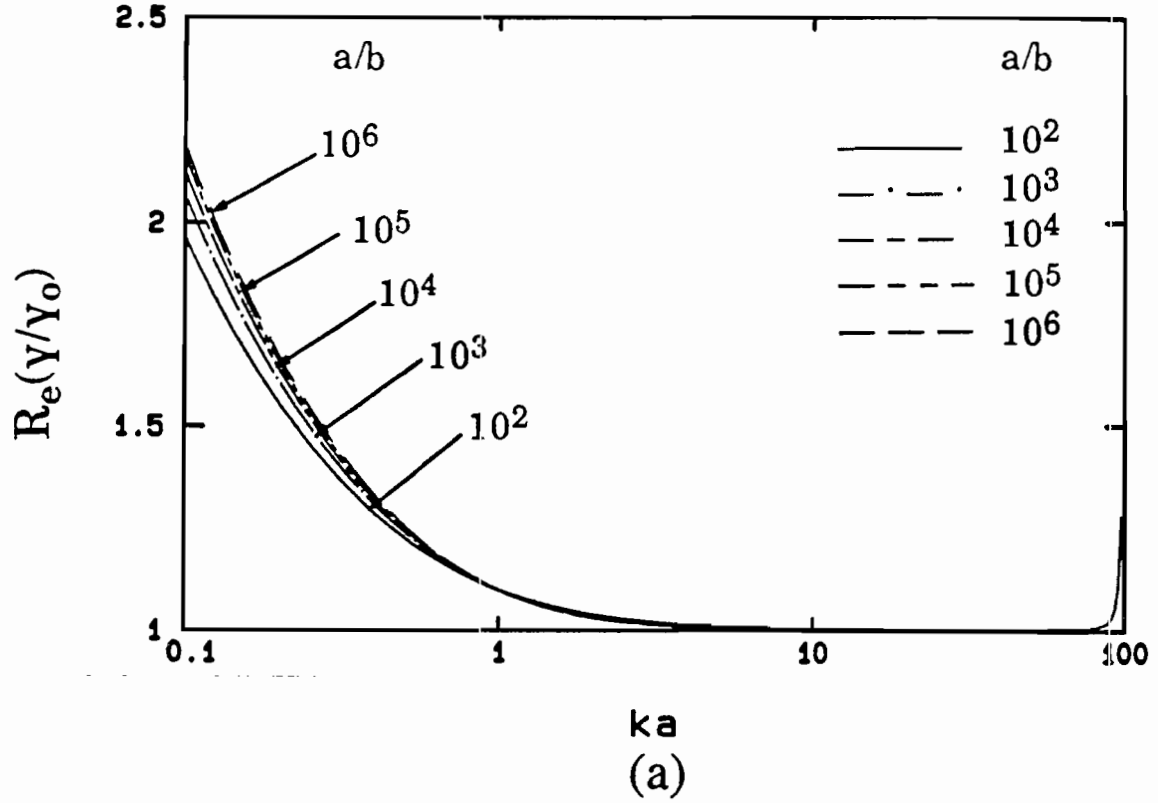

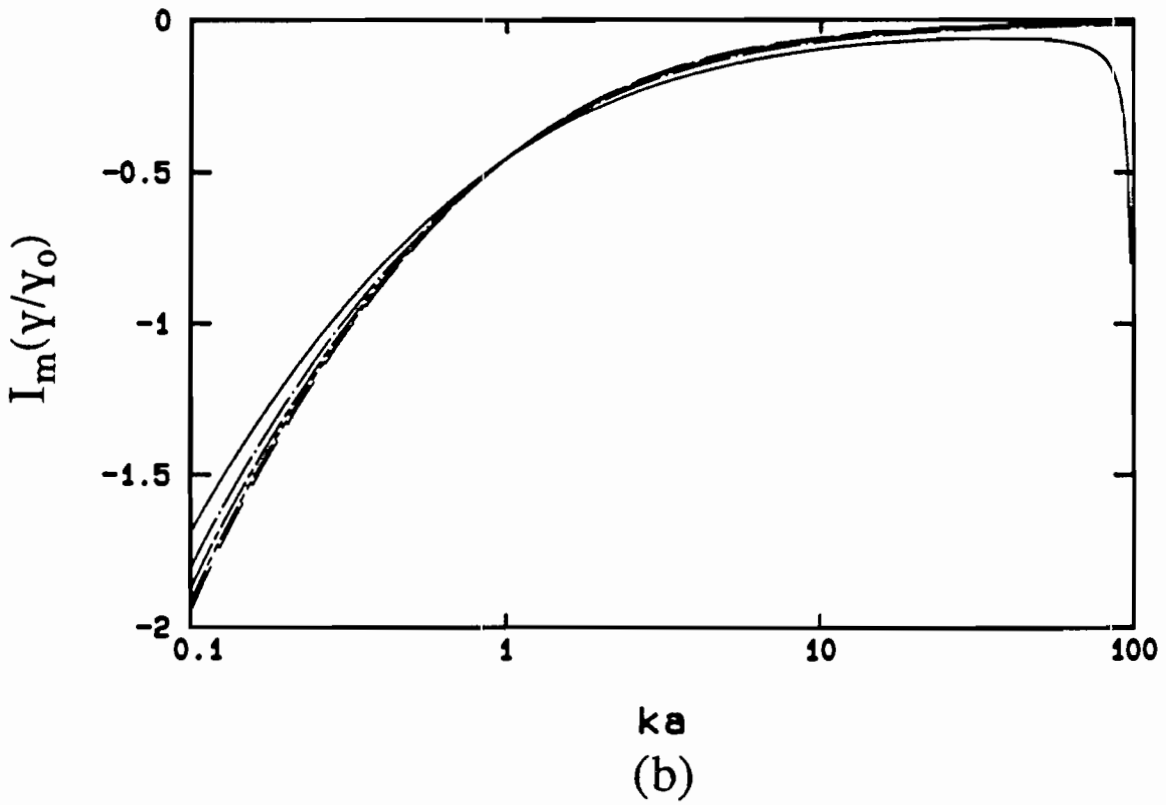

Figure 2. γ/γ_0 real and imaginary parts. Note: for $a/b = 10^2$ the model breaks down when ka approaches 1.00.

caused by the term ln(ka) + ln(b/a) in Eq. 13 which vanishes. However, the asymptotic antenna theory breaks down when kb becomes 1 or larger and one should not use the results for $a/b = 10^2$ when ka approaches 100.

1.1.2 Time-Domain Antenna Current

Equation 11 represents the antenna current in the frequency-domain. It is interesting to calculate the antenna current in the time domain. This is obtained by performing an inverse Fourier transform. For the case that the driving voltage is a unit step function this amounts to calculating

$$I_\phi(t,\phi) = -\frac{1}{2\pi}\int_{-\infty}^{+\infty} \frac{I_\phi(\phi,\omega)}{i\omega} e^{-i\omega t} d\omega \tag{14}$$

where $I_\phi(\phi, \omega)$ is given by Eq. 11 with $\omega = kc$. However one still needs to truncate the integration at some point to be able to carry it out numerically. To avoid the singularity at $\omega = 0$ Eq. 14 can be evaluated as

$$\begin{aligned} I_\phi(t,\phi) = -\frac{1}{2\pi}\Bigg\{ & \int_{-L}^{L} \frac{I'(\omega,\phi) - I'(0,\phi)}{i\omega} e^{-ik(ct-a\phi)} d\omega \\ & + \int_{-\infty}^{L} \frac{I'(\omega,\phi) - I'(0,\phi)}{i\omega} e^{-ik(ct-a\phi)} d\omega + \int_{L}^{\infty} \frac{I'(\omega,\phi) - I'(0,\phi)}{i\omega} e^{-ik(ct-a\phi)} d\omega \\ & + \int_{-\infty}^{+\infty} \frac{I'(0,\phi)}{i\omega} e^{-ik(ct-a\phi)} d\omega \Bigg\} \end{aligned} \tag{15}$$

where $I'(\omega,\phi) = I(\omega,\phi)\, e^{-ika\phi}$ and $I'(0,\phi) = \lim_{\omega \to 0} I'(\omega,\phi)$. The first integral is evaluated numerically without making approximations on the kernel. The limit of integration is selected so that $kb << 1$ and Eq. 1.d holds. We have chosen to terminate the integration at $ka = 30$, corresponding to $kb = 0.03$. The second and third integrals compensate for the numerical truncation by adding a contribution evaluated analytically. Such contribution, which is dependent on the truncation value, is calculated by approximating γ with ik and keeping ka, kb fixed at the values 30 and 0.03, respectively. This approximation is justified by the fact that the integrand of the second and third integrals is decreasing and the phase varies very rapidly at high frequencies. Therefore one is left with

$$-\frac{1}{\pi} \mathrm{Re}\left\{ [I'_{h.f.}(\omega,\phi) - I'(0,\phi)] \int_{L}^{\infty} \frac{e^{-ik(ct-a\phi)}}{i\omega} d\omega \right\} \tag{16}$$

with $I'_{h.f.}(\omega,\phi) = \lim_{\omega\to\infty} I'(\omega,\phi)$ obtained using $\gamma = ik$ in $I(\omega,\phi)$ given by Eq.11. By making a suitable change of variable Eq. 16 can be evaluated analytically also, yielding

$$-\frac{1}{\pi}\mathrm{Re}[I'_{h.f.}(\omega,\phi) - I'(0,\phi)]\,\mathrm{si}\left[ka\left(\frac{ct}{a} - \phi\right)\right] \tag{17}$$

with si(z) being the sine integral defined as

$$\mathrm{si}(z) = -\int_z^{\infty} \frac{\sin(t)}{t}\,dt \tag{18}$$

The fourth integral on the right-hand side of Eq. 15 can be evaluated analytically and it yields the unit step function of amplitude $I'(0,\phi)$ excited at the time $t = a\phi/c$.

Figure 3 presents the time domain current response at three different values of ϕ, i.e. $\phi = 0^\circ$, $\phi = 90^\circ$, and 180°, respectively.

1.1.3 Input Impedance

From Eq. 11 calculated at $\phi = 0^\circ$, simply by dividing by V_o and taking the reciprocal of the ratio, the input impedance Z_{in} is derived. It is found

$$Z_{in} = \frac{R_o}{\pi}\, 1/Y\ (W + iT)\ \frac{\ln(kb)}{\ln(a/b)}\ \frac{e^{-ikan\,Y^{-1/2}(W+iT)} - e^{ikan\,Y^{-1/2}(W+iT)}}{e^{-ikan\,Y^{-1/2}(W+iT)} + e^{ikan\,Y^{-1/2}(W+iT)}} \tag{19}$$

with

$$X = \frac{\ln(a/b)}{ka[\ln(ka) + \ln(b/a)]} \tag{20.a}$$

$$Y = \frac{1}{\sqrt{1+X^2}} \tag{20.b}$$

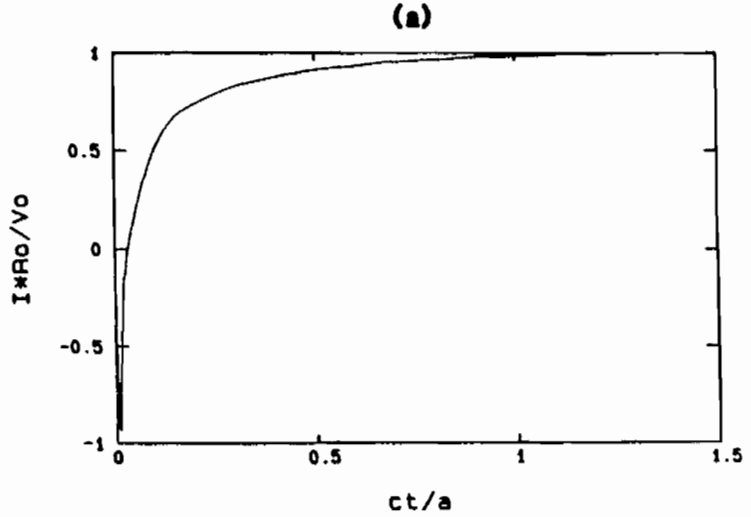

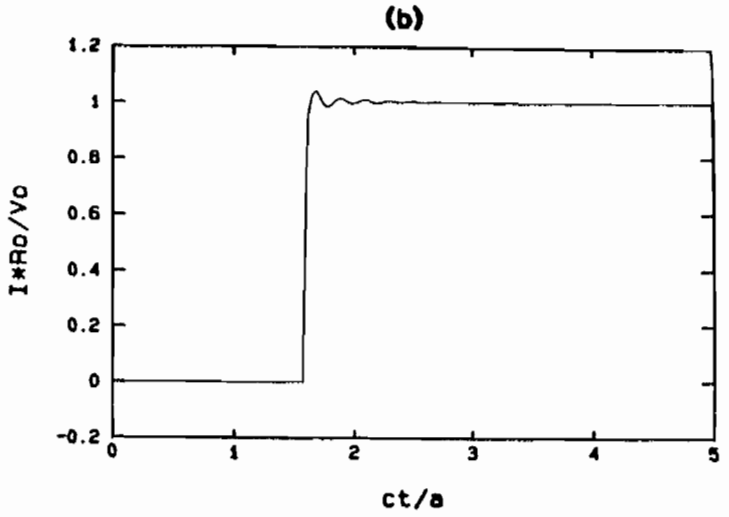

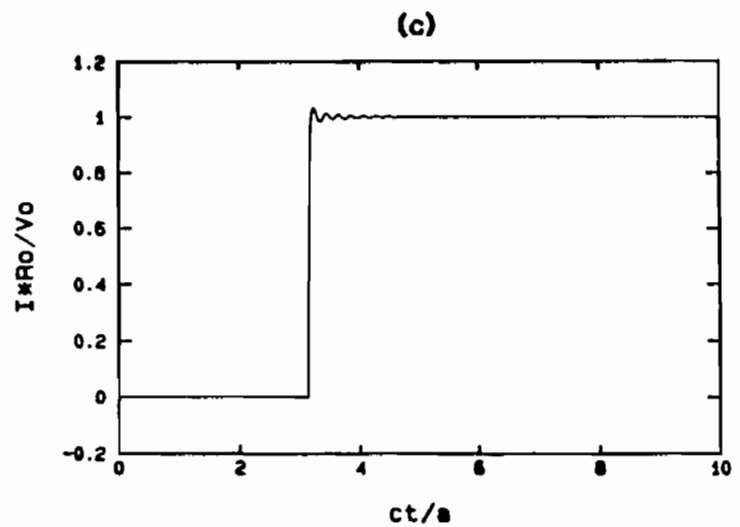

Figure 3. Time domain current response to step function excitation calculated at (a) $\phi = 0^o$ (b) $\phi = 90^o$ (c) $\phi = 180^o$.

$a/b = 10^3$ $R_0 = \eta_0 \ln(a/b)$

Note: since the results in the frequency domain are good only for ka up to 10^2 ($kb \rightarrow 0.1$) the time response at (a) $t < 10^{-1} a/c$ (b) $t < 10^{-1} a/c + \pi/2$ (c) $t < 10^{-1} a/c + \pi$ is affected by error.

$$T = \pm \sqrt{\frac{1-Y}{2}} \qquad \begin{cases} + \; X>0 \\ - \; X<0 \end{cases} \tag{20.c}$$

$$W = \sqrt{\frac{1+Y}{2}} \tag{20.d}$$

The calculation of Eq. 19 resulted in the two curves presented in Fig. 4 for the real and imaginary part, respectively. Because of the lack of the singular term in the solution for the current at $\phi = 0^o$ one should expect to see large errors in the calculation of the input impedance at $\phi = 0^o$, particularly as far as the reactance is concerned. In fact, theoretically, the reactance shuld be zero. On the other hand, since the antenna is resistively loaded, the resistive part is controlled by such load. However, one should remember that the singularity in the current is associated with the presence of a slice generator, which is not a realistic generator. In practice, measurements of input impedances associated with use of feasible sources would reveal the presence of a reactance different from zero. At low frequency the calculated impedance is purely resistive and equal to the value R_o of the loading resistance. As the frequency increases the resistance gradually decreases to zero. The reactance is always inductive and decreases to zero also, both at the low and high frequencies. Intuitively it was at first expected the reactance to change sign, maybe even several times, before vanishing (transmission line behavior); however this does not happen. Mathematically this can be understood if Eq. 19 is rewritten in the form

$$Z_{in} = \frac{R_o}{\pi} \sqrt[4]{1+X^2}\,(W+iT)\,\frac{\ln(kb)}{\ln(a/b)}\,\frac{e^{B}(\cos A - i\sin A) - e^{-B}(\cos A + i\sin A)}{e^{B}(\cos A - i\sin A) + e^{-B}(\cos A + i\sin A)} \tag{21}$$

with $A = ka\pi \sqrt[4]{1+X^2}\,W$, $B = ka\pi \sqrt[4]{1+X^2}\,T$.

As ka increases, $T \to 0$ and $W \to 1$. However, in the range of ka considered, B assumes fairly large values anyway which cause the exponential e^{B} (e^{-B}) to become very large (small). Therefore the ratio containing A and B in Eq. 21 is not oscillatory but is always very close to 1, and the impedance does not exhibit a strong resonant behavior. It is evinced that the loading resistance R_o is causing a pronounced damping effect and only a small portion of the loop in the vicinity of the source is the "effective" antenna. A simple circuit representation is thus given by an open circuit voltage source in series with the loading resistance and the inductive reactance. A possible capacitive reactance would be in parallel to this series of elements. However, as the frequency increases, this reactive element is shorted out and the only surviving reactive element is inductive. Because of the high

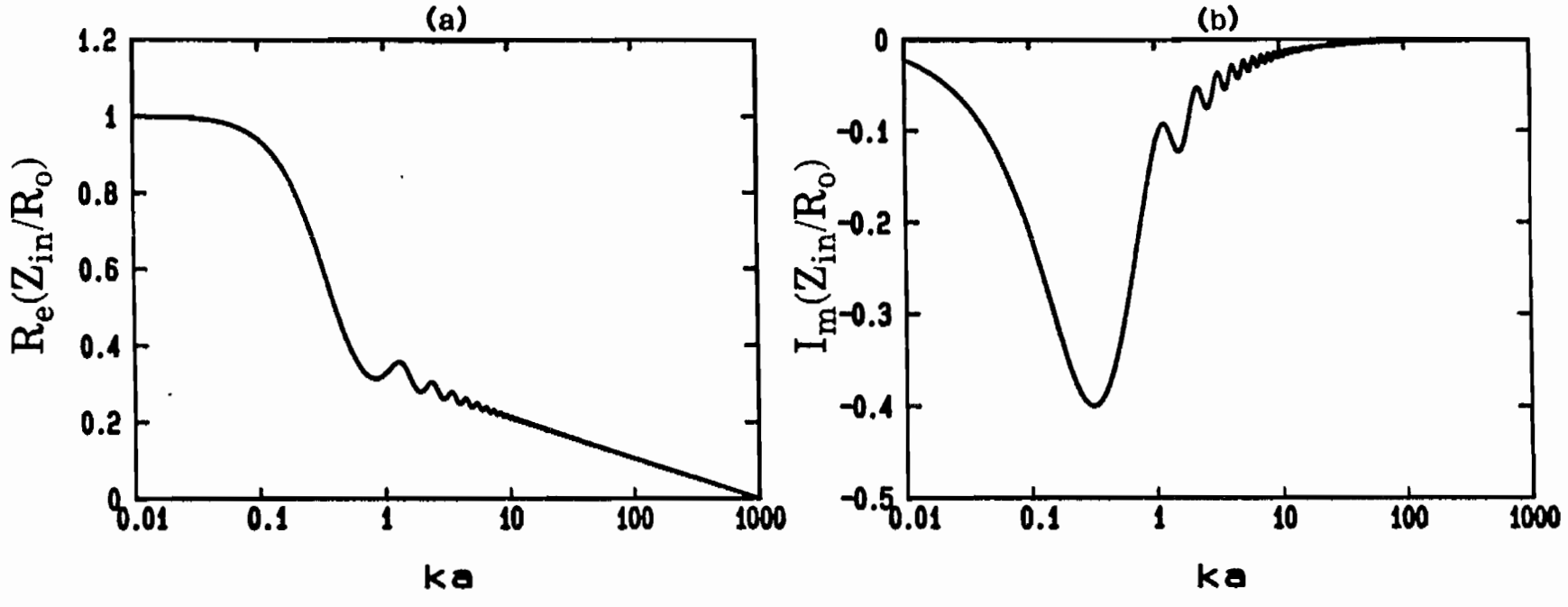

Figure 4. TORUS input impedance: (a) resistance (b) reactance

$R_o = \eta_o \ln(a/b)$ $a/b = 10^3$.

Note: asymptotic antenna theory approximation does not give exactly zero reactance at all frequencies at $\phi = 0^o$, corresponding to slice generator. In addition values beyond ka equal 100 are questionable because of theory breakdown.

value of the loading resistance the radiation resistance may become negligible and may be omitted from the circuit representation.

1.1.4 Fields At The Center Of The Antenna

Once the current is known one can calculate the potential A_ρ, A_ϕ everywhere. In general these components are given by

$$A_\rho(\rho,\phi,z) = \frac{\mu_o}{4\pi}\int_{\phi-2\pi}^{\phi} I_\phi(\phi-\phi')\frac{e^{ik\sqrt{a^2+\rho^2-2a\rho\cos\phi'+z^2}}}{\sqrt{a^2+\rho^2-2a\rho\cos\phi'+z^2}}\, a\sin\phi' d\phi' \tag{22}$$

$$A_\phi(\rho,\phi,z) = \frac{\mu_o}{4\pi}\int_{\phi-2\pi}^{\phi} I_\phi(\phi-\phi')\frac{e^{ik\sqrt{a^2+\rho^2-2a\rho\cos\phi'+z^2}}}{\sqrt{a^2+\rho^2-2a\rho\cos\phi'+z^2}}\, a\cos\phi' d\phi' \tag{23}$$

Consequently, the electromagnetic field at the center of the TORUS, i.e. for $z = 0$, $\rho = 0$, is

$$\bar{B}_c = (\nabla \times \bar{A}) = \bar{a}_z \lim_{\rho,z\to 0}\frac{1}{\rho}\left[\frac{\partial}{\partial\rho}(\rho A_\phi) - \frac{\partial}{\partial\phi}A_\rho\right] \tag{24}$$

$$= \bar{a}_z\left[2\frac{\partial A_\phi}{\partial\rho} - \frac{\partial^2 A_\rho}{\partial\phi\partial\rho}\right]_{z=\rho=0}$$

$$\bar{E}_c = (-c^2/i\omega)\nabla\times\bar{B}\Big|_{z=0,\rho=0} \tag{25}$$

$$\nabla\times\bar{B}\Big|_{z=\rho=0} = \lim_{\rho,z\to 0}\left\{\bar{a}_\rho\left[\frac{1}{\rho}\frac{\partial B_z}{\partial\phi} - \frac{\partial B_\phi}{\partial z}\right]\right.$$

$$\left. + \bar{a}_\phi\left[\frac{\partial B_\rho}{\partial z} - \frac{\partial B_z}{\partial\rho}\right] + \bar{a}_z\left[\frac{1}{\rho}\frac{\partial(\rho B_\phi)}{\partial\rho} - \frac{1}{\rho}\frac{\partial B_\rho}{\partial\phi}\right]\right\} \tag{26}$$

and

$$B_\rho = \frac{-\partial A_\phi}{\partial z},\quad B_\phi = \frac{\partial A_\rho}{\partial z},\quad B_z = \frac{1}{\rho}\left[\frac{\partial}{\partial\rho}(\rho A_\phi) - \frac{\partial A_\rho}{\partial\phi}\right] \tag{27}$$

Taking the limit in Eq.25 , it is obtained

$$\bar{E}_c = (-c^2/i\omega)\left\{\bar{a}_\rho\left|\frac{1}{2}\frac{\partial^3 A_\phi}{\partial\rho^2\partial\phi} - \frac{\partial^2 A_\rho}{\partial z^2}\right| - \bar{a}_\phi\left|\frac{3}{2}\frac{\partial^3 A_\phi}{\partial\rho^2\partial\phi} - \frac{1}{2}\frac{\partial^3 A_\rho}{\partial\phi\partial\rho^2} + \frac{\partial^2 A_\phi}{\partial z^2}\right|\right\}_{\rho=0,z=0} \tag{28}$$

Equations 24 and 28 can be carried out analytically for $\rho = z = 0$ by first calculating the derivatives in ρ and z and taking the limits for $\rho, z \to 0$ of the integrand and then performing the integration and finally the derivative with respect to ϕ.

It is obtained

$$\bar{B}_c = \frac{\mu_o}{4\pi}(1 - ika)\frac{e^{ika}}{a}\left(\frac{-PV_o}{\gamma^2 a}\right)\bar{a}_z \tag{29}$$

$$\bar{E}_c = \frac{\eta_o}{4\pi}\left(1 + \frac{i}{ka} - ika\right)\frac{e^{ika}}{a}\left(\frac{PV_o a}{\gamma^2 a^2 + 1}\right)\bar{a}_y \tag{30}$$

By evaluating $-PV_o/(\gamma^2 a)$ and $PV_o/(\gamma^2 a^2 + 1)$ in the low frequency limit the same results of Eq. 6.13 and Eq. 6.22 of Ref. 1 are obtained. Similarly, in the high frequency limit, by evaluating Eq. 30 with use of Eq. 1.c, a result equivalent to that of Eq. 6.28 of Ref. 1 can be easily established.

Furthermore, the ratio $\Lambda_o = -E_c/\eta_o H_c$ is given by

$$\Lambda_o = \frac{1 + i/ka - ika}{1 - ika} \times \frac{\gamma^2 a^2}{\gamma^2 a^2 + 1} \tag{31}$$

It is noted that in both the low frequency and high frequency limit, the value of Λ_o is 1, in agreement with Ref. 1. Equations 29 and 30 have been plotted in Fig. 5 together with the correspondent quantities from Ref. 1. It is noted that they compare quite well, especially at low and intermediate frequency. At high frequency the asymptotic antenna theory breaks down when kb approaches 1.

The fields at the center have been obtained in the time domain also by performing the inverse Fourier transforms of Eqs. 29 and 30 as

$$\bar{E}_c(t) = -\frac{1}{2\pi}\int_{-\infty}^{+\infty}\frac{\bar{E}_c(ka)}{i\omega}e^{-i\omega t}d\omega \tag{32}$$

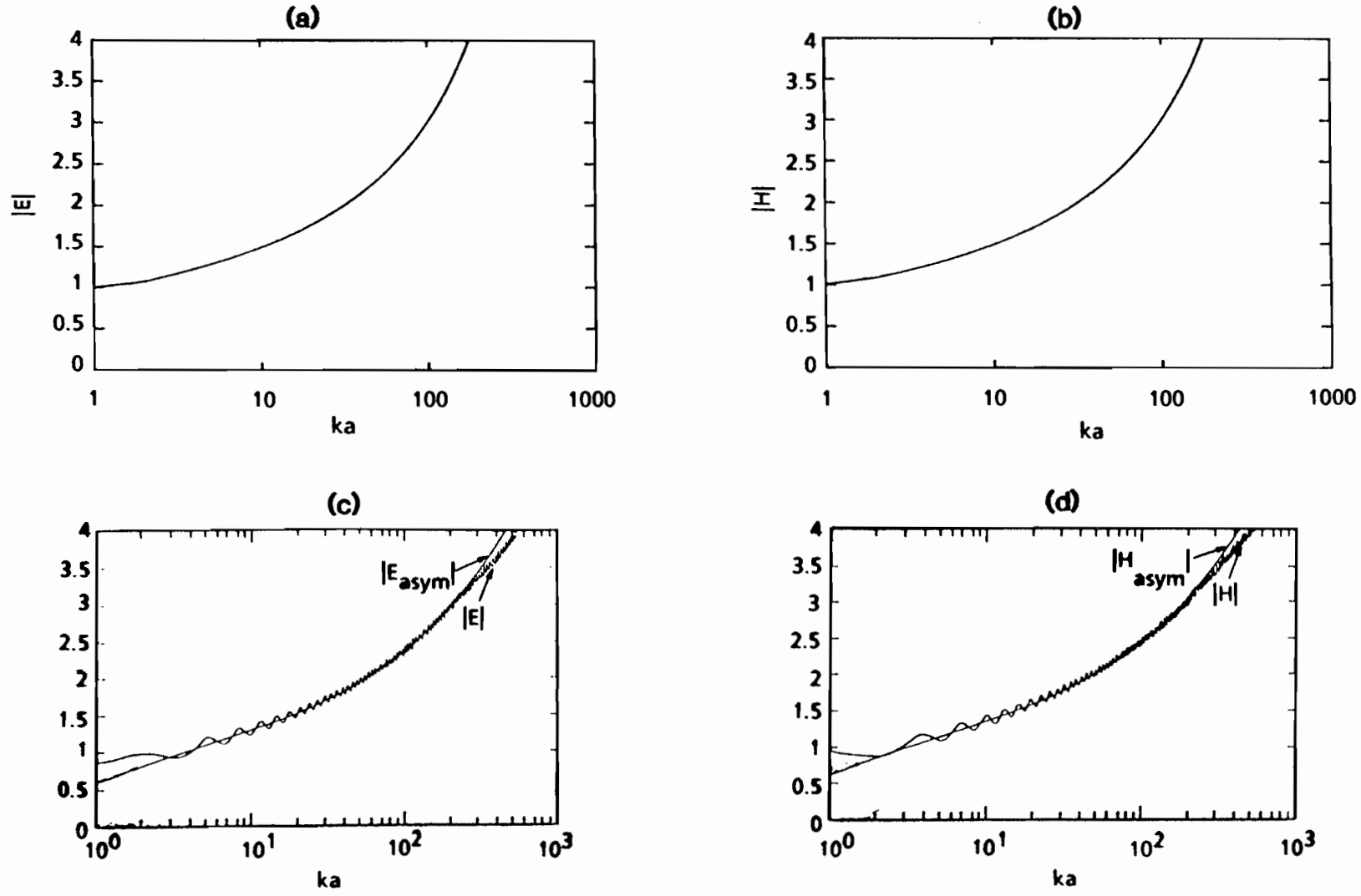

Figure 5. Comparison between the fields at the center obtained with the asymptotic antenna theory ((a), (b)) and those calculated by C. Baum [1] ((c), (d)). In both cases $R_o = \eta_o \ln(a/b)$, $a/b = 10^3$. The fields are normalized to their respective static values. Note: The asymptotic antenna theory starts breaking down at ka around 100.

$$\bar{B}_c(t) = -\frac{1}{2\pi}\int_{-\infty}^{+\infty}\frac{\bar{B}_c(ka)}{i\omega}\,e^{-i\omega t}\,d\omega \tag{33}$$

where, again, it was assumed that the source was a step function of amplitude V_0. By following a similar procedure to that illustrated in Section 1.1.3, (see Eqs. 15 through 17) one can write

$$\begin{aligned}\bar{E}_c(t) = -\frac{1}{2\pi}\Bigg\{&\int_{-L}^{L}\frac{\bar{E}_c'(ka)-E_c'(0)}{i\omega}\,e^{-ik(ct-a)}\,d\omega\\ &+\int_{-\infty}^{-L}\frac{\bar{E}_c'(ka)-E_c'(0)}{i\omega}\,e^{-ik(ct-a)}\,d\omega+\int_{L}^{\infty}\frac{\bar{E}_c'(ka)-E_c'(0)}{i\omega}\,e^{-ik(ct-a)}\,d\omega\\ &+\int_{-\infty}^{+\infty}\frac{E_c'(0)}{i\omega}\,e^{-ik(ct-a)}\,d\omega\Bigg\}\end{aligned} \tag{34}$$

$$\begin{aligned}\bar{B}_c(t) = -\frac{1}{2\pi}\Bigg\{&\int_{-L}^{L}\frac{\bar{B}_c'(ka)-B_c'(0)}{i\omega}\,e^{-ik(ct-a)}\,d\omega\\ &+\int_{-\infty}^{-L}\frac{\bar{B}_c'(ka)-B_c'(0)}{i\omega}\,e^{-ik(ct-a)}\,d\omega+\int_{L}^{\infty}\frac{\bar{B}_c'(ka)-B_c'(0)}{i\omega}\,e^{-ik(ct-a)}\,d\omega\\ &+\int_{-\infty}^{+\infty}\frac{B_c'(0)}{i\omega}\,e^{-ik(ct-a)}\,d\omega\Bigg\}\end{aligned} \tag{35}$$

with $E_c'(ka)=E_c(ka)\,e^{-ika}$, $B_c'(ka)=B_c(ka)\,e^{-ika}$. The results shown in Figs. 6 and 7 were obtained, for the magnetic and the electric field, respectively. In this case the time domain response is triggered at $t=a/c$ to account for the propagation delay between the source and the center of the antenna. It is stressed that, because of the error at high frequency due to the failure of the asymptotic antenna theory as well as the numerical error introduced in performing the integrations in Eqs. 34 and 35, the early time results are certainly affected by error. This is confirmed by the fact that the ratio $E_y/(B_z c)$ obtained from the curves in Figs. 6 an 7 is not exactly 1 at all times, but deviates from it at early times by as much as 20%. This must be accepted as a penalty intrinsic to the approximations used.

1.1.5 Fields Off The Center Of The Antenna

At points other than the center the fields cannot, in general, be evaluated analytically. However the computation of Eqs. 22 and 23 and their derivatives is straightforward and can be handled with relatively modest computational resources. This section presents the derivation of the fields and their computation in some regions of practical interest.

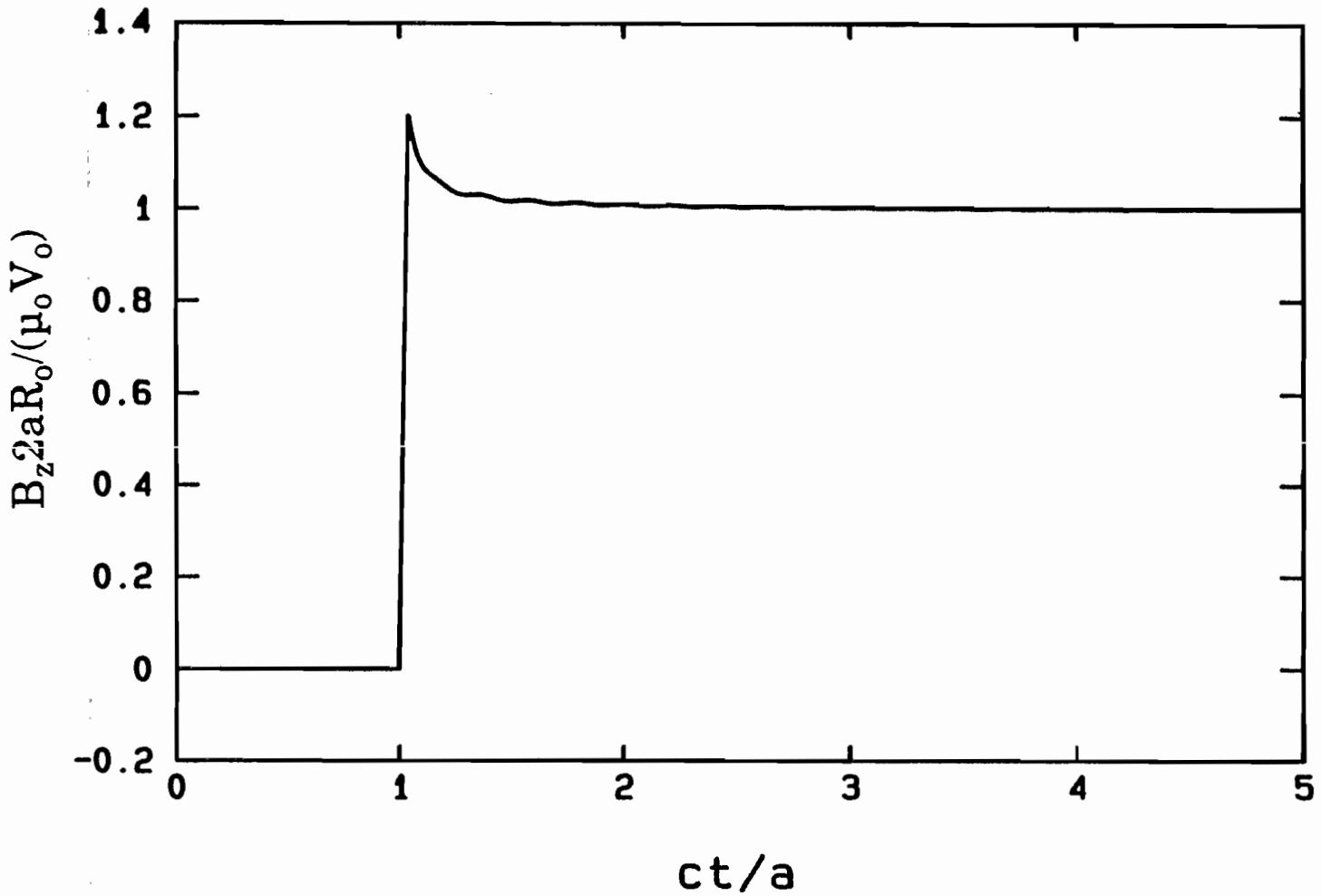

Figure 6. Time domain response to step function excitation for B_z field at the center of the TORUS. Single source at $\phi = 0^o$ $a/b = 10^3$ $R_o = \eta_o \ln(a/b)$

Note: since the results in the frequency domain are good only for ka up to 10^2 (kb→0.1) the time response at $t < 10^{-1}$ a/c is affected by error.

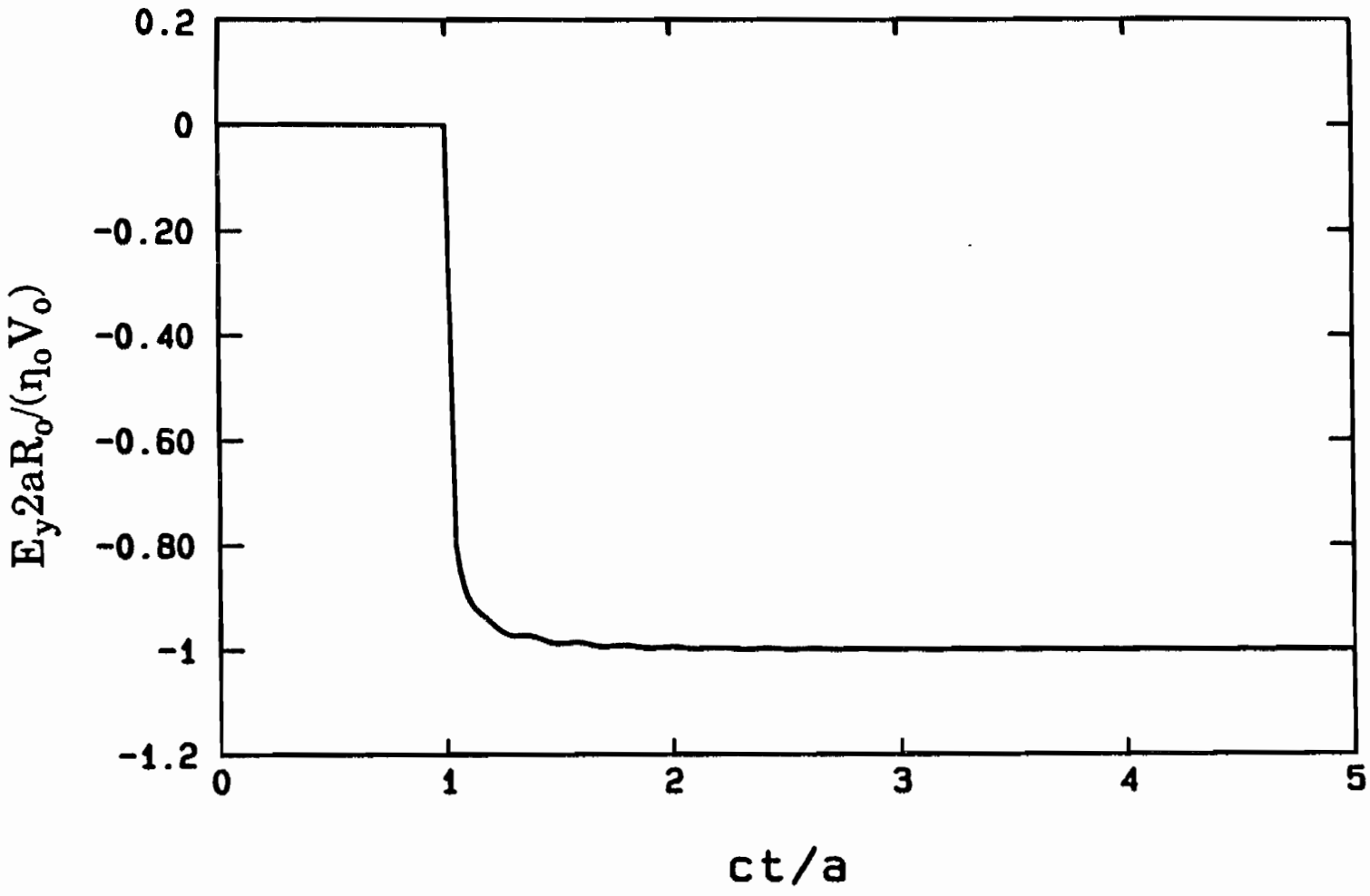

Figure 7. Time domain response to step function excitation for E_y field at the center of the TORUS. Single source at $\phi = 0^o$. $a/b = 10^3$, $R_o = \eta_o \ln(a/b)$

Note: since the results in the frequency domain are good only for ka up to 10^2 (kb→0.1) the time response at $t < 10^{-1}$ a/c is affected by error.

In these calculations the delta gap source is supposed to be located at $\phi = 0^{o}$. From Maxwell's equations $\overline{B} = \nabla x \overline{A}$, $-i\omega\varepsilon_o\mu_o \overline{E} = \nabla x \overline{B}$ it is obtained:

$$B_\rho = \frac{-\partial A_\phi}{\partial z} \qquad B_\phi = \frac{\partial A_\rho}{\partial z} \qquad B_z = \frac{1}{\rho}\left[\frac{\partial}{\partial \rho}(\rho A_\phi) - \frac{\partial A_\rho}{\partial \phi}\right] \tag{36}$$

$$-i\omega\varepsilon_o\mu_o E_\rho = \frac{1}{\rho^2}\frac{\partial A_\phi}{\partial \phi} + \frac{1}{\rho}\frac{\partial^2 A_\phi}{\partial \phi \partial \rho} - \frac{1}{\rho^2}\frac{\partial^2 A_\rho}{\partial \phi^2} - \frac{\partial^2 A_\rho}{\partial z^2} \tag{37}$$

$$-i\omega\varepsilon_o\mu_o E_\phi = -\left[\frac{\partial^2 A_\phi}{\partial \rho^2} + \frac{1}{\rho}\frac{\partial A_\phi}{\partial \rho} - \frac{1}{\rho^2}A_\phi + \frac{1}{\rho^2}\frac{\partial A_\rho}{\partial \phi} - \frac{1}{\rho}\frac{\partial^2 A_\rho}{\partial \phi \partial \rho} + \frac{\partial^2 A_\phi}{\partial z^2}\right] \tag{38}$$

$$-i\omega\varepsilon_o\mu_o E_z = \frac{1}{\rho}\frac{\partial A_\rho}{\partial z} + \frac{\partial^2 A_\rho}{\partial z \partial \rho} + \frac{1}{\rho}\frac{\partial^2 A_\phi}{\partial \phi \partial z} \tag{39}$$

In the following we report the expressions of the partial derivatives of the vector potential $\overline{A}$. All pairs of derivatives of A_ρ, A_ϕ whose expressions are very similar except for some factors having been written as a single equation with the derivative of A_ϕ appearing inside braces { }. This means that the reader can switch from one quantity to the other by substituting the correspondent quantity within braces on the right-hand side of the equation.

Letting $\sqrt{a^2+\rho^2-2a\rho\cos\phi+z^2} = C(a, \rho, \phi, z)$, it was found

$$\frac{\partial A_\rho}{\partial \phi}\left\{\frac{\partial A_\phi}{\partial \phi}\right\} = \frac{\mu o}{4\pi}\int_{\phi-2\pi}^{\phi}\frac{\partial}{\partial \phi}[\Pi(\phi-\phi')]\,\frac{e^{ikC}}{C}\,a\sin\phi'\{\cos\phi'\}\,d\phi' \tag{40}$$

$$\frac{\partial^2 A_\rho}{\partial \phi^2}\left\{\frac{\partial^2 A_\phi}{\partial \phi^2}\right\} = \frac{\mu_o}{4\pi}\int_{\phi-2\pi}^{\phi}\gamma^2 a^2\, I(\phi-\phi')\frac{e^{ikC}}{C}\,a\sin\phi'\{\cos\phi'\}\,d\phi'$$

$$+\frac{\mu_o}{4\pi}PV_o a^2\sin\phi\{\cos\phi\}\frac{e^{ikC}}{C} \tag{41}$$

Writing v for either ρ or z and S for either ρ-a $\cos\phi'$ or z, correspondingly, it was obtained

$$\frac{\partial A_\rho}{\partial v}\left\{\frac{\partial A_\phi}{\partial v}\right\} = \frac{\mu_o}{4\pi}\int_{\phi-2\pi}^{\phi} I(\phi-\phi')\frac{e^{ikC}}{C}\, a\sin\phi'\{\cos\phi'\} S\,(ik-\frac{1}{C})\,d\phi' \tag{42}$$

$$\frac{\partial^2 A_\rho}{\partial v^2}\left\{\frac{\partial^2 A_\phi}{\partial v^2}\right\} = \frac{\mu_o}{4\pi}\int_{\phi-2\pi}^{\phi}\left(I(\phi-\phi')\frac{e^{ikC}}{C}\, a\sin\phi'\{\cos\phi'\}\, x\right.$$

$$\left.\frac{1}{C^2}[-1+ikC+\frac{S^2}{C^2}(3-3ikC-k^2C^2)]\right)d\phi' \tag{43}$$

$$\frac{\partial^2 A_\rho}{\partial\phi\partial v}\left\{\frac{\partial^2 A_\phi}{\partial\phi\partial v}\right\} = \frac{\mu_o}{4\pi}\int_{\phi-2\pi}^{\phi}\frac{\partial I(\phi-\phi')}{\partial\phi}\,\frac{e^{ikC}}{C}\, a\sin\phi'\{\cos\phi'\} S\,(ik-\frac{1}{C})\,d\phi' \tag{44}$$

The principal components of the electromagnetic fields B_z and E_y have been computed using the above equations along the line x/a = 0 or 0.5 and at the heights y/a = 0.1, 0.2 and 0.25. The results are presented in Figs. 8 and 9.

1.1.6 Field Uniformity Error

In practice one is interested in the behavior of the electromagnetic fields in a volume around the center of the antenna or, in the case of a semicircular loop above the ground, in a region elevated above the ground plane itself. Ideally one would like to design the antenna in such a way that the principal components of the fields are as uniform as possible in such region and, in addition, the non principal components are small. One convenient and well accepted quantifier of the deviation from field uniformity in a certain domain is the 2-norm error.

Two domains have been considered for this case; for simplicity they are taken to be one dimensional. One is a semi-circle. This is suitable to quantify a uniformity error intrinsically related to the circular geometry of the antenna. Another domain, perhaps more interesting from a practical viewpoint, when the test article is an aircraft, is a straight segment of total length equal to the radius a, located above the ground at a variable distance y in a symmetrical position with respect to the y axis. These domains are visualized in Fig. 10. The 2-norm error, 2-N, written here for the principal component P_δ of the fields, is given by

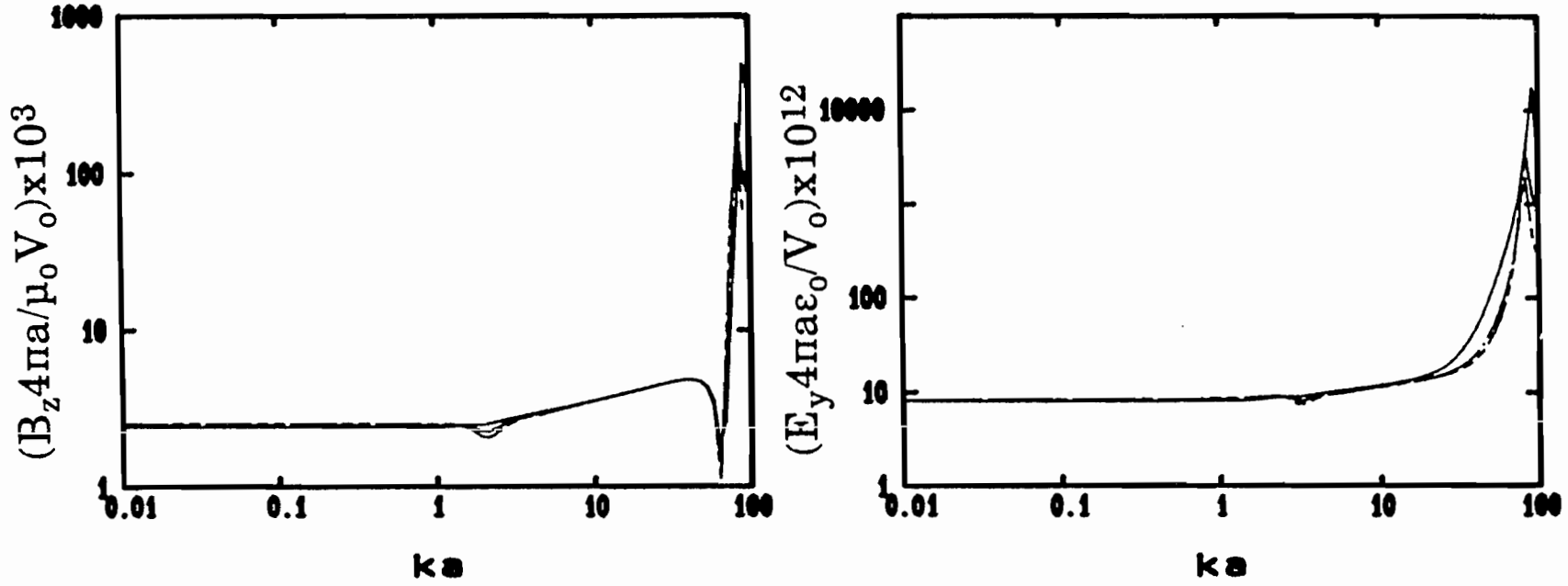

Figure 8. Principal field components of TORUS calculated at x/a = 0, z/a = 0 and

_____ y/a = 0.1

_____ y/a = 0.2

_____ y/a = 0.25

Source is at $\phi = 0^o$, $a/b = 10^3$, $R_o = \eta_o \log(a/b)$. Note: Results for ka approaching 100 might be affected by error since the asymptotic antenna theory starts breaking down. Magnetic field has units of Siemens, electric field has units of Farad/meter.

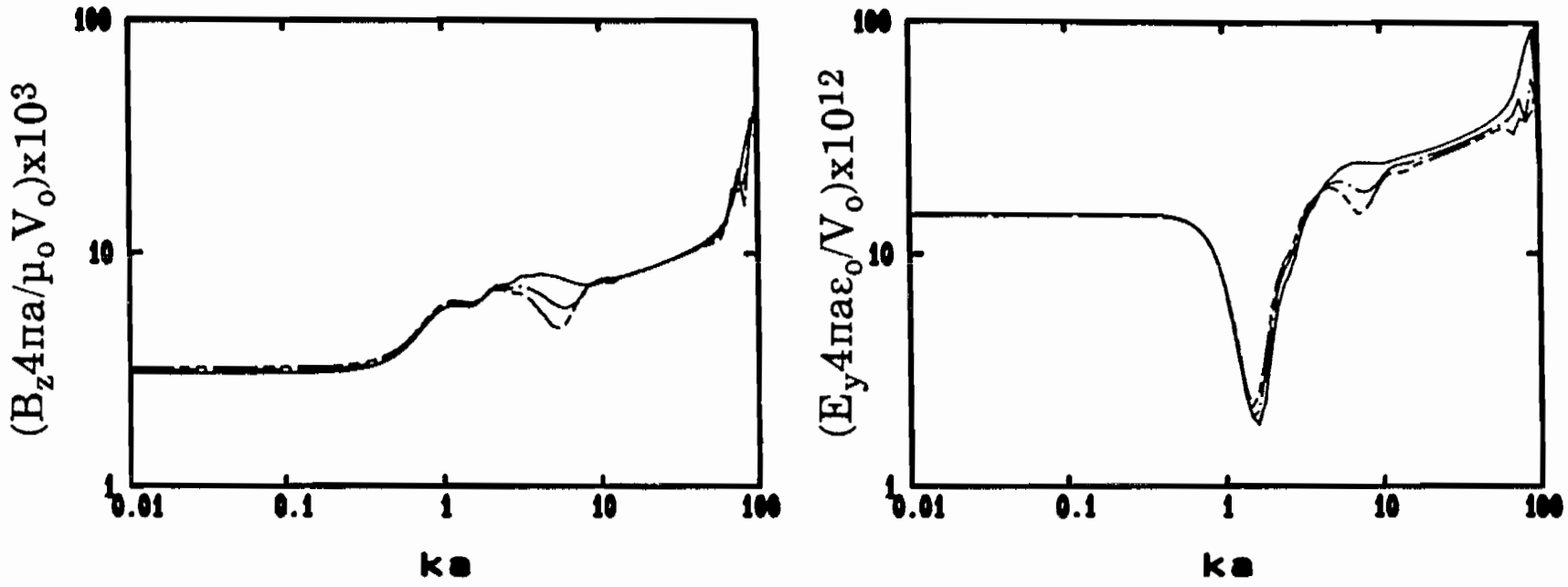

Figure 9. Principal field components of TORUS calculated at x/a = 0.5, z/a = 0 and

——————— y/a = 0.1

——— · ——— y/a = 0.2

——— — — ——— y/a = 0.25

Source is at $\phi = 0^o$, $a/b = 10^3$, $R_o = \eta_o \log(a/b)$. Note: Results for ka approaching 100 might be affected by error since the asymptotic antenna theory starts breaking down. Magnetic field has units of Siemens, electric field has units of Farad/meter.

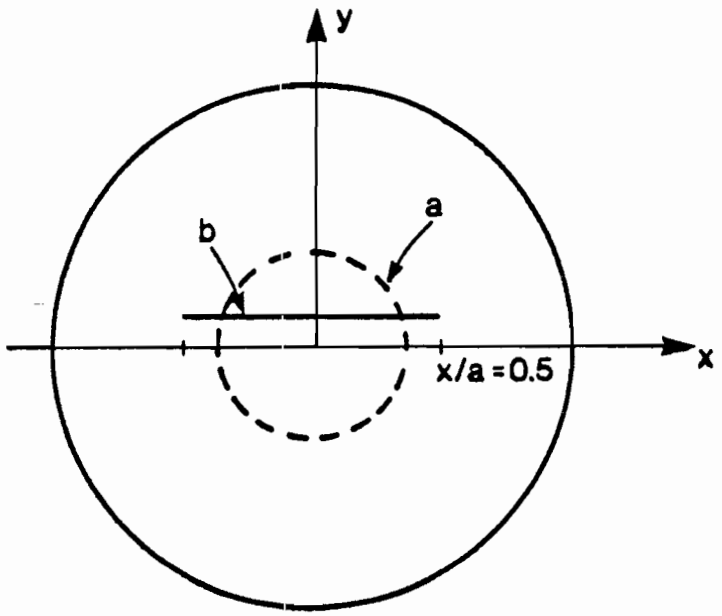

Figure 10. Illustration of the domains of integration used in evaluating (a) Eqs. 45 and 46, (b) Eqs. 47 and 48 for computation of 2-norm errors.

$$2-N=\frac{\left[\frac{1}{\pi}\int_0^{\pi}|P_\delta(ka,\rho/a,z/a,\phi)-P_\delta^{ave}|^2\,d\phi\right]^{1/2}}{|P_\delta^{ave}|} \tag{45}$$

$$P_\delta^{ave}=\frac{1}{\pi}\int_0^{\pi}P_\delta(ka,\rho/a,z/a,\phi)\,d\phi \tag{46}$$

for the circular domain of integration and

$$2-N=\frac{\left[\int_{-0.5}^{0.5}|P_\delta(ka,x/a,y/a,z/a)-P_\delta^{ave}|^2 d(x/a)\right]^{1/2}}{|P_\delta^{ave}|} \tag{47}$$

$$P_\delta^{ave}=\int_{-0.5}^{0.5}P_\delta(ka,x/a,y/a,z/a)\,d(x/a) \tag{48}$$

for a straight line. P_δ is either E_y or B_z for the case of a single δ-gap source located at $\phi=0^o$.

Figures 11 and 12 illustrate the results for the two chosen domains. As intuitively expected, the 2-norm error is smaller when calculated along the circle (ρ/a = const) than along the straight line (y/a = const). At low frequency ($ka < 1$) the error can be made quite small, i.e. about 10% for either field component up to the distance of $\rho = 0.2a$ from the center. For frequencies such that $ka > 1$ the deviation from uniformity increases quite dramatically and the effect of the resonances of the antenna clearly appears in the 2-norm error in the form of spikes.

1.2. MULTIPLE δ-GAP GENERATORS

1.2.1 Current Calculation

The results of Eqs. 11 and 12 for the current can be generalized for the case when there are two δ-gap sources, located one at $\phi = \phi_o$ and the other at $\phi = 2\pi - \phi_o$, this being the image of the first source with respect to a conducting plane perpendicular to the plane of the antenna. This situation arises in practical systems where large semicircular antennas are erected above conducting grounds. The problem amounts to solving Eq. 7 with $\delta(\phi)$ replaced by $\{\delta(\phi - \phi_o) + \delta(\phi + \phi_o - 2\pi)\}$.

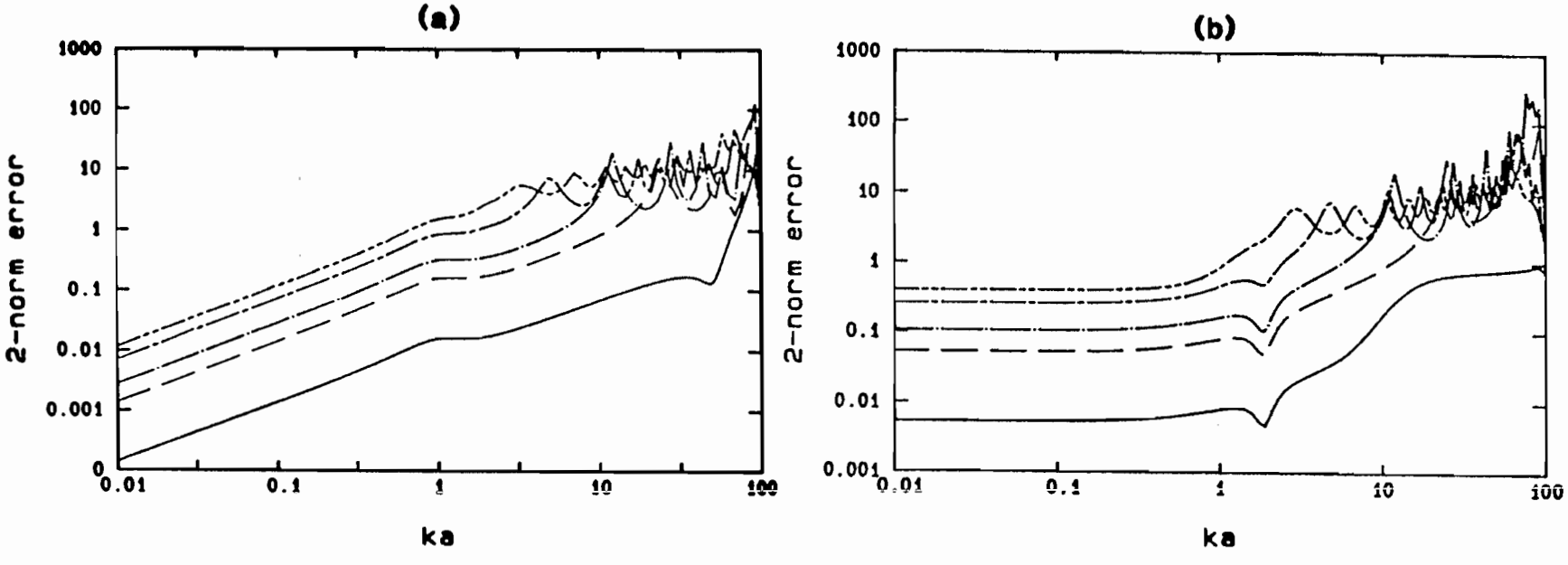

Figure 11. TORUS: Two-norm error calculated according to Eq. 45 (a) B_z; (b) E_y. Source is located at $\phi = 0°$.

———————	ρ/a = 0.01
—— —— ——	ρ/a = 0.1
——— . ———	ρ/a = 0.2
——— — ———	ρ/a = 0.5
—— — — ——	ρ/a = 0.8

$0° < \phi < 360°$

$z/a = 0$

$a/b = 10^3$, $R_0 = \eta_0 \log(a/b)$

Note: Since fields at high frequencies (ka approaching 100) might be affected by error, also 2-norm error must be taken cautiously.

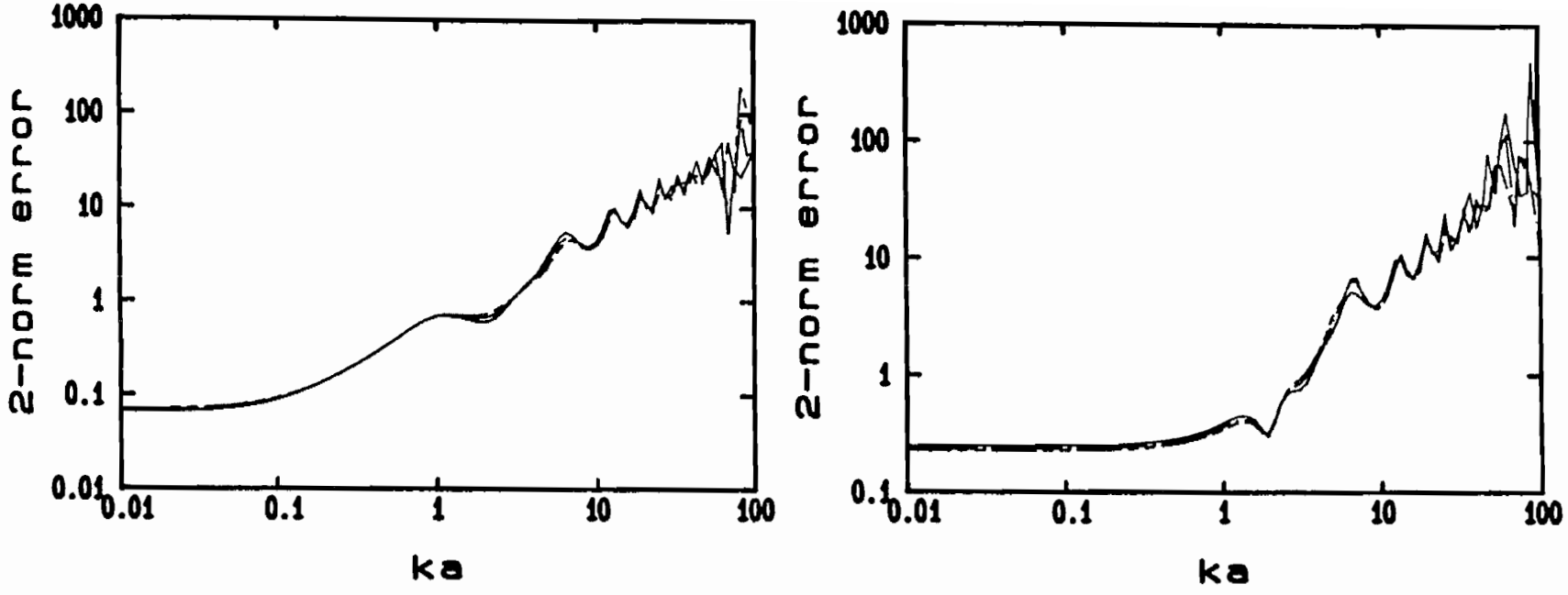

Figure 12. TORUS: Two-norm error calculated according to Eq. 47 (a) B_z; (b) E_y. Source is located at $\phi = 0^\circ$.

———————— y/a = 0.1

———— · ———— y/a = 0.2

———— – – – ———— y/a = 0.25

$-0.5 < x/a < 0.5, z/a = 0$

$a/b = 10^3$, $R_o = \eta_o \log(a/b)$

Note: Since fields at high frequencies (ka approaching 100) might be affected by error, also 2-norm error must be taken cautiously.

The solution for $I_\phi(\phi)$ can be written in the following form, with the symmetry condition $I_\phi(\phi) = I_\phi(2\pi - \phi)$ imposed,

$$I_\phi(\phi) = \begin{cases} C e^{\gamma a(\phi-\phi_0)} + D e^{-\gamma a(\phi-\phi_0)} & (I_1)\quad 0<\phi<\phi_0 \\ F e^{\gamma a(\phi-\phi_0)} + G e^{-\gamma a(\phi-\phi_0)} & (I_2)\quad \phi_0<\phi<\pi \\ C e^{-\gamma a(\phi+\phi_0-2\pi)} + D e^{\gamma a(\phi+\phi_0-2\pi)} & (I_3)\quad 2\pi-\phi_0<\phi<2\pi \\ F e^{-\gamma a(\phi+\phi_0-2\pi)} + G e^{\gamma a(\phi+\phi_0-2\pi)} & (I_4)\quad \pi<\phi<2\pi-\phi_0 \end{cases} \tag{49}$$

with the coefficients C, D, F and G chosen such as to satisfy

$$1)\quad \left.\frac{\partial I_\phi}{\partial \phi}\right|_{\phi=0,\phi=\pi} = 0 \tag{50.a}$$

$$2)\quad I_1 = I_2 \text{ at } \phi = \phi_0 \tag{50.b}$$

$$3)\quad \left.\frac{\partial I_2}{\partial \phi} - \frac{\partial I_1}{\partial \phi}\right|_{\phi=\phi_0} = PV_0 a \tag{50.c}$$

The solution for C, D, F and G is

$$F = \frac{PV_0(1 + e^{2\gamma a\phi_0})}{2\gamma(1 - e^{2\gamma a\pi})} \tag{51}$$

$$D = F\,\frac{1 + e^{2\gamma a(\pi-\phi_0)}}{1 + e^{2\gamma a\phi_0}} \tag{52}$$

$$G = F e^{2\gamma a(\pi-\phi_0)} \tag{53}$$

$$C = D e^{2\gamma a\phi_0} \tag{54}$$

1.2.2 Electromagnetic Fields

As for the fields at the center of the antenna, from the results for a single δ-gap source, the magnetic field $\bar{B}_c$ is found to be 2 times Eq. 25 , because there are two sources with the same strength V_o. Such field is still directed along z. To calculate E_c one must account for the different polarization of the electric field which arises when the source is displaced from the original location at $\phi = 0°$. Such polarization is in the direction perpendicular to the line passing through the center and the source location. As a result, at the center of the antenna the two sources give rise to both E_y components oriented in the same direction ($E_{y,TOT} = 2E_c \cos\phi_o$) and E_x components oriented in opposite directions, thus resulting in a cancellation of the latter. When ϕ_o is equal to 90°, the E_y components are zero. The results were verified by using Eqs.36, through 39 to calculate the fields at the center.

The general expressions of the fields everywhere in space are given by Eqs.36 through 39. The derivatives of the vector potential, as given by Eqs. 40 through 44 can still be used provided the function $I(\phi)$ is given by Eq. 49. In this case the integration $\int_{\phi-2\pi}^{\phi}$ appearing in each of the equations Eqs. 40 through 44 must be performed as follows

$$\int_{\phi-2\pi}^{\phi} I(\phi-\phi')\cdot\cdot\cdot d\phi' = \int_{\phi-\phi_o}^{\phi} I_1(\phi-\phi')\cdot\cdot\cdot d\phi' + \int_{\phi-\pi}^{\phi-\phi_o} I_2(\phi-\phi')\cdot\cdot\cdot d\phi'$$

$$+ \int_{\phi-2\pi}^{\phi_o+\phi-2\pi} I_3(\phi-\phi')\cdot\cdot\cdot d\phi' + \int_{\phi_o+\phi-2\pi}^{\phi-\pi} I_4(\phi-\phi')\cdot\cdot\cdot d\phi' \qquad (55)$$

One change occurs affecting Eq.41. In fact the finite term outside the integral sign becomes

$$\frac{\mu_o}{4\pi} PV_o a^2 \left[\frac{e^{ikC(\phi-\phi_o)}}{C(\phi-\phi_o)} \sin(\phi-\phi_o)\{\cos(\phi-\phi_o)\} + \frac{e^{ikC(\phi-\phi_o)}}{C(\phi+\phi_o)} \sin(\phi+\phi_o)\{\cos(\phi+\phi_o)\} \right] \qquad (56)$$

in place of $\frac{\mu_o}{4\pi} PV_o a^2 \frac{e^{ikC}}{C} \sin\phi\{\cos\phi\}$. It is pointed out that $C(\phi-\phi_o) = \sqrt{a^2+\rho^2-2a\rho\cos(\phi-\phi_o)+z^2}$ and $C(\phi+\phi_o) = \sqrt{a^2+\rho^2-2a\,\rho\cos(\phi+\phi_o)+z^2}$.

Using the above equations the principal components of the electromagnetic fields, E_x and B_z have been computed along the lines $x = 0$ and $x/a = 0.5$ at the heights $y/a = 0.1$, 0.2, and 0.25. The results

are reported in Figs. 13 and 14. By comparing Figs. 13, 14 with Figs. 8, 9 one can see that, at low frequency, B_z is indeed nearly twice as large for the present case than for the single source case. On the other hand the electric field is nearly a factor of 10 lower in the present case because of the close proximity to the conducting ground which makes the tangential E field small.

By using equations similar to Eqs. 34 and 35 except for the different locations and delay factor ct/(a-y) the time domain response to a step function excitation was calculated at x/a = 0, y/a = 0.1, z/a = 0 and is illustrated in Fig. 15. The large peak of the E field is very likely affected by error since the early time results suffer from the difficulty of the asymptotic antenna theory to give correct results at the highest frequencies.

1.2.3 Field Uniformity Error (Two sources: One at $\phi = 90^\circ$ and its image at $\phi = 270^\circ$)

Analogously to what was done for the single source configuration, the 2-norm error was calculated in the case of the double source also, using the same definitions Eqs. 45 through 48 already introduced. It is noted that in this case the principal component of the electric field is E_x while the principal component of the magnetic field is still H_z. The results are reported in Fig. 16 (integration on the circular domain) and in Fig. 17 (integration on the straight line). By comparison of Fig. 11 with Fig. 16 and of Fig. 12 with Fig. 17, one can notice that: 1) the uniformity of the magnetic field improves for the two sources over the single source case. In fact the magnetic fields add up, therefore resulting, by symmetry, in a more uniform distribution along a circumference. Again the uniformity is worse along the straight line than along the circle, for a given distance from the center. 2) the uniformity for the electric field is in general worse. This is due to the fact that now the principal component is E_x, which vanishes along the ground plane. Precisely, each source produces equal and opposite E_x contributions along the ground plane. Therefore the variation of E_x along a circle, for any value of the radius ρ, is much larger than in the case of the single source. This explains why the 2-norm error at the lower values of ρ/a is much higher in this case than in the single source one (compare Fig. 11 to Fig. 16). In addition one must consider that a further cause of error might originate from numerical problems, like round-off errors in the computations. These tend to affect particularly the calculations at the lowest values of ρ when E_x is very small and theoretically vanishing at the ground plane. On the other hand, given a certain distance from the center, unlike for the case of a single source, the uniformity along a straight line is better than that along a circle. (See Fig. 12 and Fig. 17). From what has already been explained one can intuitively understand that the variation of E_x along a circle is more drastic than along a line, since E_x vanishes along the ground plane.

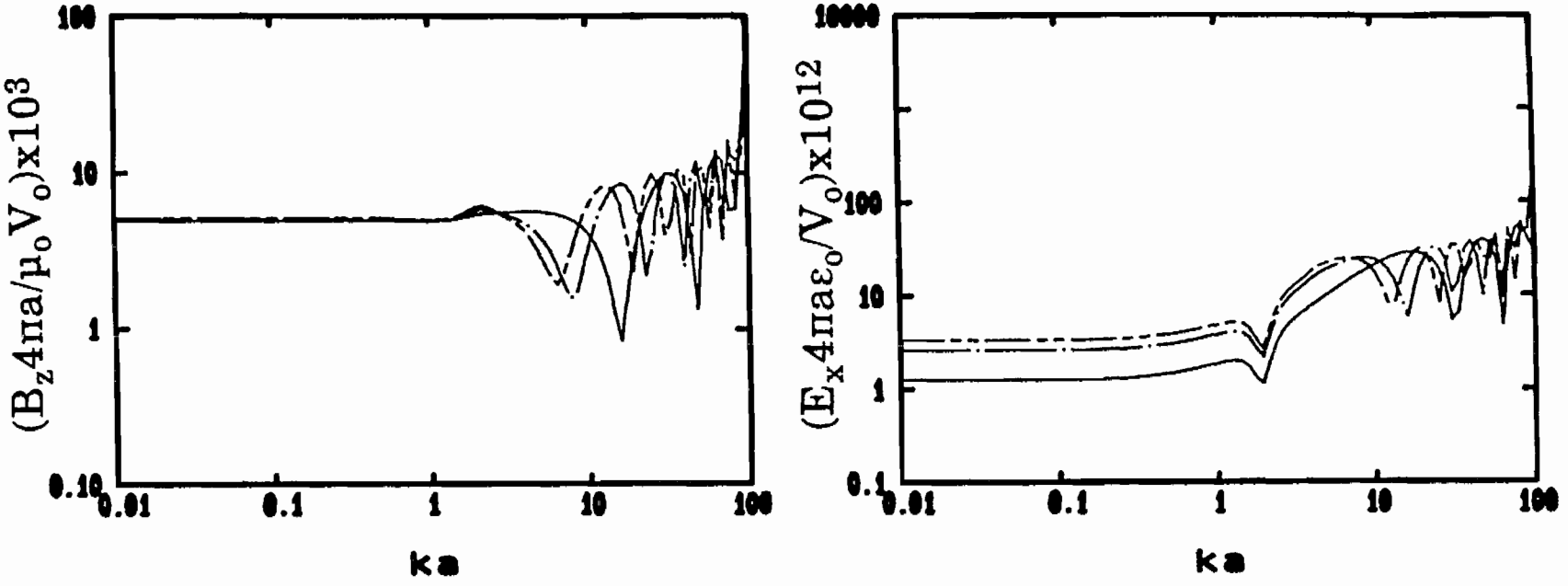

Figure 13. Principal field components of TORUS calculated at x/a = 0, z/a = 0 and

——————— y/a = 0.1

——— · ——— y/a = 0.2 $R_o = \eta_o \log(a/b)$

——— — — ——— y/a = 0.25

Source is at $\phi = 90^\circ$ with image at $\phi = 270^\circ$, a/b = 10^3. Note: Results for ka approaching 100 might be affected by error since the asymptotic antenna theory starts breaking down. Magnetic field has units of Siemens, electric field has units of Farad/meter.

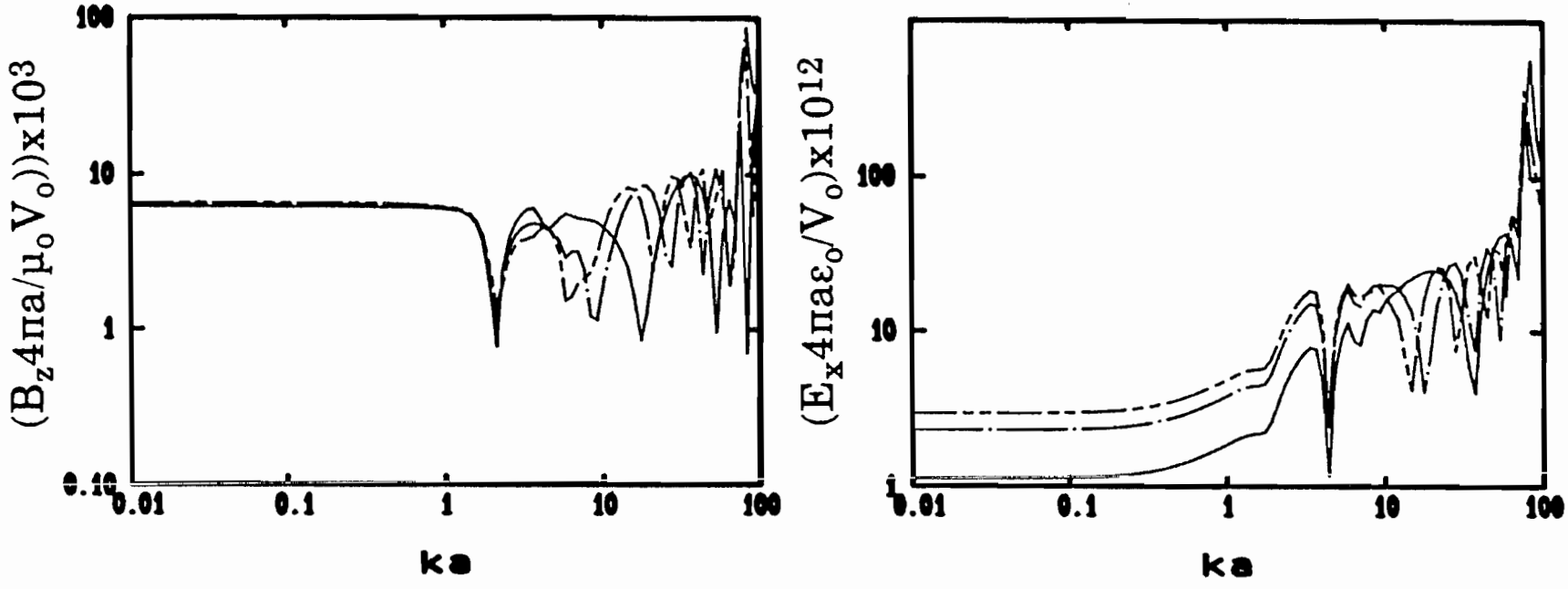

Figure 14. Principal field components of TORUS calculated at x/a = 0.5, z/a = 0 and

_____ y/a = 0.1

_____ . _____ y/a = 0.2 $R_o = \eta_o \log(a/b)$

_____ y/a = 0.25

Source is at $\phi = 90^\circ$ with image at $\phi = 270^\circ$, $a/b = 10^3$. Note: Results for ka approaching 100 might be affected by error since the asymptotic antenna theory starts breaking down. Magnetic field has units of Siemens, electric field has units of Farad/meter.

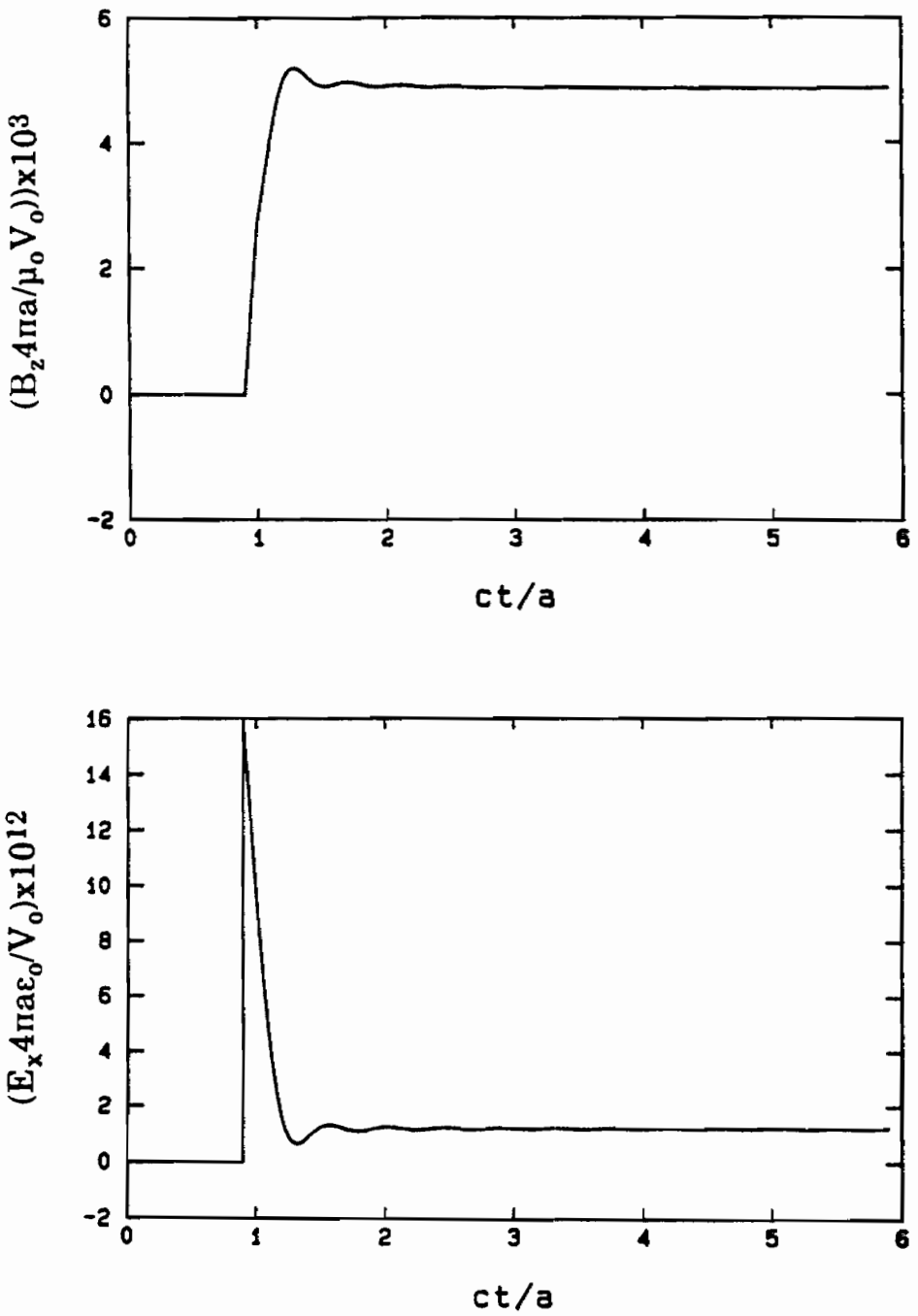

Figure 15. TORUS: Time domain response to step function excitation at $\phi = 90°$ plus image at $\phi = 270°$. Calculation at $x/a = 0$, $y/a = 0.1$, $z/a = 0$, $a/b = 10^3$, $R_o = \eta_o \log(a/b)$. Note: since the results in the frequency domain are good only for ka up to 10^2 (kb→0.1) the time response at $t < 10^{-1}$ (a-y)/c is affected by error. Magnetic field has units of Siemens, electric field has units of Farad/meter.

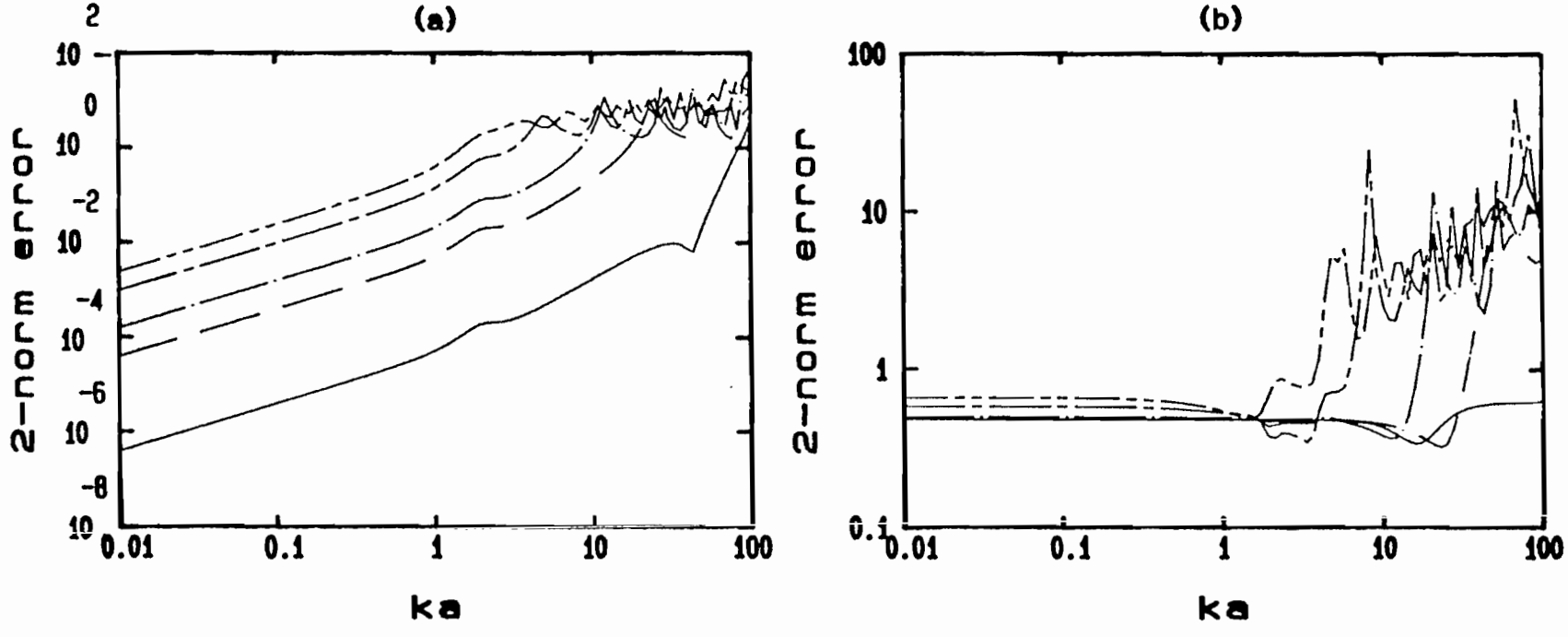

Figure 16. TORUS: Two-norm error calculated according to Eq. 45 (a) B_z; (b) E_x. Source is located at $\phi = 90^\circ$ with image at $\phi = 270^\circ$.

_____	ρ/a = 0.01	
_ _ _ _	ρ/a = 0.1	
_____ . _____	ρ/a = 0.2	$0^\circ < \phi < 360^\circ$
_____ _ _ _____	ρ/a = 0.5	z/a = 0
_____ _ _ _ _____	ρ/a = 0.8	$a/b = 10^3$, $R_0 = \eta_0 \log(a/b)$

Note: Since fields at high frequencies (ka approaching 100) might be affected by error, also 2-norm error must be taken cautiously.

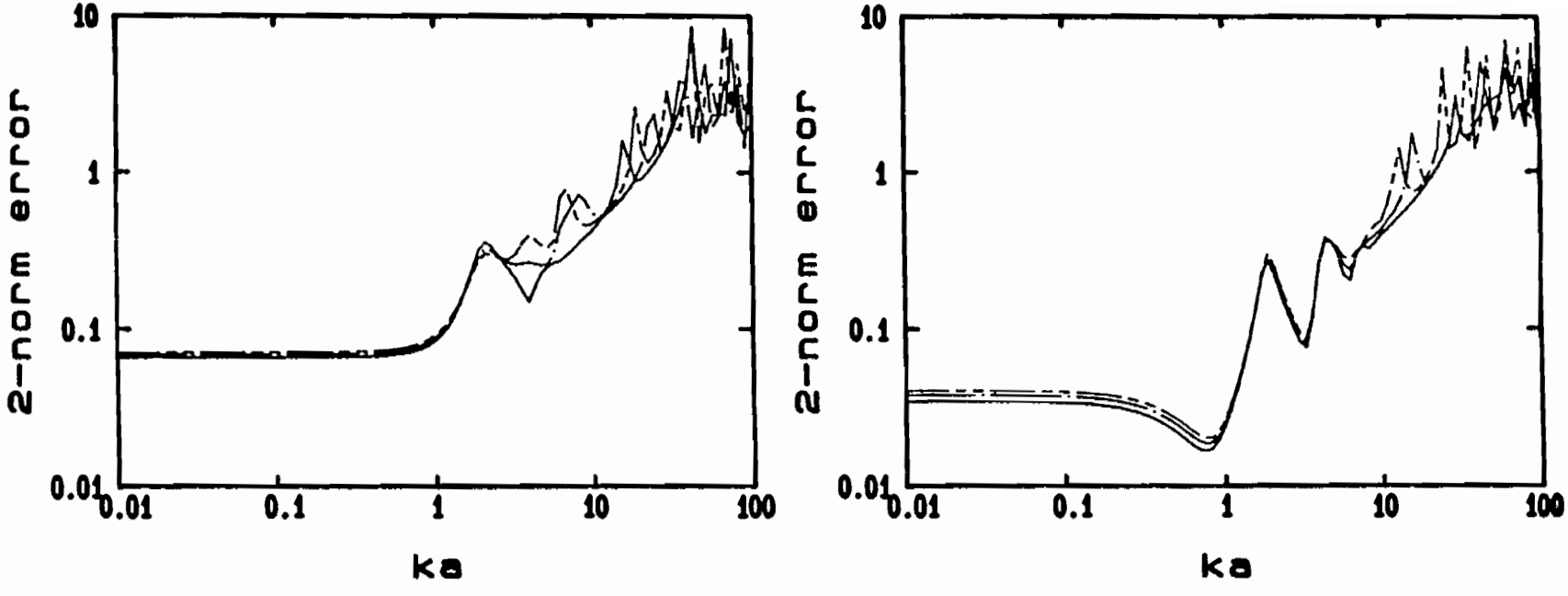

Figure 17. TORUS: Two-norm error calculated according to Eq. 47 (a) B_z; (b) E_y. Source is located at $\phi = 90^\circ$ with image at $\phi = 270^\circ$.

$-0.5 < x/a < 0.5, z/a = 0$

_____ y/a = 0.1

_____ y/a = 0.2

_____ y/a = 0.25

$a/b = 10^3$, $R_o = \eta_o \log(a/b)$

Note: Since fields at high frequencies (ka approaching 100) might be affected by error, also 2-norm error must be taken cautiously.

1.3 DISTRIBUTED SOURCE

So far the discussion has been concerned only with δ-gap generators. In practice, however, such sources do not exist. A realistic source extends over a certain length along the antenna, let's say $(-\zeta_s, +\zeta_s)$ chosen for convenience around the origin. Figure 18 illustrates the distributed source together with the coordinate ζ running along the surface S which is the finite antenna gap, for an infinitely long cylindrical antenna. The choice of the value of ζ_s is related to the physical size of the pulser, or CW source, which are selected according to the overall performances of the system. For an infinitely long cylindrical antenna the distribution of the electric field at the mathematical surface S can be approximated by that associated with a biconical antenna whose angle is such that the conical surface intersects a circular cylinder of radius b at $\pm\zeta_s$, as shown in Fig. 18. Such biconical antenna radiates a spherical wave emanating from its apex. The corresponding electric field tangential to S has been derived in Ref. 8. Assuming that the bicone voltage is a unit step function $V_o u(t)$, then the electric field in the frequency domain turns out to be (Ref. 8)

$$\bar{E}_s(r_s,\omega) = \frac{V_o f_o}{\sqrt{b^2+\zeta^2}} \frac{e^{i\omega\sqrt{b^2+\zeta^2}/c}}{i\omega} \bar{a}_\zeta \tag{57}$$

where both $r_s = \sqrt{b^2+\zeta^2}$ and $\bar{a}_\zeta$ are indicated in Fig. 18 and $f_o = \{2 \ln(\cot(\theta_o/2))\}^{-1}$. Strictly speaking this expression is valid for an infinitely long linear antenna. In the case of a circular antenna the curvature introduces a distortion in the wavefront, which results in a change in the phase of the fields at the surface S with respect to the distribution corresponding to Eq. 57. However, for very large antennas compared to the size of the source section one can, as a first approximation, neglect the effect of the curvature. Therefore one can find the electric field at the origin by integrating Eq. 26 over the source while using, in place of the voltage per unit length, the expression given by Eq. 57. By making again $R_o = \eta_o \ln(a/b) = 2\pi a Z^i$, it is obtained, for the field at the center of the antenna

$$\bar{E}_{c,dis} = -\frac{1}{2}\frac{\eta_o}{R_o}\left|\frac{-ika+1-k^2a^2}{-ika-1+k^2a^2}\right|\frac{e^{ika}}{a}\int_{-\zeta_s}^{\zeta_s}\frac{V_o f_o \cos(\zeta/a)}{\sqrt{b^2+\zeta^2}}\frac{e^{i\omega\sqrt{\zeta^2+b^2}/c}}{i\omega}d\zeta\,\bar{a}_y \tag{58}$$

Similarly for the magnetic field

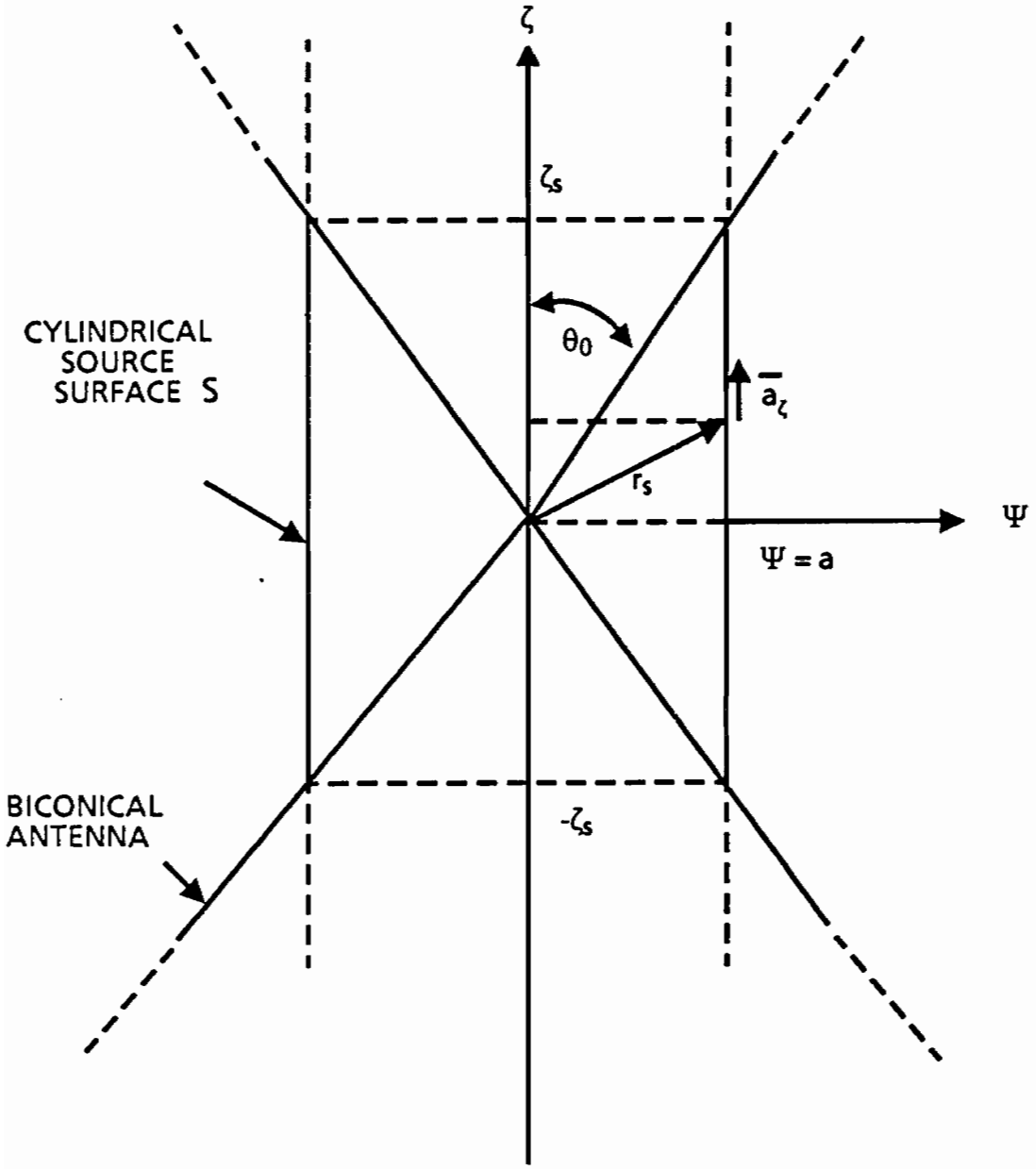

Figure 18. Cylindrical distributed source specified by an infinitely long biconical antenna.

$$\bar{H}_{c,dis} = \frac{1}{2R_o}\left(\frac{1-ika}{1+ika}\right)\frac{e^{ika}}{a}\int_{-\zeta_s}^{\zeta_s}\frac{V_o f_o}{\sqrt{\zeta^2+b^2}}\frac{e^{i\omega\sqrt{\zeta^2+b^2}/c}}{i\omega}d\zeta\ \bar{a}_z \tag{59}$$

Therefore the ratio of E over $\eta_0 H$ becomes

$$\Lambda^o_{dis} = \frac{E_{c,dis}}{\eta_0 H_{c,dis}} = \left[\frac{ika-1+k^2a^2}{-ika-1+k^2a^2}\right] x$$

$$\left[\frac{ika+1}{-ika+1}\right]\frac{\int_{-\zeta_s}^{\zeta_s}\frac{V_o f_o \cos(\zeta/a)}{\sqrt{\zeta^2+b^2}}\frac{e^{i\omega\sqrt{\zeta^2+b^2}}}{i\omega}d\zeta}{\int_{-\zeta_s}^{\zeta_s}\frac{V_o f_o}{\sqrt{\zeta^2+b^2}}\frac{e^{i\omega\sqrt{\zeta^2+b^2}/c}}{i\omega}d\zeta} \tag{60}$$

At low frequency, i.e. $\omega\rightarrow 0$, Eq. 60 can be evaluated analytically. The result is

$$\Lambda^o_{dis} = 1 + \frac{b^2}{4a^2} - \frac{\zeta_s}{4a^2}\sqrt{\zeta_s^2+b^2}\,/\ln\left[\frac{\zeta_s+\sqrt{\zeta_s^2+b^2}}{b}\right] \tag{61}$$

Equation 61 provides the expression for the dependence of Λ^o_{dis} on the extent of the source relative to the radius of the antenna. Figure 19 illustrates Λ^o_{dis} at low frequency as a function of ζ_s/a, while b/a is being used as a parameter. Figure 20 shows Λ^o_{dis} as a function of ka for different values of ζ_s/a. In this calculation b/a was assumed equal to 10^{-3}. It is pointed out that the variation is contained within a few percent of the value Λ^o calculated for the δ-gap generator.

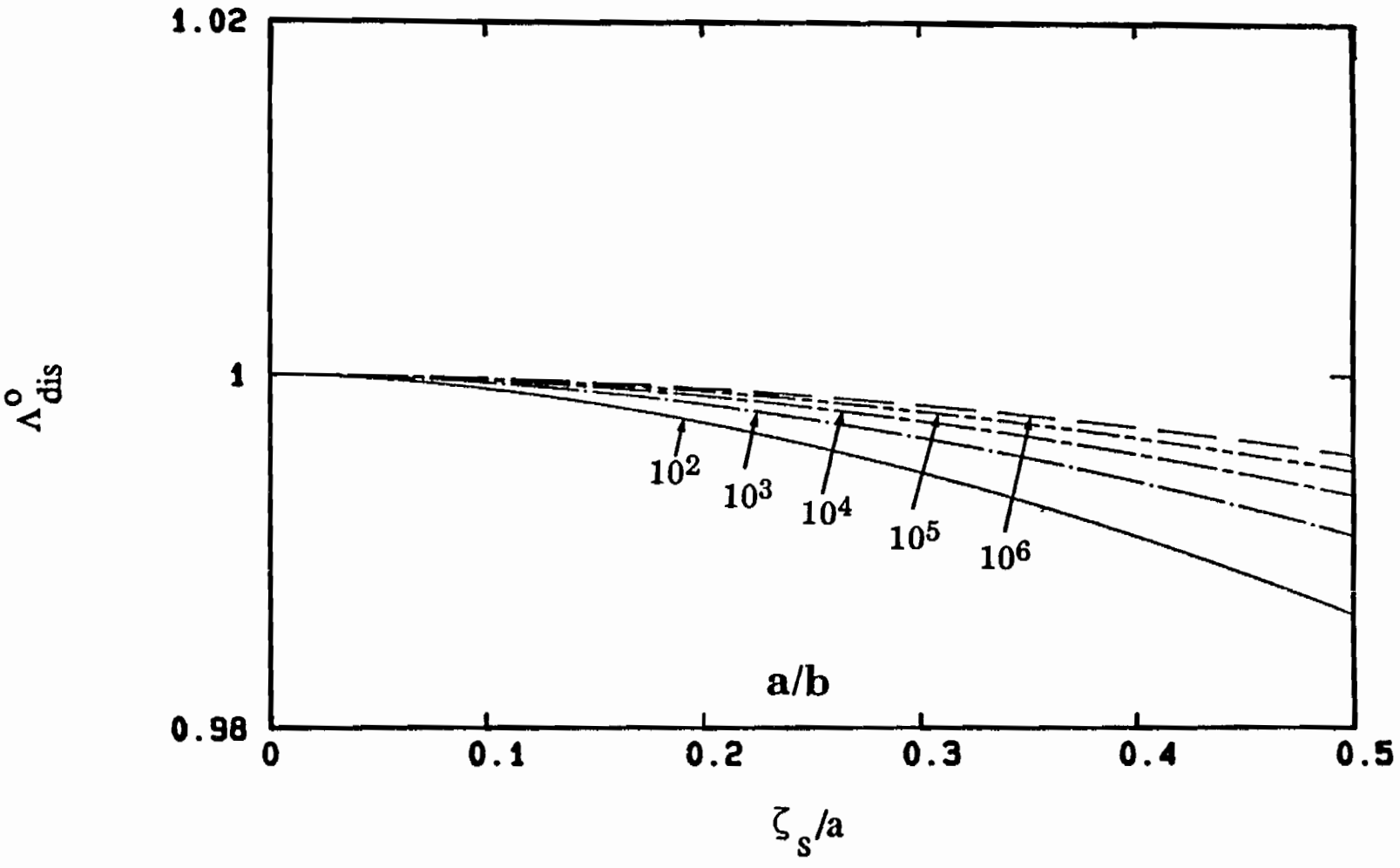

Figure 19. Λ^o_{dis} at low frequency.

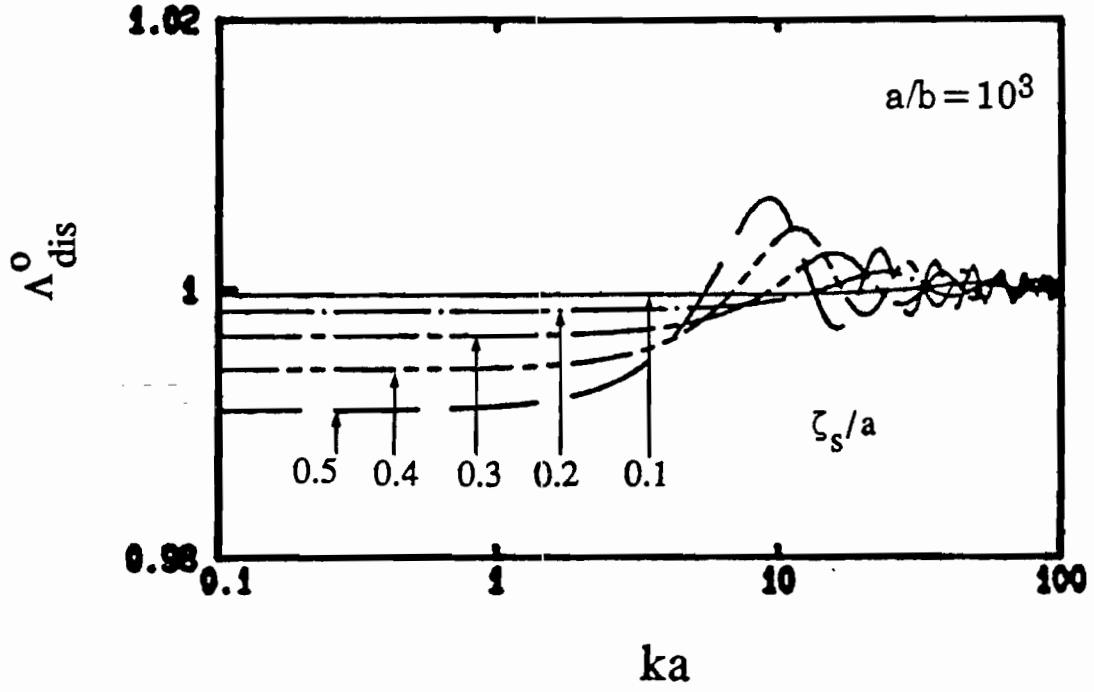

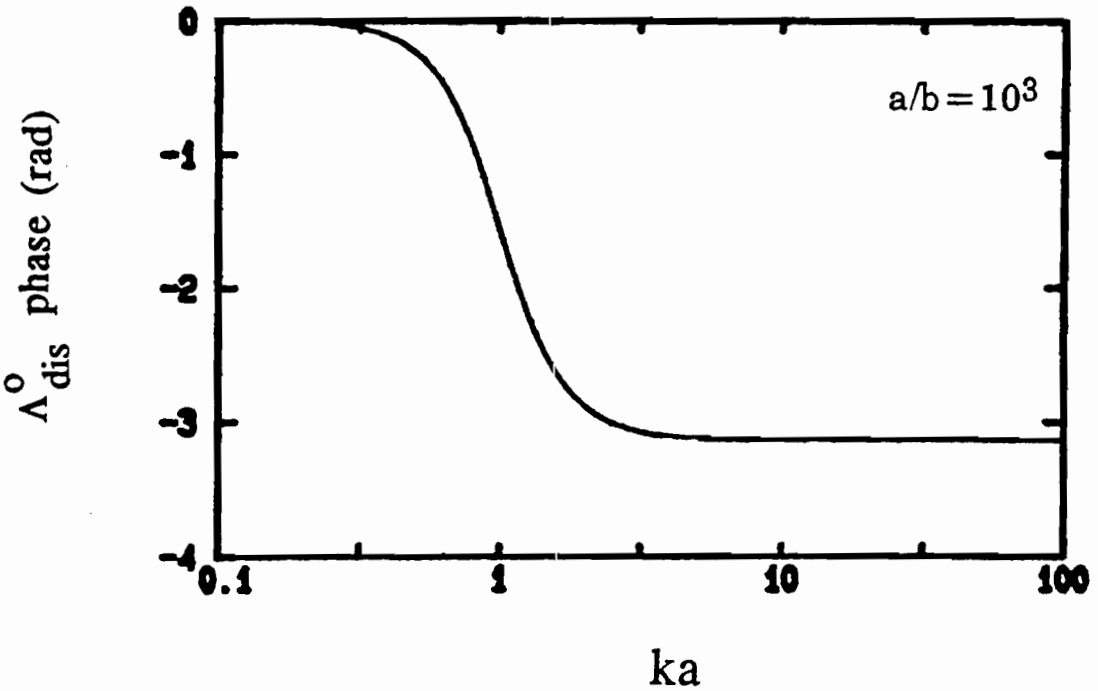

Figure 20. Λ^o_{dis} as a function of frequency with a/b = 10^3.

2.0 PART II: THIN ELLIPTICAL ANTENNA

2.1 SINGLE δ-GAP GENERATOR

2.1.1 Description

Consider an antenna of elliptical geometry, fed at one point with a δ-gap generator. By analogy with the noun "TORUS", this antenna is referred to as "ELLIPTICUS." Figure 21 illustrates the geometry of the system and the elliptical coordinate system used to analyze the problem. The antenna is located at $\xi = \xi_0$ and the δ-gap generator is at $v = 0^o$. The transformation between elliptical and Cartesian coordinates is given by

$$x = d\xi \cos v \qquad y = d\sqrt{\xi^2 - 1}\ \sin v \qquad z = z \tag{62}$$

The semi axes of the ELLIPTICUS are thus deduced to be

$$a = d\xi_0 \qquad a' = d\sqrt{\xi_0^2 - 1} \tag{63}$$

where $(\pm d, 0)$ are the locations of the foci.

Please note that in Part II of this note we indicate with a the major semiaxis of the ellipse, while in Part I a has a different meaning. The reciprocal of ξ_0 is also called eccentricity. From Fig. 21 it is seen that the unit vectors are indicated with $\bar{a}_\xi$, normal to the elliptical cylinders ξ = const, $\bar{a}_v$, normal to the hyperbolae v = const, and $\bar{a}_z$, normal to the planes z = const. The relationships between $\bar{a}_\xi$, $\bar{a}_v$ and $\bar{a}_x$ and $\bar{a}_y$ were found to be the following

$$\begin{aligned} \bar{a}_\xi &= \bar{a}_x \frac{\sqrt{\xi^2 - 1}\cos v}{\sqrt{\xi^2 - \cos^2 v}} + \bar{a}_y \frac{\xi \sin v}{\sqrt{\xi^2 - \cos^2 v}} \\ \bar{a}_v &= \bar{a}_x \frac{-\xi \sin v}{\sqrt{\xi^2 - \cos^2 v}} + \bar{a}_y \frac{\sqrt{\xi^2 - 1}\cos v}{\sqrt{\xi^2 - \cos^2 v}} \end{aligned} \tag{64}$$

and, conversely,

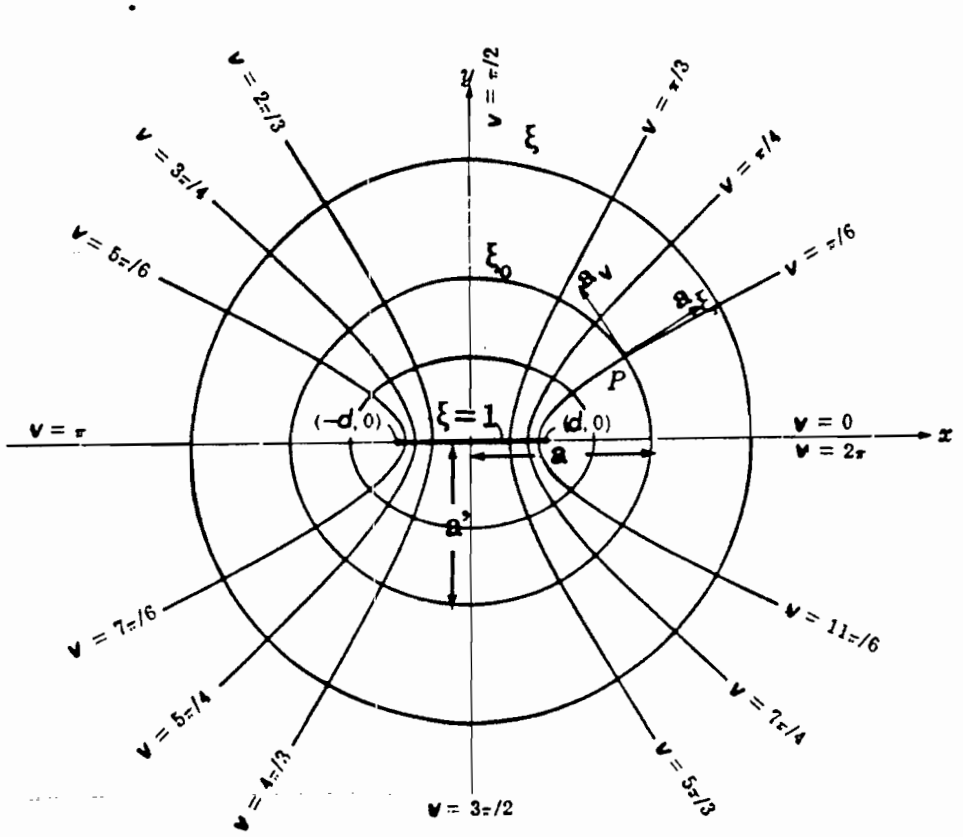

Figure 21. ELIPTICUS geometry showing elliptical coordinate system, a - major semiaxis, a' - minor semiaxis,

$\xi_0 = 1/\sqrt{[1 - (a'/a)^2]}$

$$\bar{a}_x = \bar{a}_\xi \frac{\sqrt{\xi^2-1}\cos v}{\sqrt{\xi^2-\cos^2 v}} + \bar{a}_v \frac{-\xi \sin v}{\sqrt{\xi^2-\cos^2 v}}$$

$$\bar{a}_y = \bar{a}_\xi \frac{\xi \sin v}{\sqrt{\xi^2-\cos^2 v}} + \bar{a}_v \frac{\sqrt{\xi^2-1}\cos v}{\sqrt{\xi^2-\cos^2 v}} \qquad (65)$$

The length of an arc of ellipse s(v) is given by

$$s(v) = a \int_0^v \sqrt{1 - \frac{\cos^2 v'}{\xi_0^2}}\, dv' \qquad (66)$$

where the integral is referred to as the elliptic integral of the second kind, and is indicated with $E(v, 1/\xi_0)$. The total perimeter of the ellipse is given by $s_u = 4aE(\pi/2, 1/\xi_0)$.

2.1.2 Current Calculation

To calculate the current flowing along a thin elliptical antenna one can apply the same line of reasoning as for the case of the thin TORUS. However, in this case one must work with the elliptic coordinates, which introduce some complication in the calculations. To simplify the problem we assumed that the current of a thin elliptical antenna and that of a thin toroidal antenna of the same total length, i.e. $s_0 = 4a\, E(\pi/2, 1/\xi_0) = 2\pi a_{eq}$ are the same, provided a correspondence is established between the position along the equivalent TORUS, $a_{eq}\phi$, and that along the ellipse, s(v), namely $s(v) = a_{eq}\phi$. Therefore, within this approximation, the current is then given by:

$$I_v(v) = A' e^{\gamma s(v)} + B' e^{-\gamma s(v)} \qquad (67)$$

where

$$A' = \frac{PV_0}{2\gamma(1-e^{\gamma s_0})} \quad , \quad B' = \frac{-PV_0}{2\gamma(1-e^{\gamma s_0})} \qquad (68)$$

$$\gamma/\gamma_0 = \sqrt[4]{1+\left(\frac{2\pi R_0}{s_0 k \eta_0 \ln(kb)}\right)^2} \times \exp\left\{i\,\frac{1}{2}\arctan\left[\frac{2\pi R_0}{s_0 k \eta_0 \ln(kb)}\right]\right\} \qquad (69)$$

Such a current is directed in the v direction, i.e. longitudinal to the antenna wire.

Equations 67 and 68 are very similar to Eqs. 11 and 12 of Part I. On the other hand Eq. 69 is more general than Eq. 13 of Part I because here the loading resistance $R_o = s_o Z^i$ is not yet specified. In fact, in this case the choice $Z_o^i = \eta_o \ln(s_o/2\pi b)$ for the value of the loading resistance might not be the proper value in order to impose $E/H = \eta_o$ at the center of the antenna. The discussion on the selection of the loading resistance as a function of the geometry of the ELLIPTICUS is postponed to Section 2.1.5. Furthermore, it is noted that in Eq. 69 the quantity $s_o/2\pi$, which is the "equivalent radius" of a circle whose circumference is equal to the perimeter s_o of the ellipse, is used in place of a of Eq. 13.

Once the current is known, one can go through the same process illustrated in Part I to find the vector potential and the electromagnetic fields everywhere. In doing so the elliptical coordinate system must be used and the calculations become more cumbersome. The following sections illustrate the results obtained for this case.

2.1.3 Electromagnetic Fields Calculation

The vector potential A can be calculated from the knowledge of the current $I_v(v)$, using the free-space Green's function $e^{ikD}/(4\pi D)$ where

$$D = \sqrt{d^2[\xi^2 + \xi_o^2 - \sin^2 v - \sin^2 v' - 2\xi\xi_o \cos v \cos v' - 2\sqrt{(\xi^2-1)(\xi_o^2-1)}\sin v \sin v'] + z^2} \qquad (70)$$

It was found

$$A_\xi(\xi, v, z) = \frac{\mu_o}{4\pi}\int_0^{2\pi} I_v(v')\frac{e^{ikD}}{D}\frac{d[-\sin v'\cos v\,\xi_o^2\sqrt{\xi^2-1} + \cos v'\sin v\,\xi\sqrt{\xi_o^2-1}]}{\sqrt{\xi^2-\cos^2 v}}dv' \qquad (71)$$

$$A_v(\xi, v, z) = \frac{\mu_o}{4\pi}\int_0^{2\pi} I_v(v')\frac{e^{ikD}}{D}\frac{d[\xi\xi_o \sin v' \sin v + \sqrt{\xi^2-1}\,\sqrt{\xi_o^2-1}\cos v'\cos v]}{\sqrt{\xi^2-\cos^2 v}}dv' \qquad (72)$$

where ξ_o and the prime (') coordinates for v indicate the source point.

From Maxwell's equations the electromagnetic fields in the elliptic coordinate system are written as

$$\bar{B} = \nabla \times \bar{A} = B_\xi \bar{a}_\xi + B_v \bar{a}_v + B_z \bar{a}_z \qquad (73)$$

$$B_\xi = -\frac{\partial A_v}{\partial z} \tag{74}$$

$$B_v = \frac{\partial A_\xi}{\partial z} \tag{75}$$

$$B_z = \frac{1}{d\sqrt{\xi^2-\cos^2 v}}\left[\sqrt{\xi^2-1}\left(\frac{\partial A_v}{\partial \xi} + \frac{\xi}{\xi^2-\cos^2 v}A_v\right) - \frac{\partial A_\xi}{\partial v} - \frac{\cos v \sin v}{\xi^2-\cos^2 v}A_\xi\right] \tag{76}$$

and

$$\nabla \times \nabla \times \bar{A} = \left[E_\xi \bar{a}_\xi + E_v \bar{a}_v + E_z \bar{a}_z\right]\frac{-i\omega}{c^2} \tag{77}$$

$$E_\xi = \left\{\frac{1}{d\sqrt{\xi^2-\cos^2 v}}\left[\frac{-\cos v \sin v}{d(\xi^2-\cos^2 v)^{3/2}}\left(\sqrt{\xi^2-1}\,\frac{\partial A_v}{\partial \xi} - \frac{\partial A_\xi}{\partial v} + \frac{3\sqrt{\xi^2-1}\,\xi A_v}{\xi^2-\cos^2 v} - \frac{3\sin v \cos v\, A_\xi}{\xi^2-\cos^2 v}\right)\right.\right.$$

$$+\frac{1}{d\sqrt{\xi^2-\cos^2 v}}\left(\sqrt{\xi^2-1}\,\frac{\partial^2 A_v}{\partial \xi \partial v} - \frac{\partial^2 A_\xi}{\partial v^2} + \frac{\sqrt{\xi^2-1}\,\xi}{\xi^2-\cos^2 v}\,\frac{\partial A_v}{\partial v} - \frac{(\cos^2 v - \sin^2 v)A_\xi}{\xi^2-\cos^2 v}\right.$$

$$\left.\left.\left.-\frac{\sin v \cos v}{\xi^2-\cos^2 v}\,\frac{\partial A_\xi}{\partial v}\right)\right] - \frac{\partial^2 A_\xi}{\partial^2 z}\right\}\frac{ic^2}{\omega} \tag{78}$$

$$E_v = \left\{-\frac{\sqrt{\xi^2-1}}{d\sqrt{\xi^2-\cos^2 v}}\left[-\frac{\xi}{d(\xi^2-\cos^2 v)^{3/2}}\left(-\frac{\partial A_\xi}{\partial v} + \frac{3\sqrt{\xi^2-1}\,\xi A_v}{\xi^2-\cos^2 v} - \frac{3\sin v \cos v\, A_\xi}{\xi^2-\cos^2 v}\right)\right.\right.$$

$$+\frac{1}{d(\xi^2-\cos^2 v)}\left(\frac{\xi}{\sqrt{\xi^2-1}}\,\frac{\partial A_v}{\partial \xi} + \sqrt{\xi^2-1}\,\frac{\partial^2 A_v}{\partial \xi^2} - \frac{\partial^2 A_\xi}{\partial v \partial \xi} + \frac{\sqrt{\xi^2-1}\,A_v}{\xi^2-\cos^2 v}\right.$$

$$\left.\left.\left.+\frac{\xi^2 A_v}{\sqrt{\xi^2-1}\,(\xi^2-\cos^2 v)} - \frac{\sin v \cos v}{\xi^2-\cos^2 v}\,\frac{\partial A_\xi}{\partial \xi}\right)\right] - \frac{\partial^2 A_v}{\partial z^2}\right\}\frac{ic^2}{\omega} \tag{79}$$

$$E_z = \frac{\sqrt{\xi^2-1}}{d\sqrt{(\xi^2-\cos^2 v)}} \frac{ic^2}{\omega}$$

$$x\left[\frac{\xi}{\xi^2-\cos^2 v}\frac{\partial A_\xi}{\partial z} + \frac{\partial^2 A_\xi}{\partial z \partial \xi} + \frac{\sin v \cos v}{\sqrt{\xi^2-1}\sqrt{\xi^2-\cos^2 v}}\frac{\partial A_v}{\partial z} + \frac{\sqrt{\xi^2-\cos^2 v}}{\sqrt{\xi^2-1}}\frac{\partial^2 A_v}{\partial z \partial v}\right] \tag{80}$$

The derivatives of A_ξ and A_v appearing in Eqs. 83 through 86 were calculated to be

$$\frac{\partial A_\xi}{\partial v}\left\{\frac{\partial A_v}{\partial v}\right\} = \frac{\mu_o}{4\pi}\int_0^{2\pi} I_v(v')\frac{e^{ikD}}{D}\frac{X\sin v + Y\cos v}{\sqrt{\xi^2-\cos^2 v}} G\, dv' \tag{81}$$

with

$$G = d^2(-\delta\xi \sin v + \beta\sqrt{\xi^2-1}\cos v)(ik - \frac{1}{D}) + \frac{X\cos v - Y\sin v}{X\sin v + Y\cos v} - \frac{\cos v \sin v}{\xi^2-\cos^2 v} \tag{82}$$

$$\delta = \xi\cos v - \xi_o \cos v' \qquad \beta = \sqrt{\xi^2-1}\sin v - \sqrt{\xi_o^2-1}\sin v' \tag{83}$$

$$X = d\sqrt{\xi_o^2-1}\,\xi\cos v' \quad \{d\xi\xi_o \sin v'\} \tag{84}$$

$$Y = -d\sqrt{\xi^2-1}\,\xi_o \sin v \quad \{d\sqrt{\xi^2-1}\sqrt{\xi_o^2-1}\sin v'\} \tag{85}$$

Again one can switch from one derivative of A_ξ to the correspondent derivative of A_v by substituting the proper expressions appearing within braces.

$$\frac{\partial A_\xi}{\partial \xi}\left\{\frac{\partial A_v}{\partial \xi}\right\} = \frac{\mu_o}{4\pi}\int_o^{2\pi} I_v(v')\frac{ikD}{D}\frac{X'\xi + Y'\sqrt{\xi^2-1}}{\sqrt{\xi^2-\cos^2 v}} F\, dv' \tag{86}$$

with

$$F = \frac{d^2(\delta\cos v + \beta(\xi/\sqrt{\xi^2-1})\sin v)}{D}(ik - \frac{1}{D}) - \frac{\xi}{\xi^2-\cos^2 v} + \frac{X' + Y'\xi/\sqrt{\xi^2-1}}{X'\xi + Y'\sqrt{\xi^2-1}} \tag{87}$$

$$X' = d\sqrt{\xi_o^2-1}\cos v' \sin v \quad \{d\,\xi_o \sin v' \sin v\} \tag{88}$$

$$Y' = -d\ \xi_o\ \sin v' \cos v \qquad \{d\sqrt{\xi_o^2 - 1}\ \cos v' \cos v\} \tag{89}$$

It is noted that $X \sin v + Y \cos v = X'\xi + Y'\sqrt{\xi^2 - 1}$.

$$\frac{\partial^2 A_\xi}{\partial \xi \partial v}\ \left\{\frac{\partial^2 A_v}{\partial \xi \partial v}\right\} = \frac{\mu_o}{4\pi} \int_0^{2\pi} I_v(v') \frac{e^{ikD}}{D} \frac{(X \sin v + Y \cos v)}{\sqrt{\xi^2 - \cos^2 v}} \left[\frac{\partial F}{\partial v} + FG\right] dv' \tag{90}$$

with

$$\frac{\partial^2 F}{\partial \xi \partial v} = \left\{ d^2 \frac{[-\delta \sin v + \beta(\xi/\sqrt{\xi^2 - 1})\cos v]}{D} \right.$$

$$\left. - \frac{d^4 [\delta \cos v + \beta(\xi/\sqrt{\xi^2 - 1})\sin v][-\delta \xi \sin v + \beta\sqrt{\xi^2 - 1}\cos v]}{D^3} \right\} x \left(ik - \frac{1}{D}\right)$$

$$+ \frac{2\xi \cos v \sin v}{(\xi^2 - \cos^2 v)^2} + \frac{[X \cos v/\xi - Y(\xi/(\xi^2 - 1)\sin v)]}{X \sin v + Y \cos v}$$

$$+ d^4 \frac{[(\delta \cos v + \beta(\xi/\sqrt{\xi^2 - 1})\sin v)][(-\delta\xi \sin v + \beta\sqrt{\xi^2 - 1}\cos v)]}{D^4}$$

$$- \frac{[X \sin v/\xi + Y(\xi/(\xi^2 - 1))\cos v][X \cos v - Y \sin v]}{[X \sin v + Y \cos v]^2} \tag{91}$$

$$\frac{\partial^2 A_v}{\partial \xi^2} = \frac{\eta_o}{4\pi} \cdot \int_0^{2\pi} I(v)' \frac{e^{ikD}}{D} \frac{X'\xi + Y'\sqrt{\xi^2 - 1}}{\sqrt{\xi^2 - \cos^2 v}} (F^2 + \frac{\partial F}{\partial \xi})\ dv'$$

with

$$\frac{\partial F}{\partial \xi} = d^2 \left| \frac{1 - \sqrt{\xi_o^2 - 1}\ \sin v' \sin v\,[-\xi^2/(\xi^2-1) + 1]/\sqrt{\xi^2-1}}{D} \right| (ik - \frac{1}{D})$$

$$+ \frac{d^4 [\delta \cos v + \beta(\xi/\sqrt{\xi^2-1}\ ) \sin v]^2}{D^3} \times \left(\frac{2}{D} - ik \right)$$

$$+ \frac{\xi^2 + \cos^2 v}{(\xi^2 - \cos^2 v)^2} - \frac{[X'Y'\xi/\sqrt{\xi^2-1}\ (2\xi^2-1) - X'^2(\xi^2-1) - Y'^2(\xi^2+1)]\sqrt{(\xi^2-1)}}{(X'\xi + Y'\sqrt{\xi^2-1}\ )^2} \qquad (92)$$

$$\frac{\partial^2 A_\xi}{\partial v^2} = \frac{\mu_o}{4\pi} \int_0^{2\pi} I(v') \frac{e^{ikD}}{D} \frac{X \sin v + Y \cos v}{\sqrt{\xi^2 - \cos^2 v}} \left\{ G^2 + (\delta\xi \sin v + \beta\sqrt{\xi^2-1}\ \cos v)^2 \frac{d^4}{D^3} \right.$$

$$\times (ik + \frac{2}{D}) + \frac{(-\delta\xi \cos v + \beta\sqrt{\xi^2-1}\ \sin v + \xi^2 - \cos^2 v)^2}{D} d^2 (ik - \frac{1}{D})$$

$$\left. - \frac{(X \cos v - Y \sin v)^2}{(X \sin v + Y \cos v)^2} - 1 - \frac{\cos^2 v - \sin^2 v}{\xi^2 - \cos^2 v} - \frac{2 \cos^2 v \sin^2 v}{(\xi^2 - \cos^2 v)^2} \right\} dv' \qquad (93)$$

$$\frac{\partial A_\xi}{\partial z} \left\{ \frac{\partial A_v}{\partial z} \right\} = \frac{\mu_o}{4\pi} \int_o^{2\pi} I_v(v') \times \frac{X'\xi + Y'\sqrt{\xi^2-1}}{\sqrt{\xi^2 \cos^2 v}} \frac{e^{ikD}}{D} H\, dv' \qquad (94)$$

with

$$H = \frac{z}{D}(ik - \frac{1}{D}) \qquad (95)$$

$$\frac{\partial^2 A_\xi}{\partial z^2} \left\{ \frac{\partial^2 A_v}{\partial z^2} \right\} = \frac{\mu_o}{4\pi} \int_0^{2\pi} I_v(v') \frac{e^{ikD}}{D} \frac{X'\xi + Y'\sqrt{\xi^2-1}}{\sqrt{\xi^2 - \cos^2 v}} (H^2 + \frac{\partial H}{\partial z})\, dv' \qquad (96)$$

with

$$\frac{\partial H}{\partial z} = \frac{ik}{D}(1 - \frac{z^2}{D^2}) - \frac{D^2 - 2z^2}{D^4} \qquad (97)$$

$$\frac{\partial^2 A_\xi}{\partial\xi\partial z}\left\{\frac{\partial^2 A_v}{\partial\xi\partial z}\right\} = \frac{\mu_0}{4\pi}\int_0^{2\pi} I_v(v')\frac{e^{ikD}}{D}\,x\,\frac{X'\xi + Y'\sqrt{\xi^2-1}}{\sqrt{\xi^2-\cos^2 v}}\left(F\,H + \frac{\partial H}{\partial\xi}\right)dv' \tag{98}$$

with

$$\frac{\partial H}{\partial\xi} = \frac{d^2 z}{D^3}(\delta\cos v + \beta(\xi/\sqrt{\xi^2-1})\sin v)(-ik + \frac{2}{D}) \tag{99}$$

$$\frac{\partial^2 A_\xi}{\partial\xi\partial z}\left\{\frac{\partial^2 A_v}{\partial\xi\partial z}\right\} = \frac{\mu_0}{4\pi}\int_0^{2\pi} I_v(v')\frac{e^{ikD}}{D}\,\frac{X\sin v + Y\cos v}{\sqrt{\xi^2-\cos^2 v}}\left\{FH + \right.$$

$$\left.\frac{d^2 z}{D^3}(\delta\cos v + \beta(\xi/\sqrt{\xi^2-1})\sin v\,(-ik + \frac{2}{D})\right\}dv' \tag{100}$$

2.1.4 Determination Of The Loading Resistance

When designing an EMP illuminator one is interested in obtaining incident fields with certain specified characteristics in some region of space. Typically it is desired to have the ratio E/H at the center of the antenna equal to the free space intrinsic impedance, i.e. 377 Ω, so that the incident field has locally the characteristics of a plane wave, in the broadest possible frequency range of interest. This is to simulate the realistic condition of threat for a test object located on the ground. In the case of the thin circular geometry such property was established at low frequency by choosing a proper uniform loading resistance, as derived in Ref. 1. Unlike for the circular geometry, in the case of the thin elliptical geometry, the value of the uniform loading resistance which makes E/H = 377 at the center is dependent upon the location of the δ-gap generator, because the location of the source on the ellipse is not symmetric with respect to its center. In the following we discuss how we determined the loading resistance for the case of (a) a δ-gap generator at $v = 0^0$ such that $E_y/H_z = 377$ at the center and (b) a δ-gap generator at $v = 90^0$ such that $E_x/H_z = 377$ at the center, at low frequency. It is stressed that any choice of the loading resistance will approximately give such field ratio at high frequency because of the local plane wave behavior of the radiated (far-zone) fields of any source.

Using the above equations the electromagnetic fields were determined at the center of the ELLIPTICUS ($\xi = 1$, $v = \pi/2$) in the low frequency limit. From Eq. 6, when $\gamma \to 0$, by performing a Taylor series expansion and retaining terms up to the γ^2 power, it was obtained

$$I(v) = -\frac{PV_o}{2s_o}\left[s^2(v) - s(v)\,s_o + \frac{s_o^2}{6}\right] \tag{101}$$

In this limit the magnetic field at the center was calculated to be

$$H_z = \frac{1}{\pi d}\,\frac{V_o}{R_o}\,\frac{1}{\sqrt{\xi_o^2 - 1}}\,E(\pi/2;\, 1/\xi_o) \tag{102}$$

where the yet unknown loading resistance R_o appears in the denominator. This value is independent of the location of the source. The low frequency electric field component was obtained as

$$E_y = T_o \times Int_1 = T_o \int_0^{2\pi} \frac{\sqrt{\xi_o^2 - 1}\,\cos v'}{\sqrt{\xi_o^2 - \sin^2 v'}}\left(\frac{3\xi_o^2}{(\xi_o^2 - \sin^2 v')^2} - \frac{2}{\xi_o^2 - \sin^2 v'}\right)(s^2(v') - s(v')s_o)\,dv' \tag{103}$$

corresponding to the source located at $v = 0^o$ and

$$E_x = T_o \times Int_2 = T_o \int_{\pi/2}^{5\pi/2} \frac{\xi_o \sin v'}{\sqrt{\xi_o^2 - \sin^2 v'}}\left(\frac{3(\xi_o^2 - 1)}{(\xi_o^2 - \sin^2 v')^2} - \frac{2}{\xi_o^2 - \sin^2 v'}\right)[s(v')^2 - 3/2\,s(v')s_o + 5/16\,s_o^2]dv' \tag{104}$$

for the case when the source is located at $v = 90^o$. In both cases

$$T_o = \frac{V_o}{4\,\ln(s_o/2\pi b)d^2 s_o} \tag{105}$$

By imposing $E_y/H_z = \eta_o$ or $E_x/H_z = \eta_o$ one can solve for R_o obtaining

$$R_o = \frac{4\,\eta_o \ln(s_o/2\pi b)\,ds_o E(\pi/2,\, 1/\xi_o)}{Int_1\,\pi\,\sqrt{\xi_o^2 - 1}} \tag{106}$$

or

$$R_0 = \frac{4\,\eta_0 \ln(s_0/2\pi b)\, ds_0\, E(\pi/2,\, 1/\xi_0)}{Int_2 \text{ or } \sqrt{\xi_0^2 - 1}} \qquad (107)$$

Equations 106, 107 give the loading resistance required for $E_y/H_z = \eta_0$, $E_x/H_z = \eta_0$ at the center of the antenna, when the source is one δ-gap generator located at $v = 0^0$, $v = 90^0$ as a function of the geometry of the ELLIPTICUS (ξ_0). Furthermore the ratio of the equivalent radius to the thickness of the wire, b, also appears. The quantities G_0, G_{90} equal to R_0 normalized with respect to $\eta_0 \ln(s_0/(2\pi b))$ are plotted in Fig. 22 as a function of ξ_0. For ease of interpretation the scale a/a′ is also provided on the top of the plot frame. An expanded portion of G_0, G_{90} is shown in Fig. 23 corresponding to a/a′ ranging between 1.1 and 3. G_0, G_{90} represent the amount of resistance, as a fraction of $\eta_0 \ln(s_0/(2\pi b))$, that one should load the antenna with, to obtain E/H = 377 Ω at the center, in the low frequency limit. It can be seen from either curve that, for high values of the eccentricity, i.e. $\xi_0 \to 1$, the optimum resistance can be even 80% (or lower) of $\eta_0 \ln(s_0/2\pi b)$. By comparing G_0 with G_{90}, one can notice that the differences in loading resistances depending on the source location appear mainly for values of ξ_0 smaller than 3 and, in any case, are contained within 15%. These differences account for the effect of the curvature of the ellipse relative to the location of the source. Such effect is manifested in the low frequency value of the electric field only, as shown in Eqs. 103 and 104. In fact Int_1 is higher than Int_2 because the separation between the wires, where the potential difference is established, is smaller when the source is at $v = 0^0$. Because of this the value of R_0 must increase when the electric field decreases, so that the magnetic field can decrease also, to establish E/H = 377. Figures 24 through 27 illustrate the fields at the center corresponding to the choice G_0, G_{90} for two particular values of ξ_0, i.e. 1.09 and 1.34, chosen as examples. One should notice that in one case (G_0) the incident E-field is vertically polarized whereas in the other (G_{90}) the incident E-field is horizontally polarized. The calculations are made for thin antennas, i.e. $a/b = 4.7 \times 10^4$ ($\xi_0 = 1.09$) and $a/b = 2 \times 10^4$ ($\xi_0 = 1.34$). In both cases we have taken the ratio E/(H 377) and plotted it as a function of frequency in Figs. 28 and 29.

It appears that when the source is located at $v = 0^0$ the electric field is more dependent on the geometry (ξ_0) than when the source is at $v = 90^0$. This is to say that E_y of Figs. 24 ($\xi_0 = 1.09$) and 25 ($\xi_0 = 1.34$) look quite different from each other whereas E_x of Figs. 26 ($\xi_0 = 1.09$) and 27 ($\xi_0 = 1.34$) look quite similar. Perhaps when the source is at $v = 0^0$ the illuminator looks more like a guided wave system since the wires are closer together in the neighborhood of the source, exhibiting a standing wave pattern particularly apparent in the case when $\xi_0 = 1.09$. On the contrary when the source is placed at $v = 90^0$ the wires are further apart and the change of geometry does not affect this separation quite as much as it does for the other source location. As a result, by looking at Figs. 28

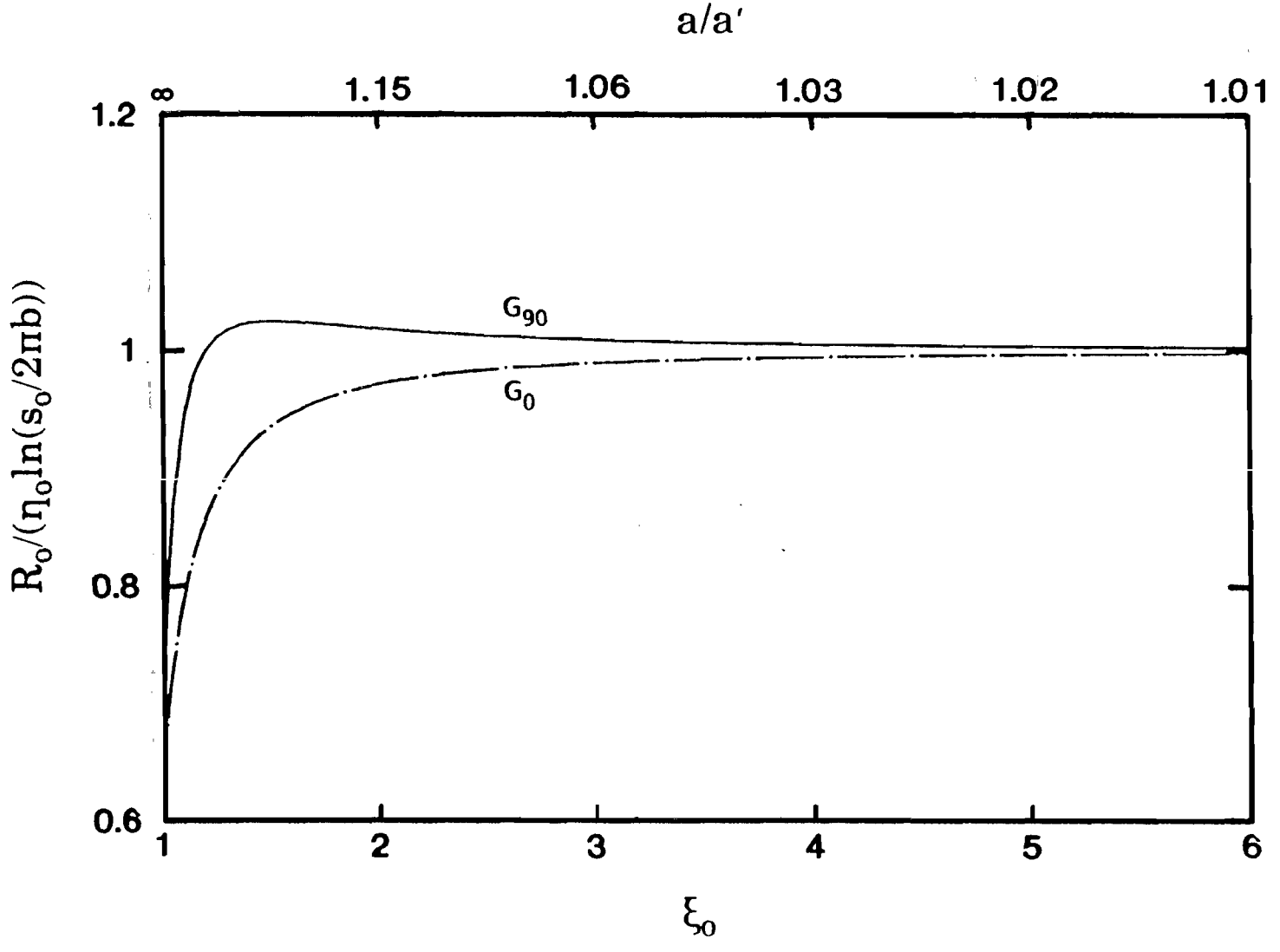

Figure 22. Normalized loading resistance G_0, (G_{90}) for ELLIPTICUS which indicates the optimum value, as a function of the geometry ξ_o (a/a'), to achieve E_y/H_z (E_x/H_z) = 377 Ω at the center (low frequency limit). G_0 corresponds to δ-gap at v = 0°, G_{90} corresponds to δ-gap at v = 90°.

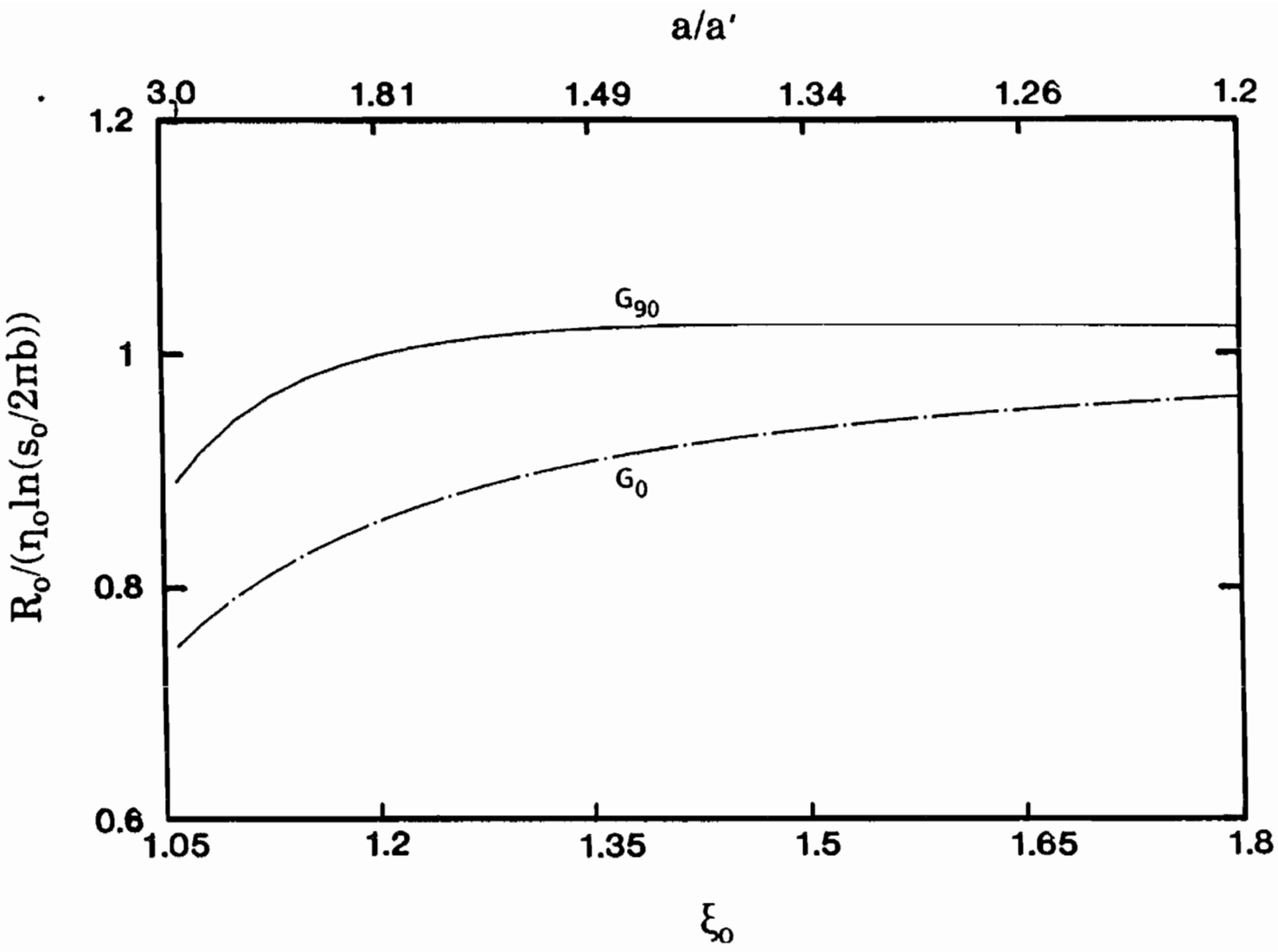

Figure 23. Expanded part of curves of Fig. 22 for ξ_o ranging between 1.05 and 1.08. Correspondingly a/a' ranges between 3 and 1.2.

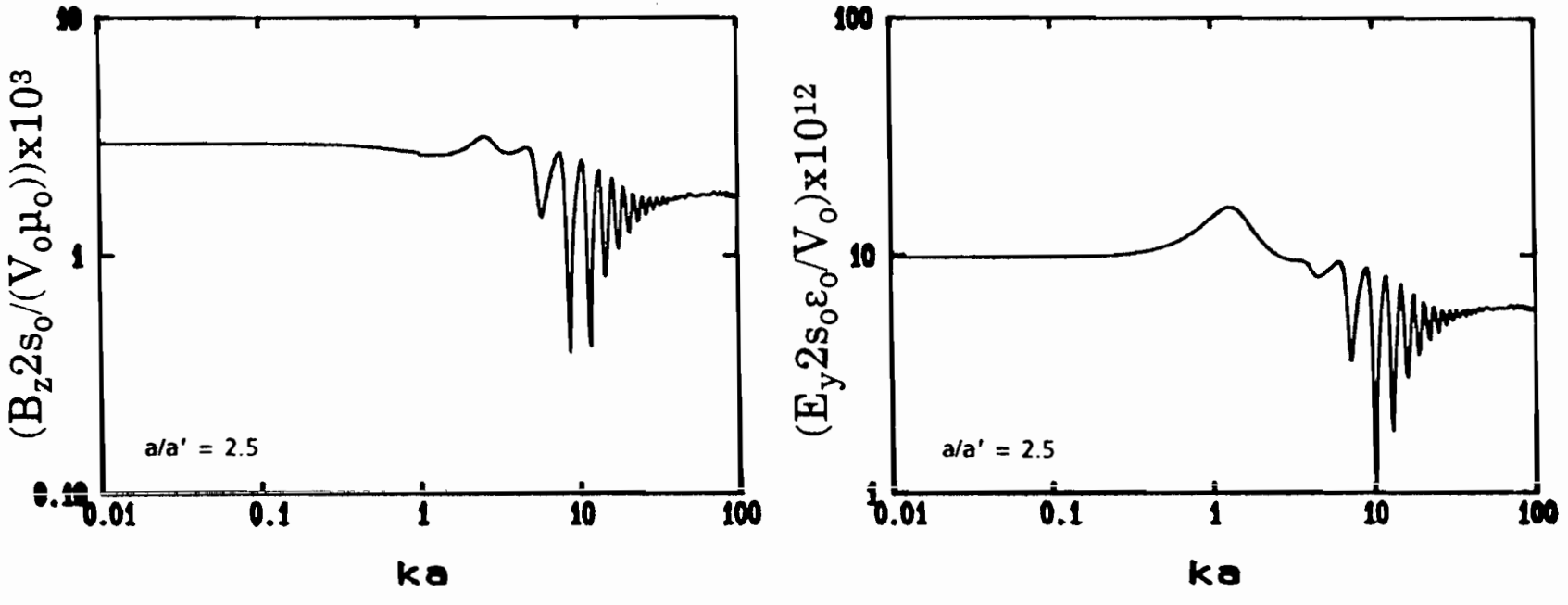

Figure 24. Principal field components of ELLIPTICUS calculated at x/a = 0, y/a' = 0, z/a = 0. Source is at v = 0°, ELLIPTICUS geometry: $\xi_o = 1.09$, a/b = 4.7x10^4, $R_o = 0.78\ \eta_o \ln|s_o/(2\pi b)|$ from G_0. Magnetic field has units of Siemens, electric field has units of Farad/meter.

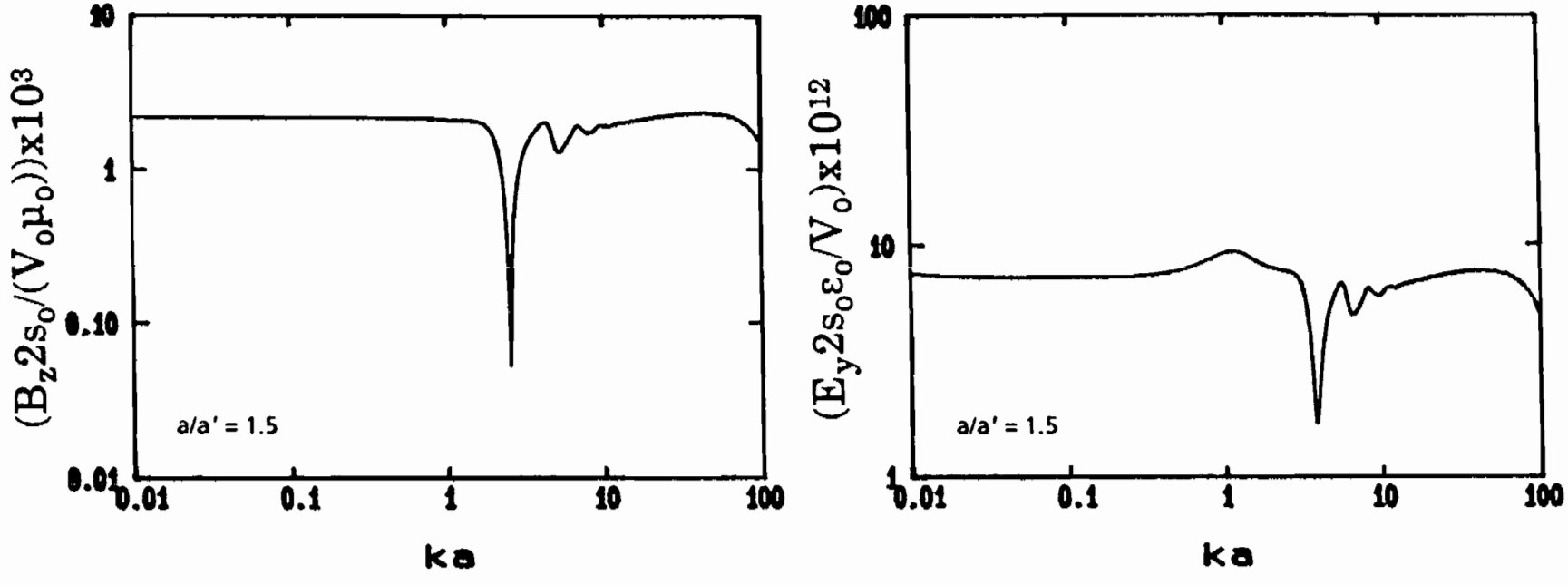

Figure 25. Principal field components of ELLIPTICUS calculated at x/a = 0, y/a' = 0, z/a = 0. Source is at v = 0^c, ELLIPTICUS geometry: $\xi_o = 1.34$, $a/b = 2x10^4$, $R_o = 0.91\ \eta_o \ln[s_o/(2nb)]$ from G_0. Magnetic field has units of Siemens, electric field has units of Farad/meter.

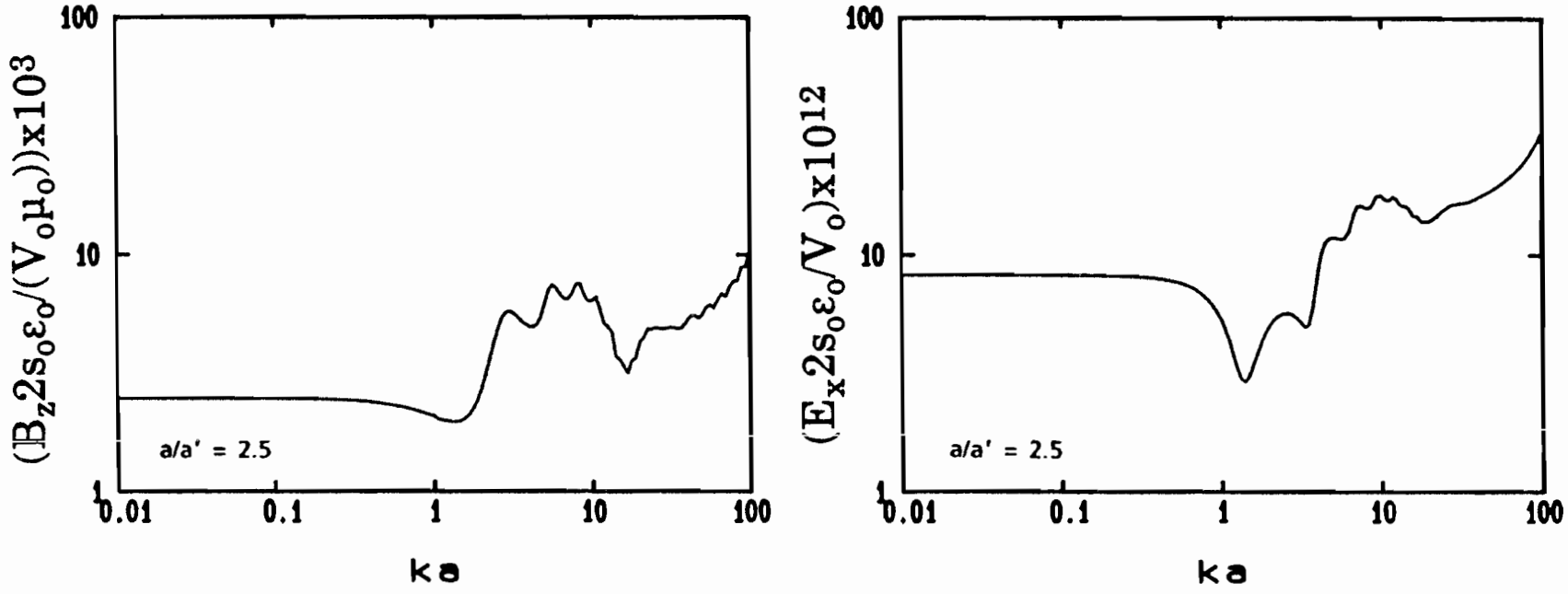

Figure 26. Principal field components of ELLIPTICUS calculated at x/a = 0, y/a' = 0, z/a = 0. Source is at v = 90°, ELLIPTICUS geometry: $\xi_o = 1.09$, a/b = $4.7x10^4$, $R_o = 0.93\ \eta_o \log[s_o/(2\pi b)]$ from G_{90}. Magnetic field has units of Siemens, electric field has units of Farad/meter.

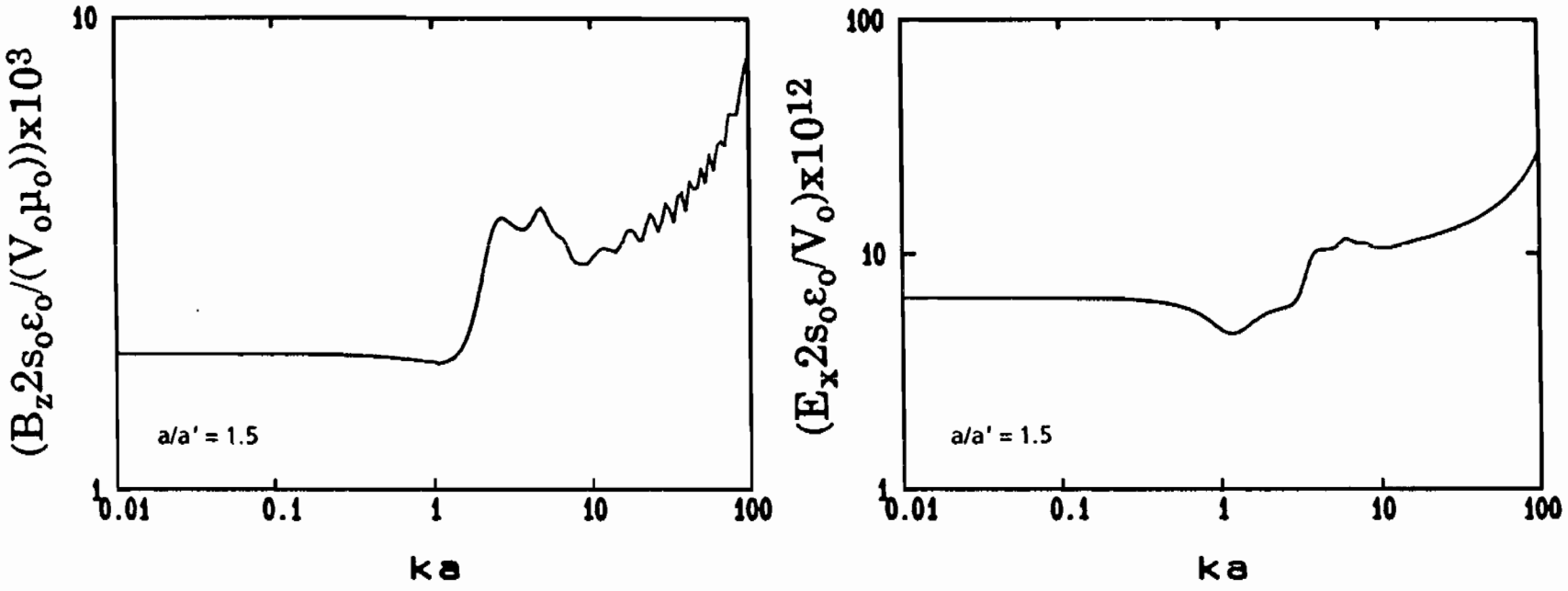

Figure 27. Principal field components of ELLIPTICUS calculated at x/a = 0, y/a' = 0, z/a = 0. Source is at v = 90°, ELLIPTICUS geometry: $\xi_o = 1.34$, a/b = $2x10^4$, $R_o = 1.02$ $\eta_o \log[s_o/(2\pi b)]$ from G_{90}. Magnetic field has units of Siemens, electric field has units of Farad/meter.

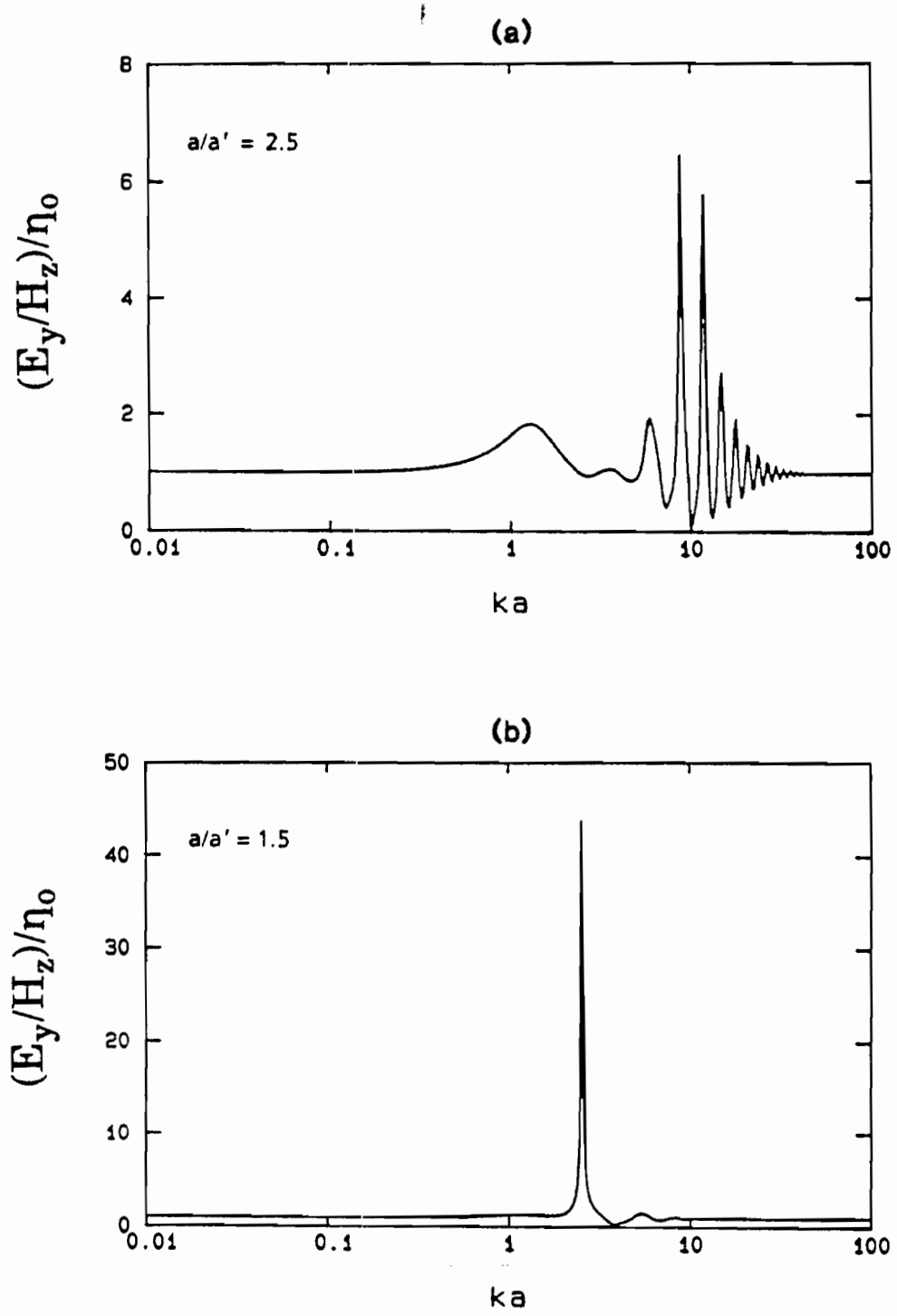

Figure 28. E_y/H_z ratio at the center for

(a) Fields of Fig. 24, $\xi_o = 1.09$, $R_o = 0.78\,\eta_o \log(a/b)$, $a/b = 4.7 \times 10^4$.
(b) Fields of Fig. 25, $\xi_o = 1.34$, $R_o = 0.91\,\eta_o \log(a/b)$, $a/b = 2 \times 10^4$.

Source is at $v = 0^o$.

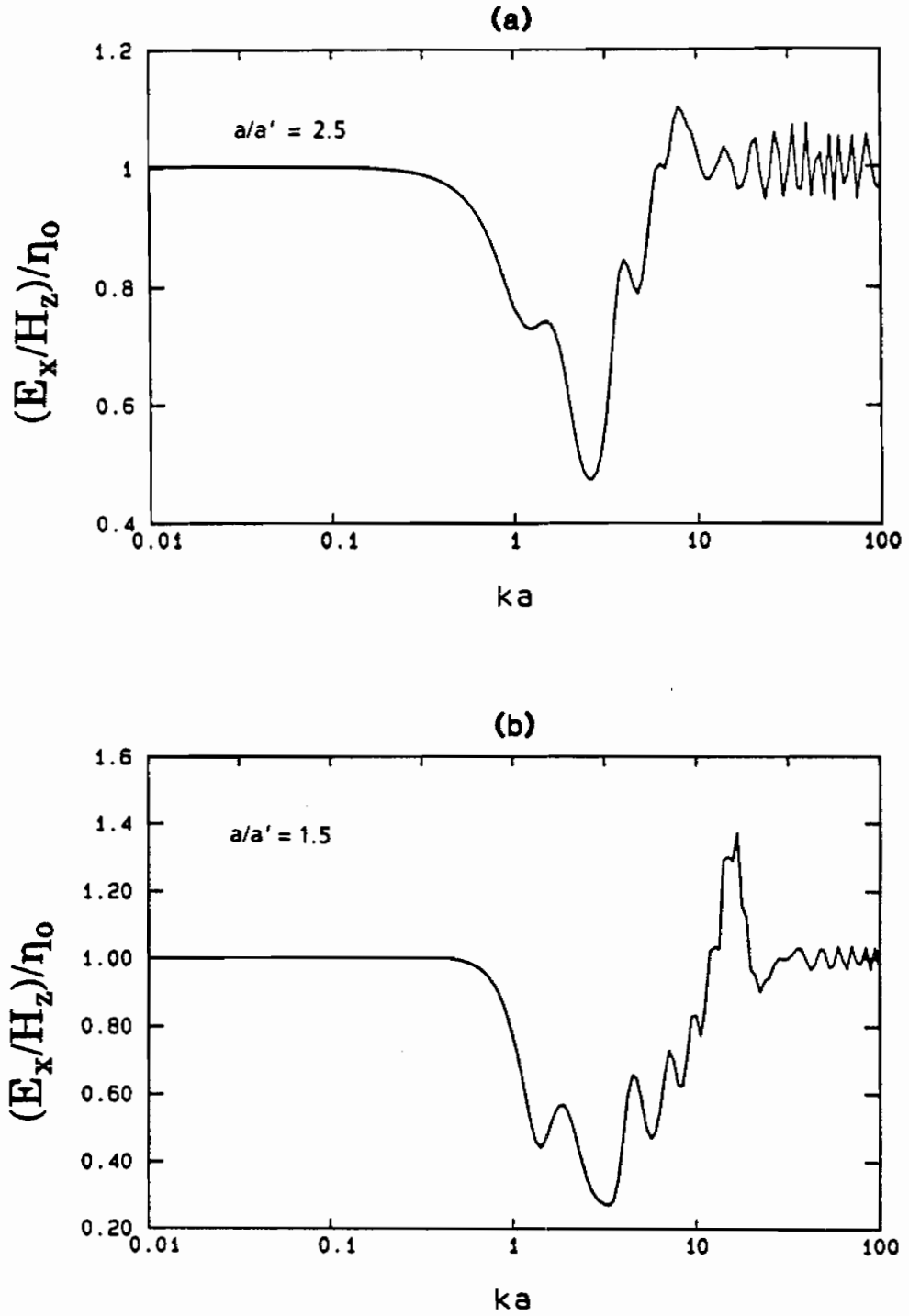

Figure 29. E_x/H_z ratio for at the center for

(a) Fields of Fig. 26, $\xi_0 = 1.09$, $R_0 = 0.93\ \eta_0 \log(a/b)$, $a/b = 4.7 \times 10^4$.
(b) Fields of Fig. 27, $\xi_0 = 1.39$, $R_0 = 1.02\ \eta_0 \log(a/b)$, $a/b = 2 \times 10^4$.

Source is at $v = 90^o$.

and 29 the field ratios are, as an overall, closer to the plane wave situation when the source is at $v = 90^0$. In any case these considerations were made to assess how the choice of the loading resistance affects the "plane wave behavior" of the incident field at the center of the antenna. In practice, however, the selection according to either G_0 or G_{90} is going to make only a very small difference in the event that the source is located at $v = 90^0$ with an image at $v = 270^0$. This point will be clarified with illustrations of calculated fields in Sec. 2.2.1.

For the two chosen geometries and a/b ratios, using Eqs. 69 through 100, the principal components of the electromagnetic fields E_y and B_z were calculated also at the observation points (x/a = 0, y/a' = 0.1, 0.2, 0.25, z/a = 0) (x/a = 0.46, y/a' = 0, 0.1, 0.2, 0.25, z/a = 0) for the case when $\xi_0 = 1.09$ and (x/a = 0, y/a' = 0.1, 0.2, 0.25, z/a = 0) (x/a = 0.37, y/a' = 0.1, 0.2, 0.25, z/a = 0) for the case when $\xi_0 = 1.34$. The geometries and the observation points are visualized in Fig. 30.

The results of the calculations are presented in Figs. 31 through 34. In these calculations the δ-gap source was assumed to be at $v = 0^0$ and R_0 was chosen according to Eq. 106. One can notice, by comparison with Figs. 8 and 9, that the field values at low frequency and the general trend are very similar for both the toroidal and the elliptical geometries but some details, particularly in the intermediate and high frequency region where the different modes of the antennas contribute their peculiar features, are quite different in the two configurations.

It is pointed out that when $\xi_0 \to \infty$, i.e. the ellipse becomes a circle, both Eqs. 106, and 107 give the value $\eta_0 \ln(a/b)$, as expected. This result was obtained by carrying out the limit of each factor of Eqs. 106 and 107 for $\xi_0 \to \infty$.

2.1.5 2-Norm Error Calculations

2-Norm errors have been calculated according to the following definitions

$$2-N = \frac{\left| \frac{1}{L} \int_{-L/2}^{L/2} |P_\delta(ka, \xi, v, z) - P_d^{ave}|^2 dl \right|^{1/2}}{|P_\delta^{ave}|} \tag{108}$$

$$P_\delta^{ave} = \frac{1}{L} \int_{-L/2}^{L/2} P_\delta(ka, \xi, v, z) dl \tag{109}$$

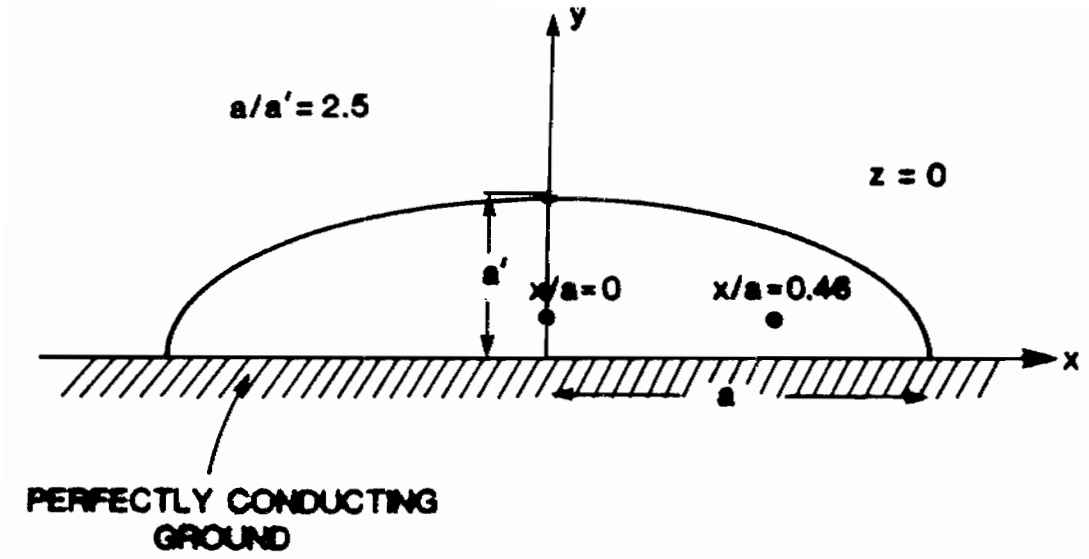

(a)

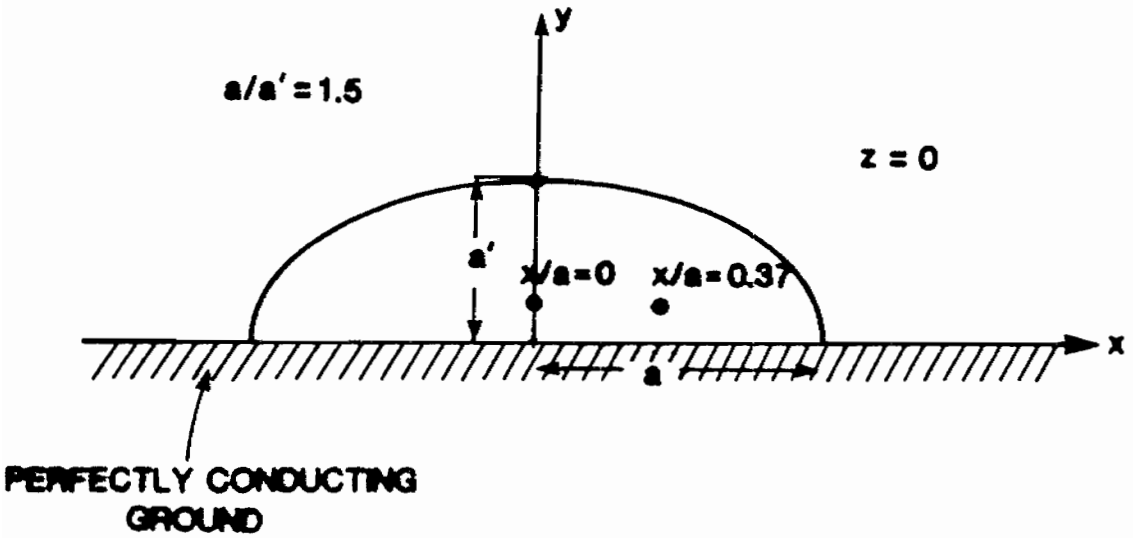

(b)

Figure 30. Illustration of location of points used in field calculation for ELLIPTICUS (a) $\xi_0 = 1.09$ (b) $\xi_0 = 1.34$.

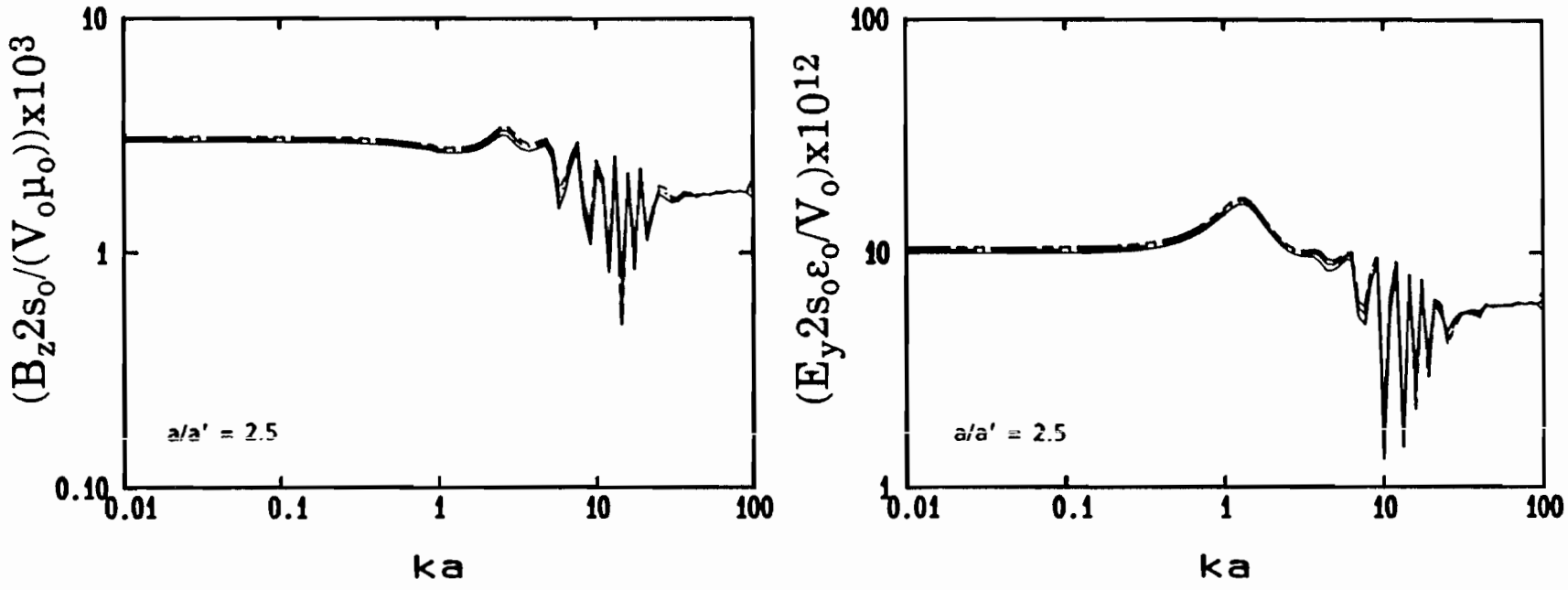

Figure 31. Principal field components of ELLIPTICUS calculated at x/a = 0, z/a = 0 and

_____ y/a' = 0.1

_____ y/a' = 0.2

_____ y/a' = 0.25

Source is at $v = 0°$, $\xi_0 = 1.09$, $a/b = 4.7x10^4$, $R_0 = 0.78\,\eta_0 \ln[s_0/(2\pi b)]$. Magnetic field has units of Siemens, electric field has units of Farad/meter.

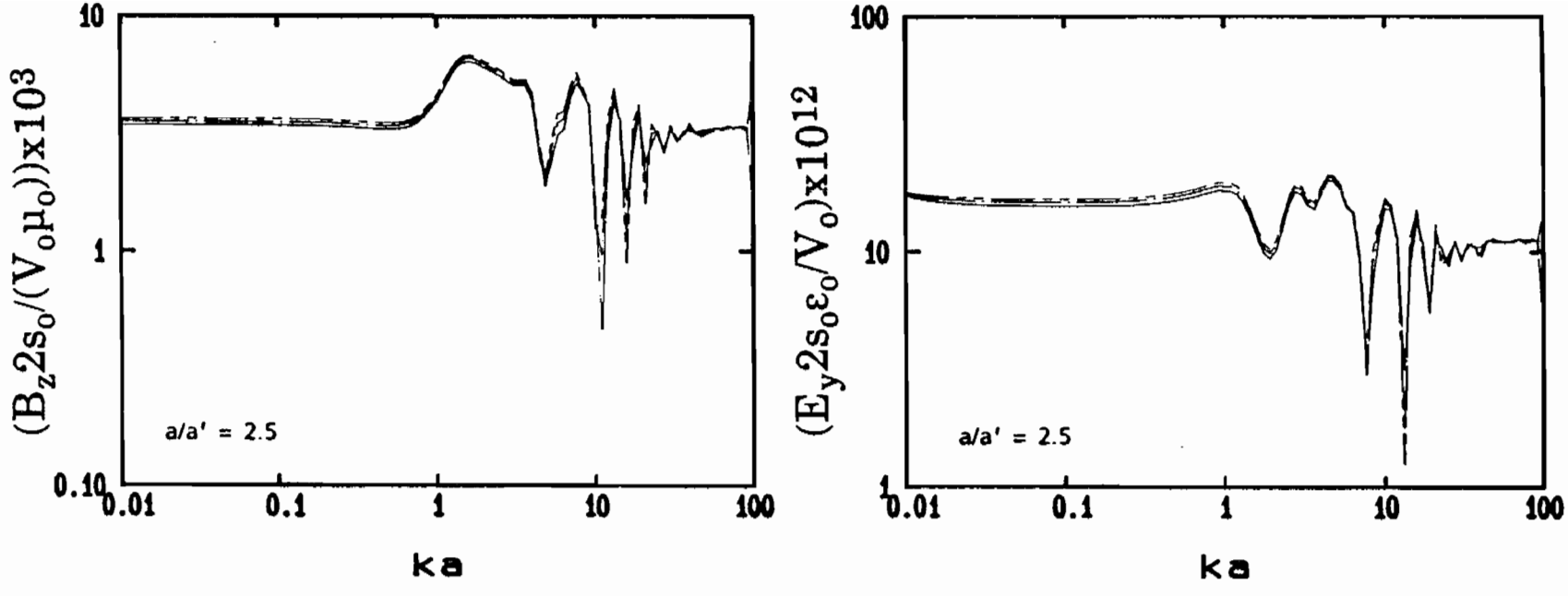

Figure 32. Principal field components of ELLIPTICUS calculated at x/a = 0.46, z/a = 0 and

_____ y/a' = 0.1

_____ . _____ y/a' = 0.2

_____ _ _ _ _____ y/a' = 0.25

Source is at $v = 0^\circ$, $\xi_0 = 1.09$, $a/b = 4.7x10^4$, $R_o = 0.78\,\eta_o\,|n|s_o/(2\pi b)|$. Magnetic field has units of Siemens, electric field has units of Farad/meter.

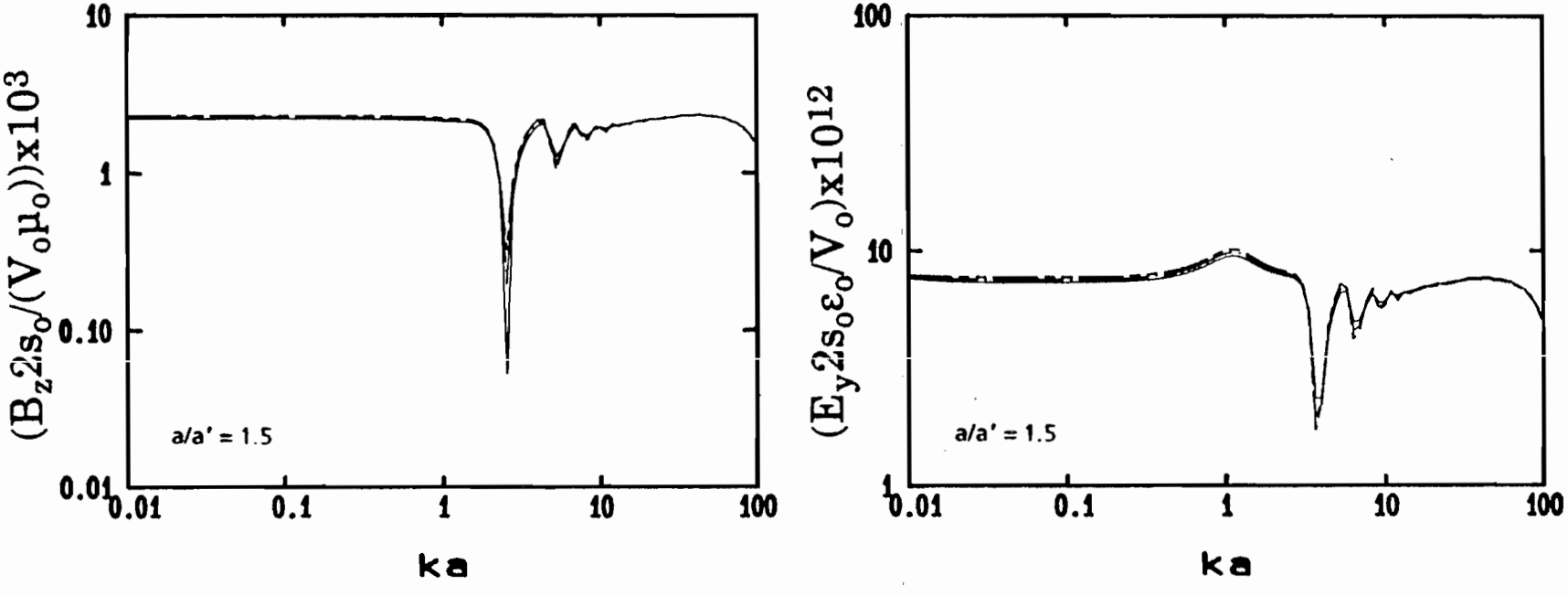

Figure 33. Principal field components of ELLIPTICUS calculated at x/a = 0, z/a = 0 and

_____ y/a' = 0.1

_____ y/a' = 0.2

_____ y/a' = 0.25

Source is at v = 0°, ELLIPTICUS geometry: $\xi_0 = 1.34$, $a/b = 2x10^4$, $R_0 = 0.91\ \eta_0 \ln[s_0/(2\pi b)]$. Magnetic field has units of Siemens, electric field has units of Farad/meter.

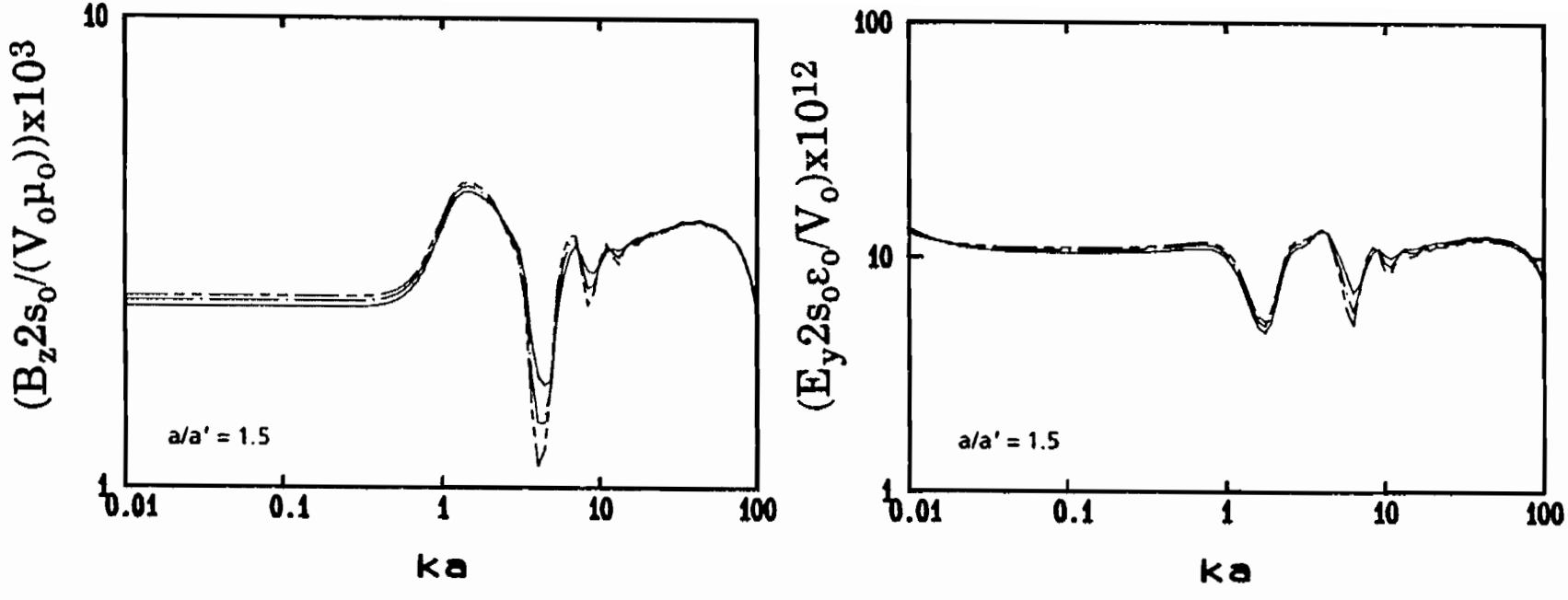

Figure 34. Principal field components of ELLIPTICUS calculated at x/a = 0.37, z/a = 0 and

_____ y/a' = 0.1

_____ y/a' = 0.2

_____ y/a' = 0.25

Source is at v = 0°, ELLIPTICUS geometry: $\xi_o = 1.34$, $a/b = 2x10^4$, $R_o = 0.91\ \eta_o \ln[s_o/(2\pi b)]$. Magnetic field has units of Siemens, electric field has units of Farad/meter.

The integrations were carried out along a straight line of length L located at a height y/a'. Such length, for a given height y/a', is determined by imposing that (see Eq. 62)

$$y/a' = d/a'(\sqrt{\xi^2 - 1}\ \sin v) \tag{110}$$

$$L = 2\, d\xi \cos v \tag{111}$$

solved for $v = 60^\circ$. Equation 110 determines the value of ξ which, once substituted in Eq. 111, gives L. It is stressed that the length of the domain of integration depends on the value of the height y/a' since v is always taken equal to 60° in Eqs. 110 and 111. Consistently with what was done for the TORUS, three different heights were considered, namely $y/a' = 0.1$, 0.2 and 0.25. The 2-Norm errors calculated for the two elliptical geometries of interest, i.e. $\xi_0 = 1.09$ and $\xi_0 = 1.34$, are illustrated in Figs. 35 and 36, respectively. They are very similar to those calculated for the TORUS and reported in Fig. 11.

2.2 MULTIPLE δ-GAP GENERATORS

2.2.1 Electromagnetic Fields (one source at $v = 90^\circ$ and its image at $v = 270^\circ$)

The case of a half ELLIPTICUS above a perfectly conducting ground with a δ-gap generator located at $v = 90^\circ$ can be treated analogously to what was done for the half TORUS. That is to say that Eqs. 49 through 54 can be used to calculate the current provided the substitution $a\phi = s(v)$ is made. The expressions for the vector potential, its derivatives and the fields everywhere in space are still given by Eqs. 70 through 100, the only difference being that the integrations between 0 and 2π must here be carried out like shown in the following

$$\int_0^{2\pi} I_v(v')\ldots = \int_0^{\pi/2} I_1(v')\ldots + \int_{\pi/2}^{\pi} I_2(v')\ldots + \int_{\pi}^{3\pi/2} I_4(v')\ldots + \int_{3\pi/2}^{\pi} I_3(v')\ldots \tag{112}$$

with I_1, I_2, I_3, and I_4 given by Eq. 49 with $a\phi$ substituted by $s(v)$ given by Eq. 66. The principal field components E_x and H_z were calculated at the points $y/a' = 0.1$, 0.2, 0.25; $x/a = 0$, $z/a = 0$ and $y/a' = 0.1$, 0.2, 0.25, $z/a = 0$, $x/a = 0.46$ ($\xi_0 = 1.09$) or 0.37 ($\xi_0 = 1.34$) and the results are presented in Figs. 37 through 40. These results can be compared with those obtained for the TORUS and reported in Figs. 13 and 14. One can notice that the trends are very similar for the two geometries, particularly at the low frequency values, while at high frequencies the higher order modes introduce

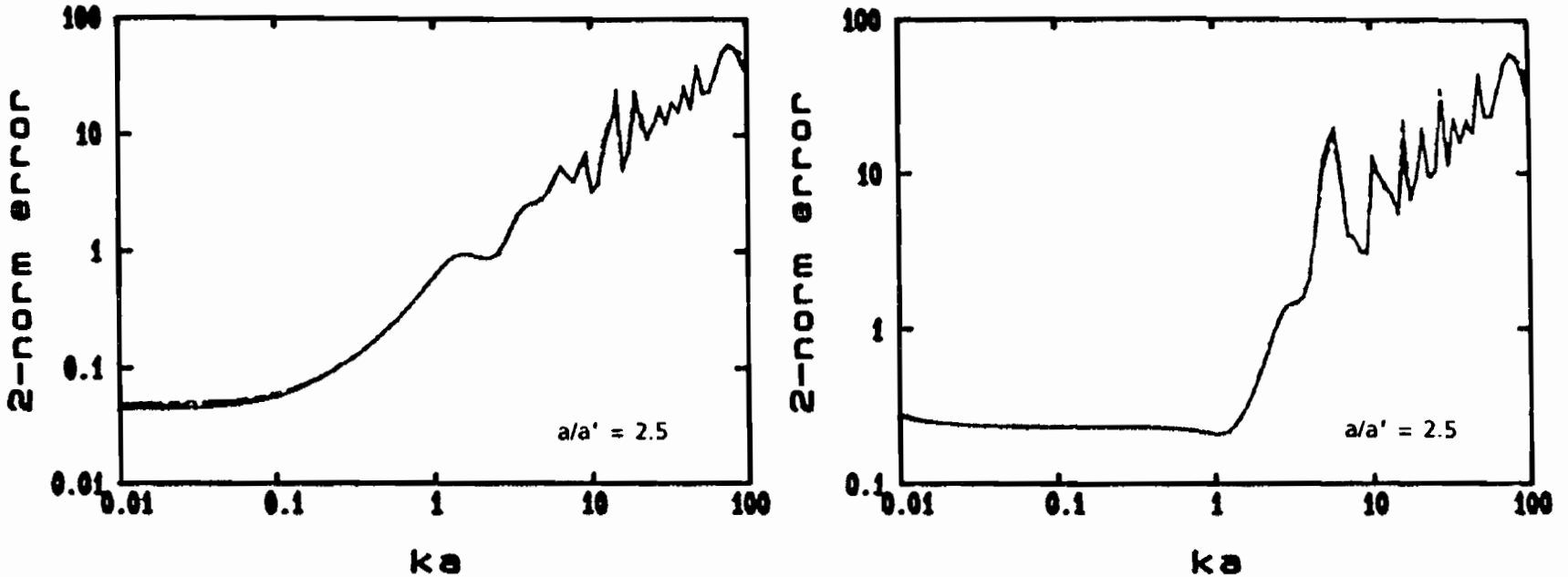

Figure 35. Two-norm error calculated according to Eq. 108(a) B_z; (b) E_x. Source is located at $v = 0^c$.

$-0.37 < x/a < 0.37$, $z/a = 0$ and

_____ $y/a' = 0.1$

_____ $y/a' = 0.2$

_____ $y/a' = 0.25$

ELLIPTICUS geometry: $\xi_0 = 1.09$, $a/b = 4.7 \times 10^4$ $R_0 = 0.78 \ln[s_0/(2\pi b)]$.

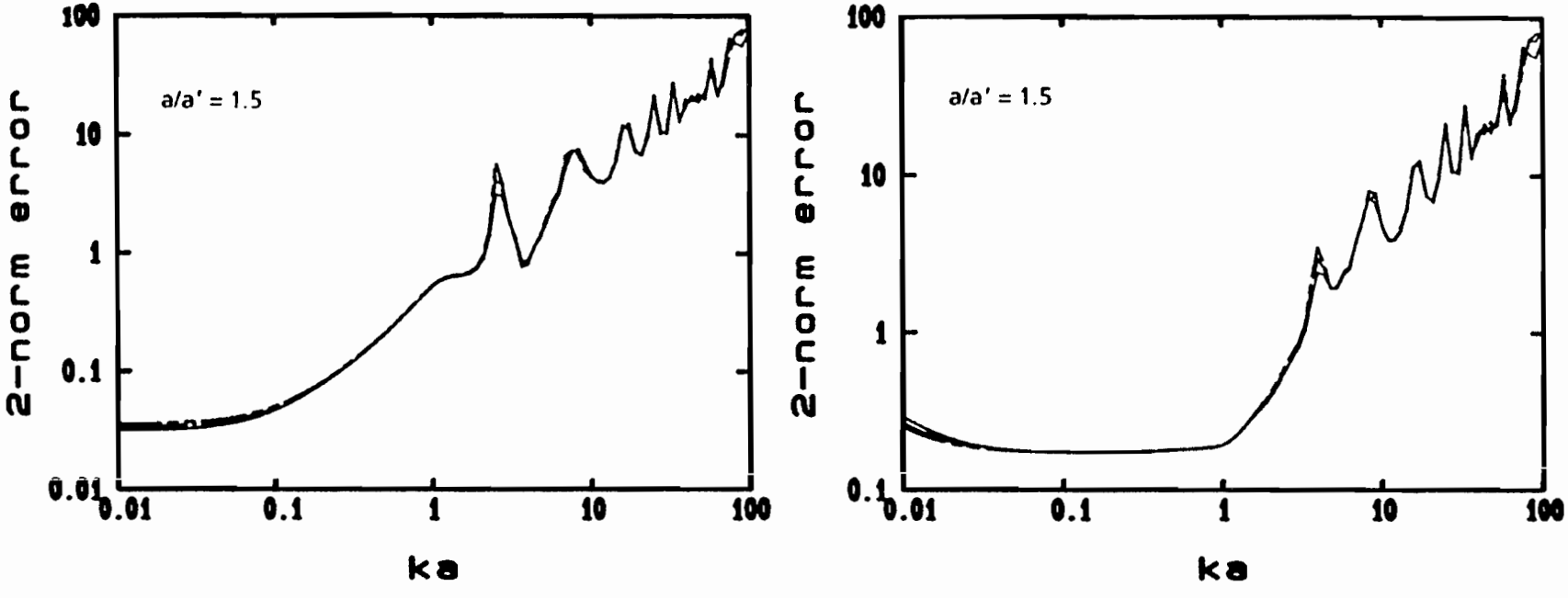

Figure 36. ELLIPTICUS: Two-norm error calculated according to Eq. 108 (a) B_z; (b) E_x. Source is located at $v = 0°$.

$-0.37 < x/a < 0.37$, $z/a = 0$ and

_____ $y/a' = 0.1$

_____ $y/a' = 0.2$

_____ $y/a' = 0.25$

ELLIPTICUS geometry: $\xi_0 = 1.34$, $a/b = 2 \times 10^4$, $R_0 = 0.91 \eta_0 \ln[s_0/(2\pi b)]$.

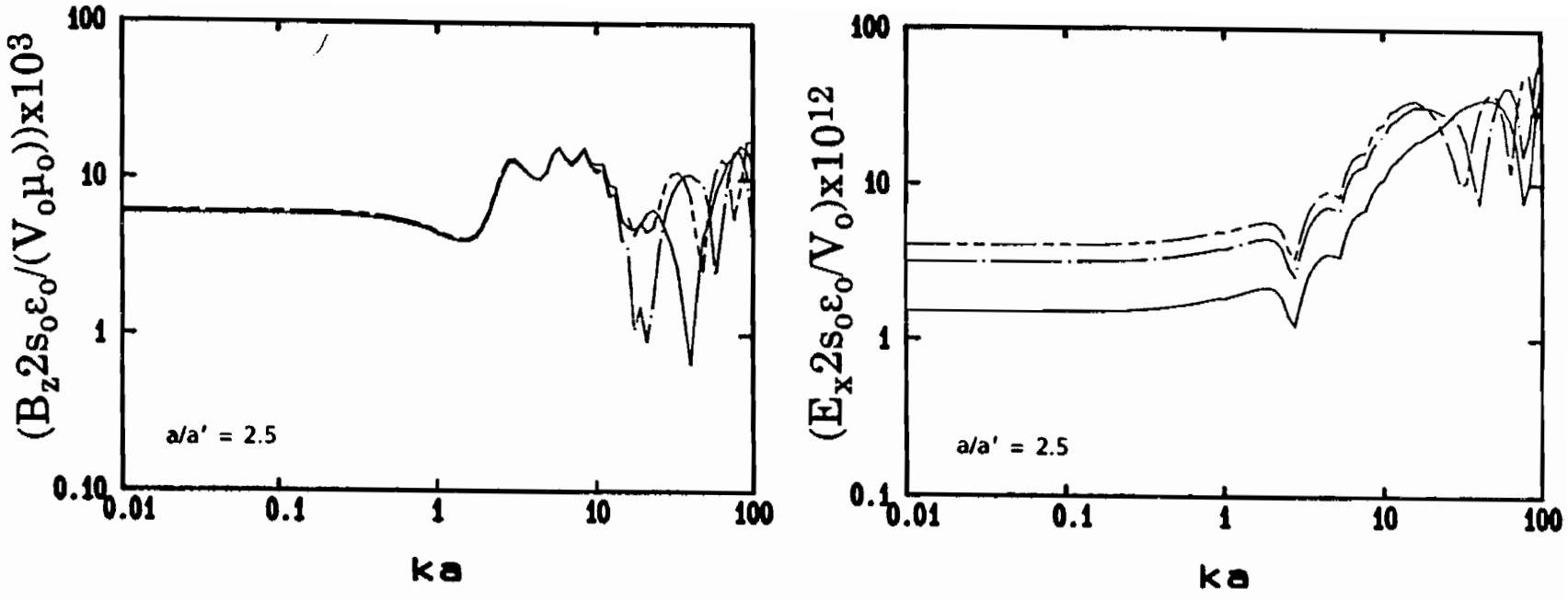

Figure 37. Principal field components of ELLIPTICUS calculated at x/a = 0, z/a = 0 and

——————— y/a' = 0.1

——— · ——— y/a' = 0.2

——— – – ——— y/a' = 0.25

Source is at v = 90° with image at v = 270°. ELLIPTICUS geometry: $\xi_o = 1.09$, $a/b = 4.7x10^4$, $R_o = 0.78\ \ln[s_o/(2nb)]$. Magnetic field has units of Siemens, electric field has units of Farad/meter.

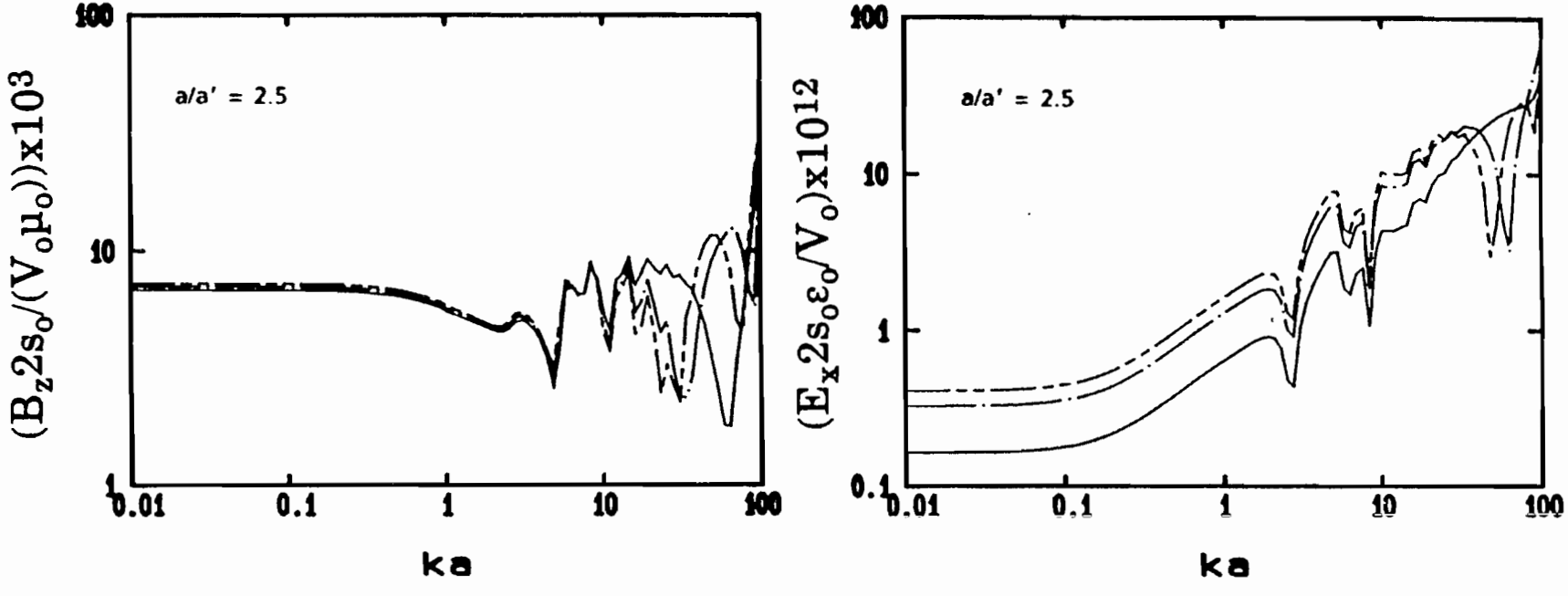

Figure 38. Principal field components of ELLIPTICUS calculated at x/a = 0.46, z/a = 0 and

_____ y/a' = 0.1

_____ y/a' = 0.2

_____ y/a' = 0.25

Source is at v = 90° with image at v = 270°. ELLIPTICUS geometry: $\xi_o = 1.09$, $a/b = 4.7x10^4$, $R_o = 0.78\ \ln[s_o/(2\pi b)]$. Magnetic field has units of Siemens, electric field has units of Farad/meter.

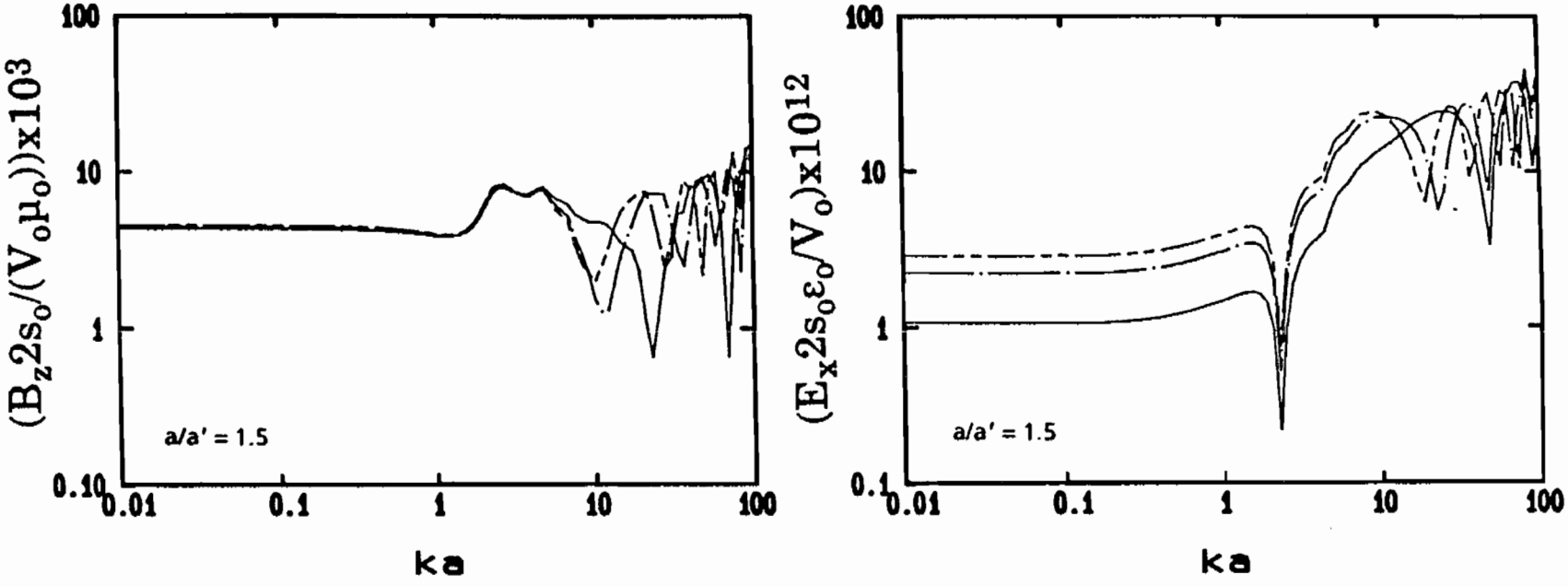

Figure 39. Principal field components of ELLIPTICUS calculated at x/a = 0, z/a = 0 and

_____ y/a' = 0.1

_____ y/a' = 0.2

_____ y/a' = 0.25

Source is at v = 90° with image at v = 270°. ELLIPTICUS geometry: $\xi_0 = 1.34$, a/b = $2x10^4$, $R_0 = 0.91\ \eta_0 \ln[s_0/(2\pi b)]$. Magnetic field has units of Siemens, electric field has units of Farad/meter.

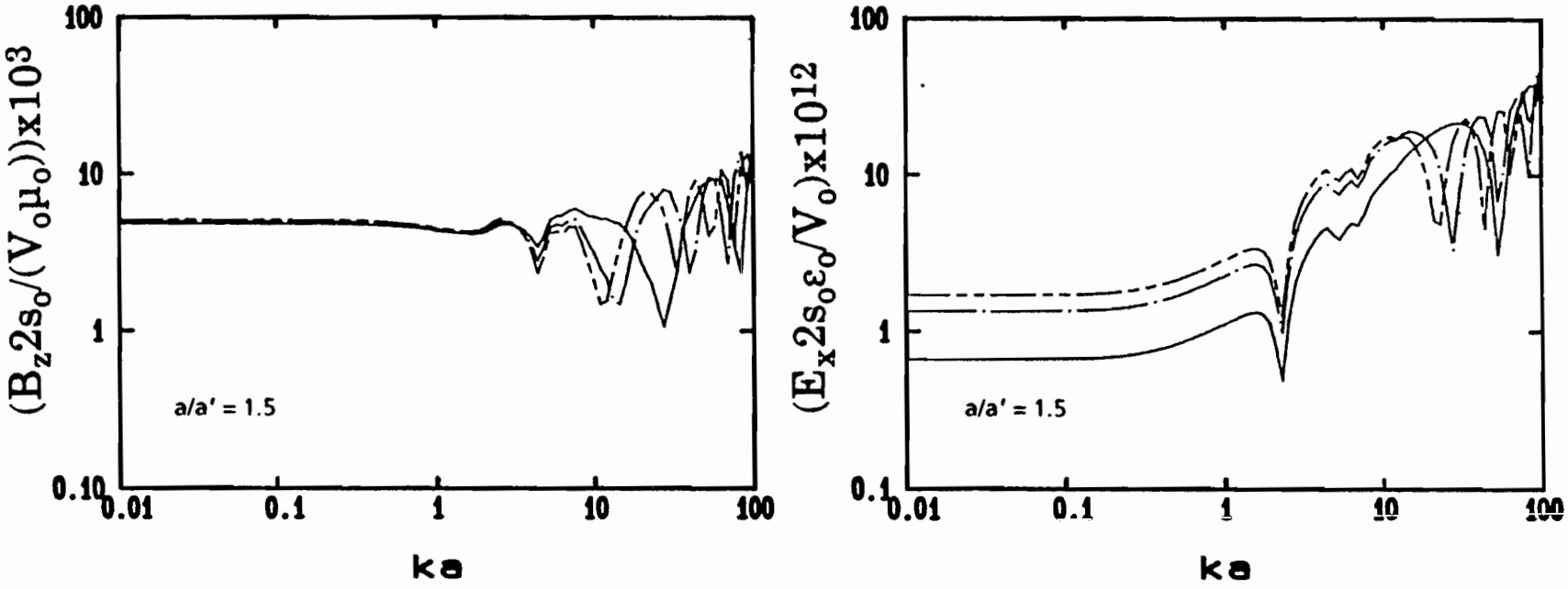

Figure 40. Principal field components of ELLIPTICUS calculated at x/a = 0.37, z/a = 0 and

_____ y/a' = 0.1

_____ y/a' = 0.2

_____ y/a' = 0.25

Source is at v = 90° with image at v = 270°. ELLIPTICUS geometry: $\xi_o = 1.34$, $a/b = 2x10^4$, $R_o = 0.91\ \eta_o \ln[s_o/(2\pi b)]$. Magnetic field has units of Siemens, electric field has units of Farad/meter.

more marked differences between them. Furthermore, in the low frequency range, i.e. ka < 1, there is more variation of E_x along the x axis the higher the eccentricity. This point is clearly illustrated in Fig. 41 which shows the behavior of the principal field components for the TORUS as well as the two elliptical configurations of interest here. In this case y/a' (y/a) was equal to 0.1 and ka = 0.01. Furthermore Fig. 42 plots the fields at x/a = 0, y/a' (y/a) = 0.1 for a TORUS and an ELLIPTICUS of very small eccentricity ($1/\xi_0 = 0.1$) to show that indeed, in the limit, our calculations for the ELLIPTICUS are consistent with those derived for the TORUS.

In the above calculations the loading resistance was that given by Eq. 106. Figures 43 through 46 illustrate the results for the case when $\bar{R}_0$ is given by Eq. 107 instead. One can notice that the results are very similar. In the remaining calculations the choice of R_0 given by Eq. 106 was retained throughout.

Time domain responses to a step function were carried out also in this case. Figures 47 through 50 illustrate the results for the case of $\xi_0 = 1.09$, 1.34, at the point x/a = 0, y/a' = 0.1 and z/a = 0. They are consistent with those obtained for the TORUS and the same limitations already pointed out in Sec. 1.1.4 and 1.2 hold. However, it is noted that the fields exhibit an oscillating behavior even for relatively late times, particularly the E-field. Such oscillations arise from the truncation of the integrand in the frequency domain, which introduces an artificial "resonance". Therefore the oscillations are somewhat dependent on the truncation point and should not necessarily be interpreted as proper resonances of the system. An attempt to correct for this unwanted effect is to account for the truncation by adding a term evaluated analytically which represents the remaining contribution to the integral (see, for instance, second line of Eq. 15, 34 and 35). Such correction however is not perfect since the integrals are evaluated analytically but approximately. Such correction process is more effective for the TORUS fields than it is for the ELLIPTICUS ones.

Realistic physical pulsed sources have a switch which when closed allows the voltage built-up at capacitors to be applied to the actual load presented by the antenna. We have modeled this capacitor inserted in series with the antenna load. Such a capacitor acts as a high-pass filter. In this case, the time domain response to a step function can be calculated by

$$\bar{E}(t) = -\frac{1}{2\pi}\int_{-\infty}^{+\infty} \bar{E}(ka)\frac{Z_{in}C}{iZ_{in}\omega C - 1}e^{-i\omega t}d\omega \qquad (113)$$

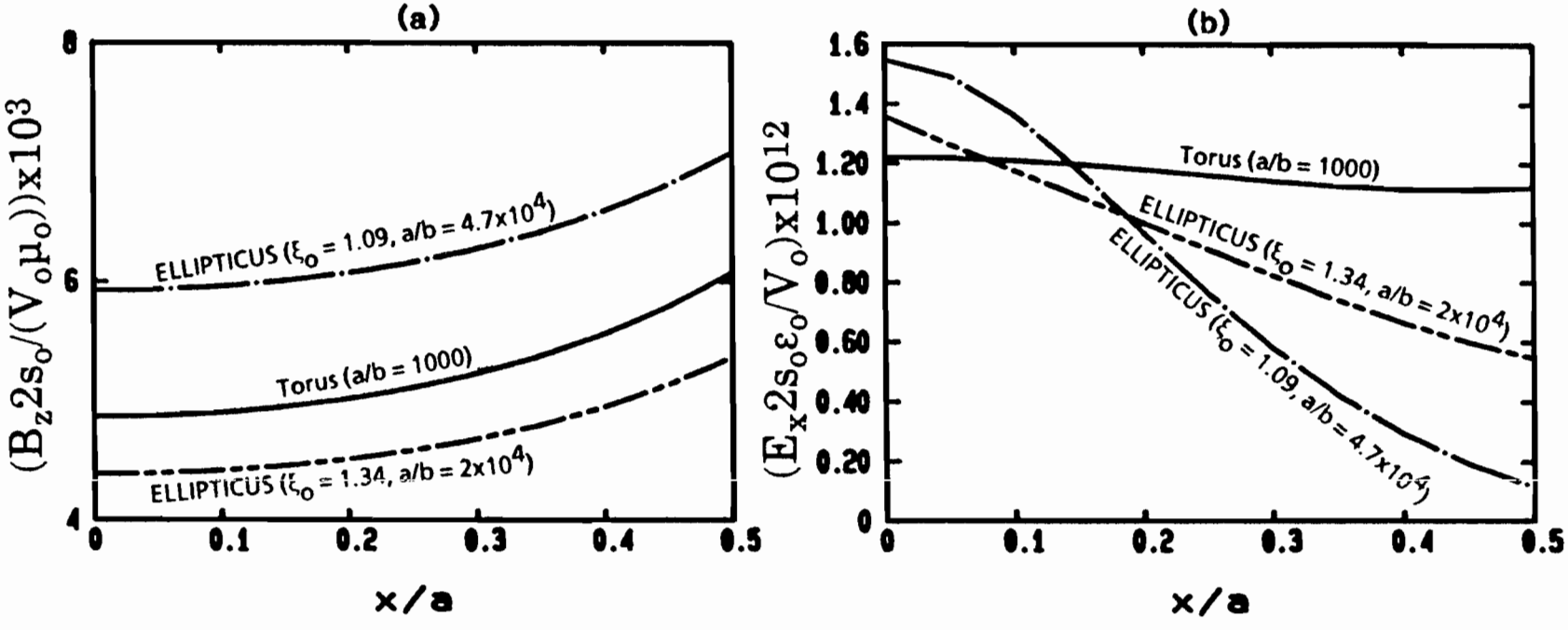

Figure 41. Comparison between the principal field components of a TORUS and of two ELLIPTICUS of different geometries. Calculations are along x-axis at the height y/a (y/a') = 0.1, ka = 10^{-2}.

$$R_o = \begin{cases} \eta_o \log(a/b) \text{ TORUS} & \\ 0.78\,\eta_o \log[s_o/2\pi b)] \text{ ELLIPTICUS } \xi_o = 1.09 & a/a' = 2.5 \\ 0.91\,\eta_o \log[s_o/(2\pi b)] \text{ ELLIPTICUS } \xi o = 1.34 & a/a' = 1.5 \end{cases}$$

Source is at $\phi = 90^0$ (or $v = 90^0$) with image at ϕ-270^0 ($v = 270^0$). Magnetic field has units of Siemens, electric field has units of Farad/meter.

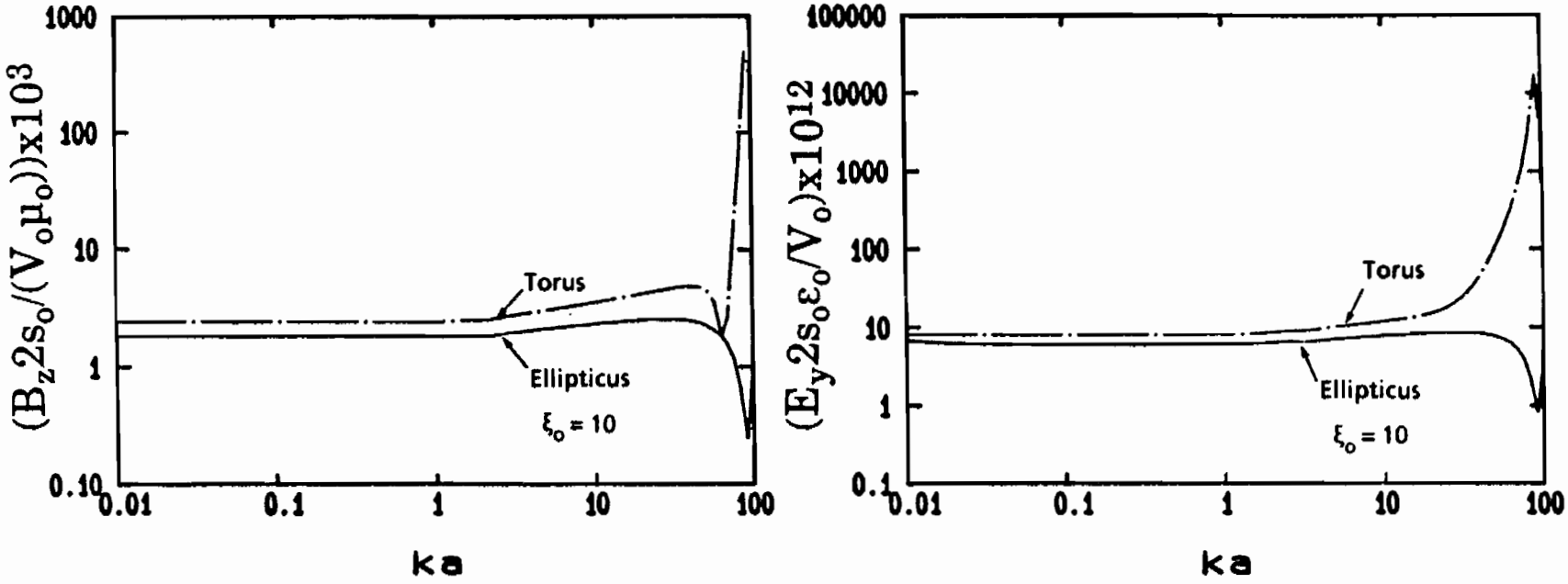

Figure 42. Comparison between the principal field components of a TORUS and of an ELLIPTICUS of low eccentricity ($\xi_o = 10$) at x/a = 0, y/a' = 0.1, z/a = 0 (single source).

$$R_o = \begin{cases} \eta_o \log(a/b) \text{ for TORUS} \\ \eta_o \log[s_o/(2\pi b)] \text{ for ELLIPTICUS} \end{cases} \qquad \xi_o = 10 \qquad a/a' = 1.005$$

$a/b = s_o/(2\pi b) = 10^3$

Magnetic field has units of Siemens, electric field has units of Farad/meter.

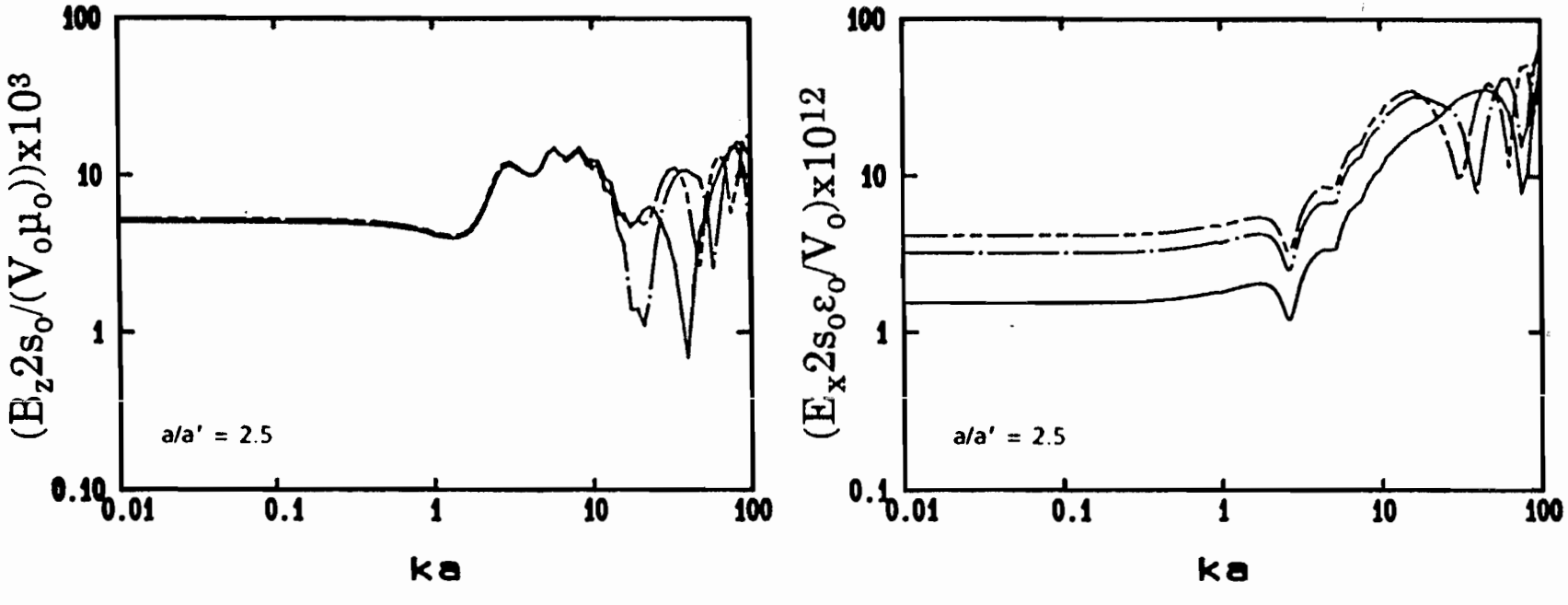

Figure 43. Principal field components of ELLIPTICUS calculated at x/a = 0, z/a = 0 and

_____ y/a' = 0.1

_____ y/a' = 0.2

_____ y/a' = 0.25

Source is at v = 90° with image at v = 270°. ELLIPTICUS geometry: $\xi_o = 1.09$, $a/b = 4.7x10^4$, $R_o = 0.93 \ln|s_o/(2nb)|$. Magnetic field has units of Siemens, electric field has units of Farad/meter.

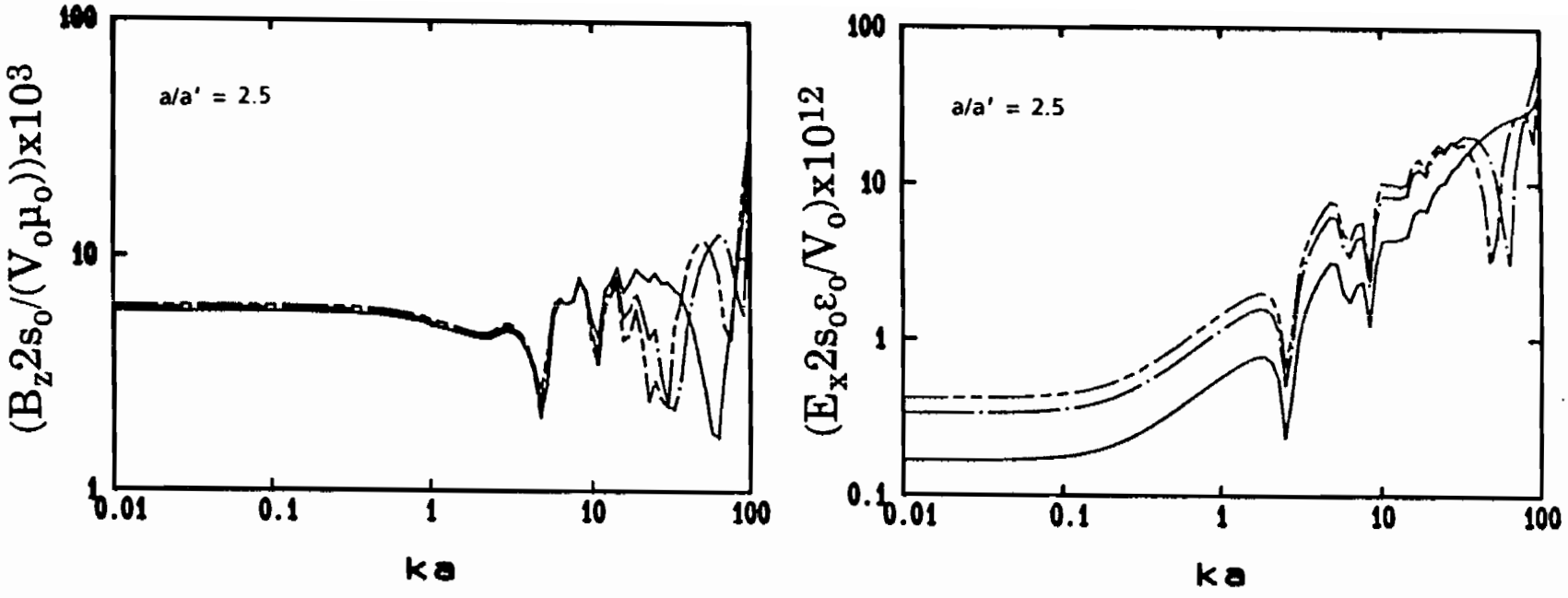

Figure 44. Principal field components of ELLIPTICUS calculated at x/a = 0.46, z/a = 0 and

———————— y/a' = 0.1

———— · ———— y/a' = 0.2

———— – – ———— y/a' = 0.25

Source is at v = 90° with image at v = 270°. ELLIPTICUS geometry: $\xi_o = 1.09$, $a/b = 4.7x10^4$, $R_o = 0.93 \ln[s_o/(2\pi b)]$. Magnetic field has units of Siemens, electric field has units of Farad/meter.

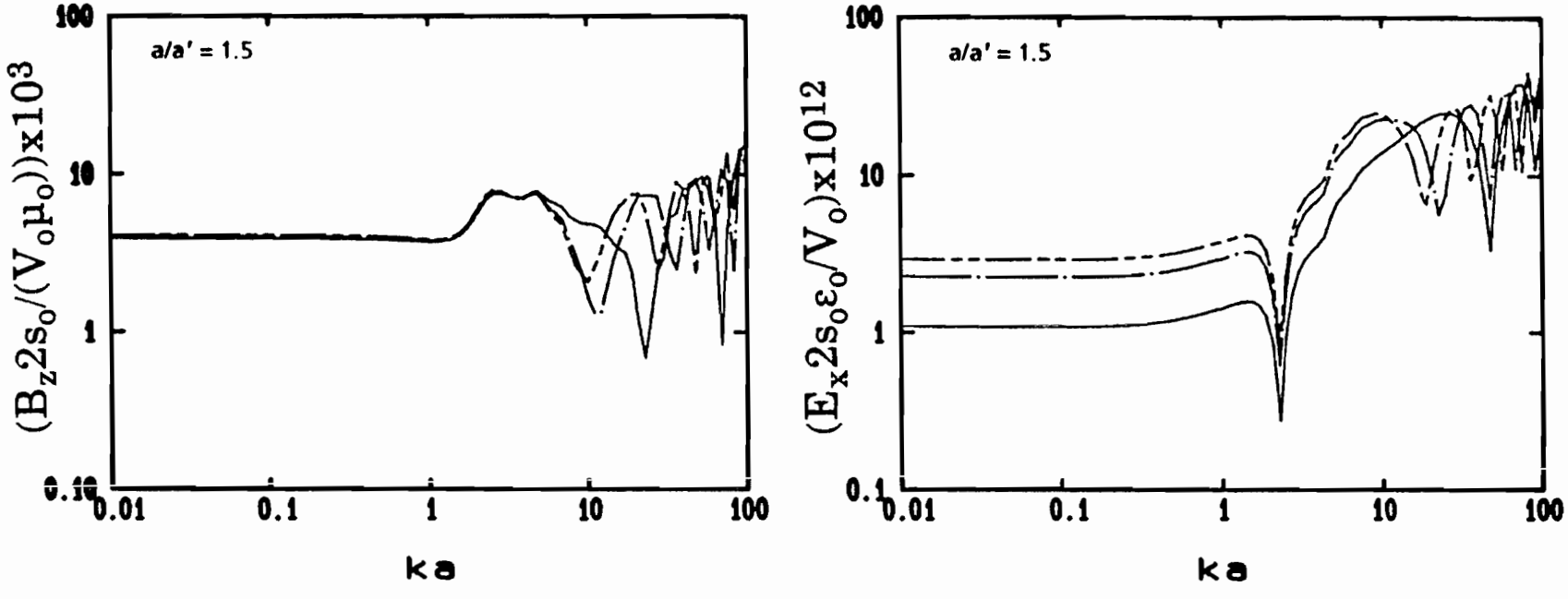

Figure 45. Principal field components of ELLIPTICUS calculated at x/a = 0, z/a = 0 and

_____ y/a' = 0.1

_____ . _____ y/a' = 0.2

____ _ _ _ ____ y/a' = 0.25

Source is at v = 90° with image at v = 270°. ELLIPTICUS geometry: $\xi_o = 1.34$, a/b = $2x10^4$, $R_o = 1.02\,\eta_o \ln[s_o/2\pi b)]$. Magnetic field has units of Siemens, electric field has units of Farad/meter.

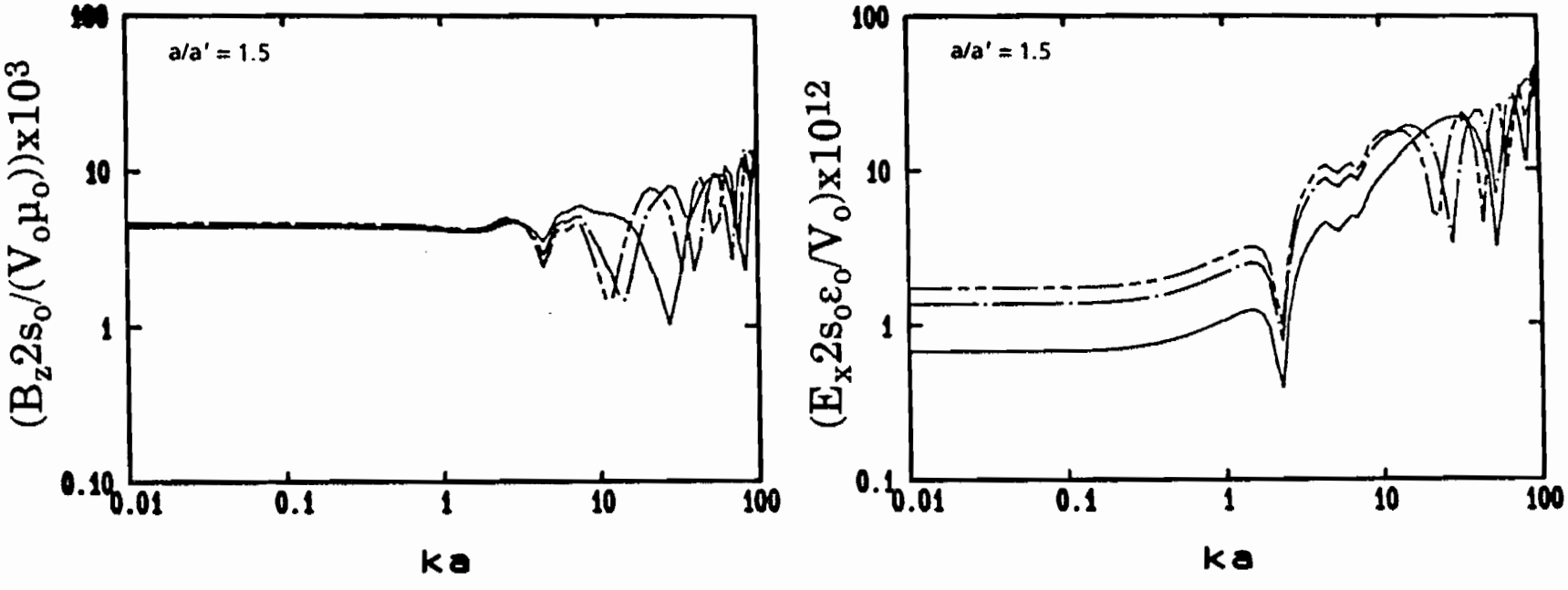

Figure 46. Principal field components of ELLIPTICUS calculated at x/a = 0.37, z/a = 0 and

——————— y/a' = 0.1

———.——— y/a' = 0.2

——— — — ——— y/a' = 0.25

Source is at v = 90° with image at v = 270°. ELLIPTICUS geometry: $\xi_o = 1.34$, $a/b = 2x10^4$, $R_o = 1.02\,\eta_o \ln[s_o/2\pi b)]$. Magnetic field has units of Siemens, electric field has units of Farad/meter.

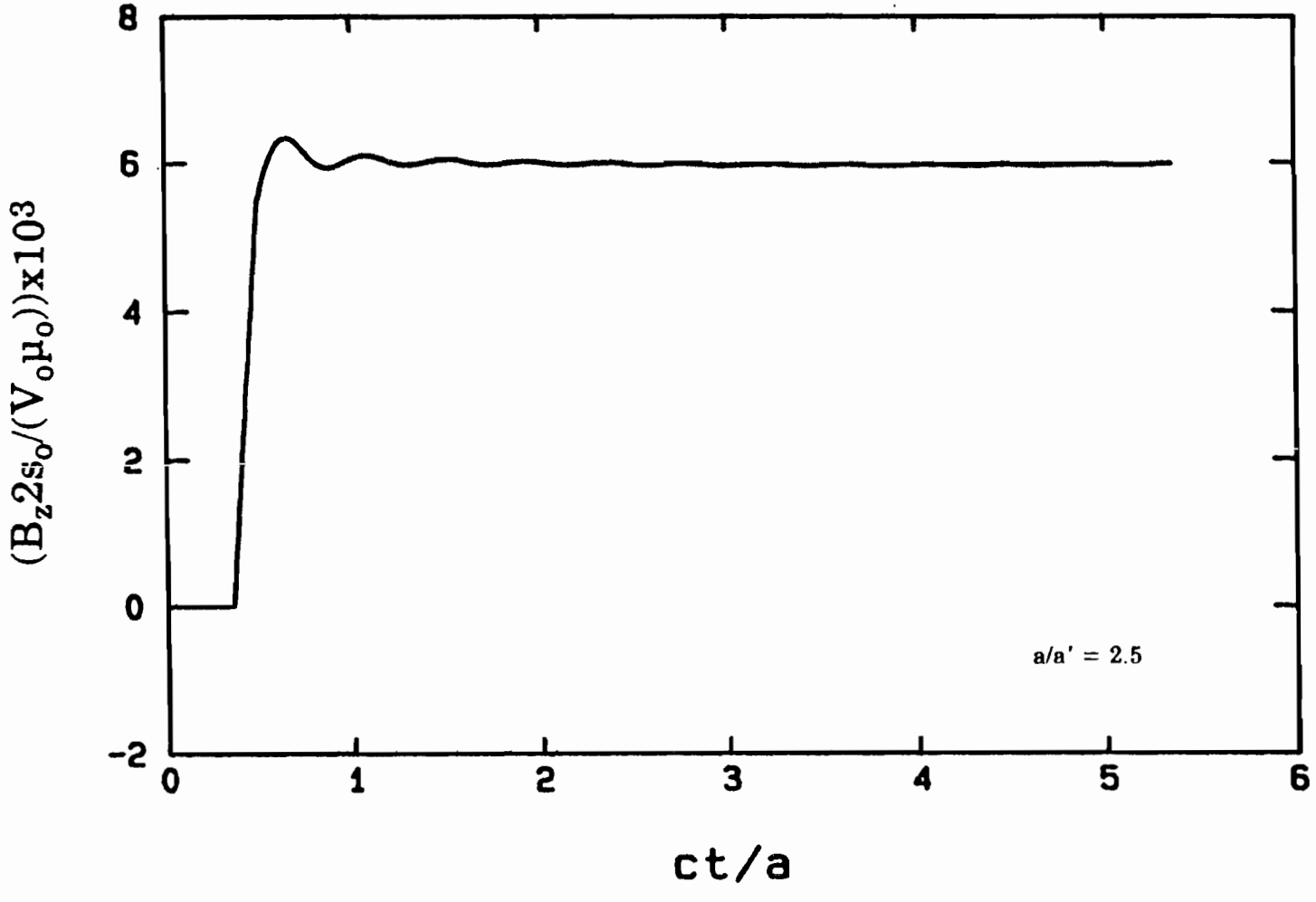

Figure 47. ELLIPTICUS: B_z time domain response to step function excitation at $v = 90^\circ$ plus image at $v = 270^\circ$. Calculation at $x/a = 0$, $y/a' = 0.1$, $z/a = 0$. ELLIPTICUS geometry: $\xi_0 = 1.09$, $a/b = 4.7x10^4$, $R_0 = 0.78\ \eta_0 \log(s_0/2nb)$. Magnetic field has units of Siemens.

Note: Peak values might not be calculated correctly due to high frequency truncation when performing inverse Fourier transform.

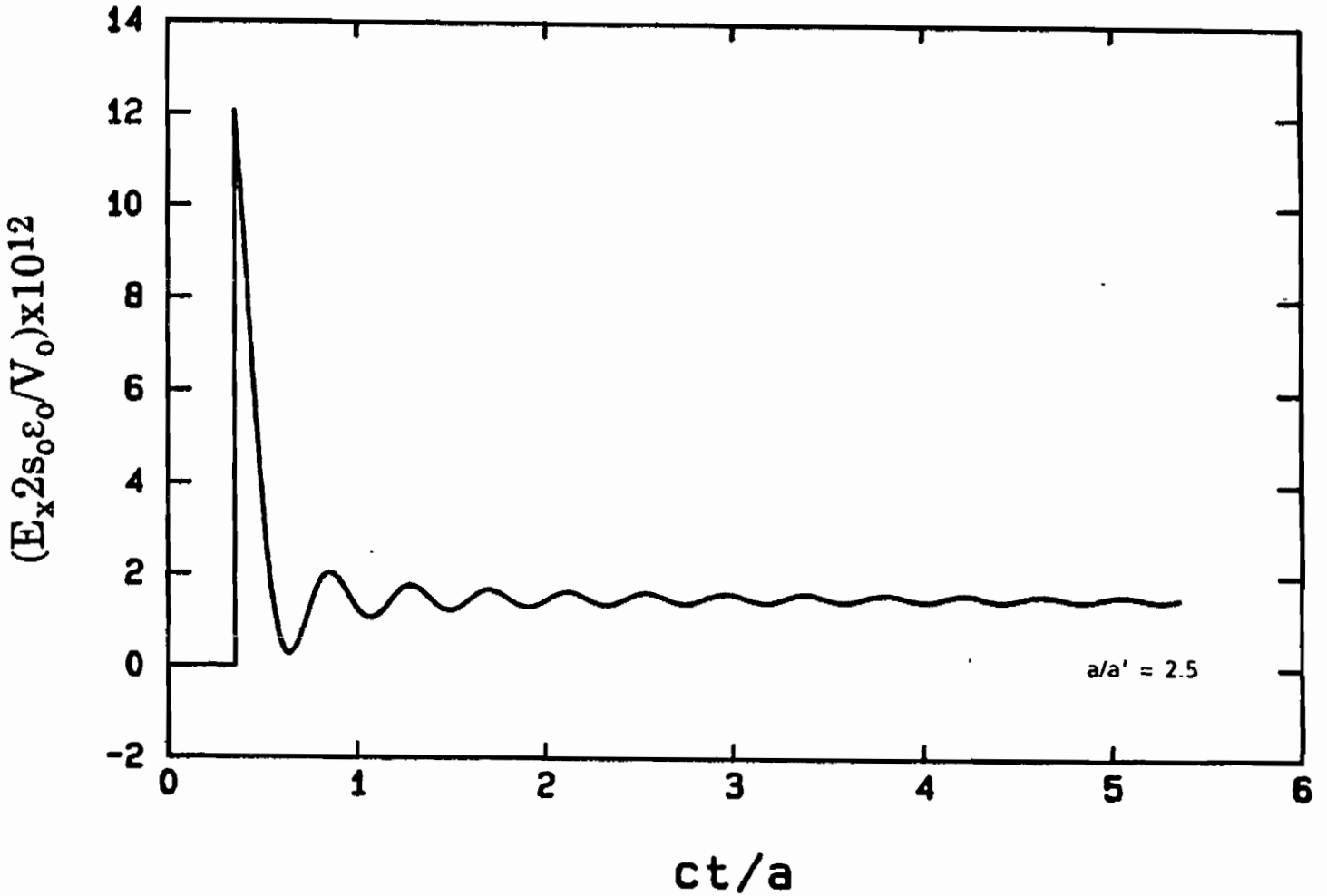

Figure 48. ELLIPTICUS: E_x time domain response to step function excitation at $v = 90°$ plus image at $v = 270°$. Calculation at $x/a = 0$, $y/a' = 0.1$, $z/a = 0$. ELLIPTICUS geometry: $\xi_o = 1.09$, $a/b = 4.7x10^{4}$, $R_o = 0.78\,\eta_o \log(s_o/2\pi b)$. Electric field has units of Farad/meter.

Note: Peak values might not be calculated correctly due to high frequency truncation when performing inverse Fourier transform.

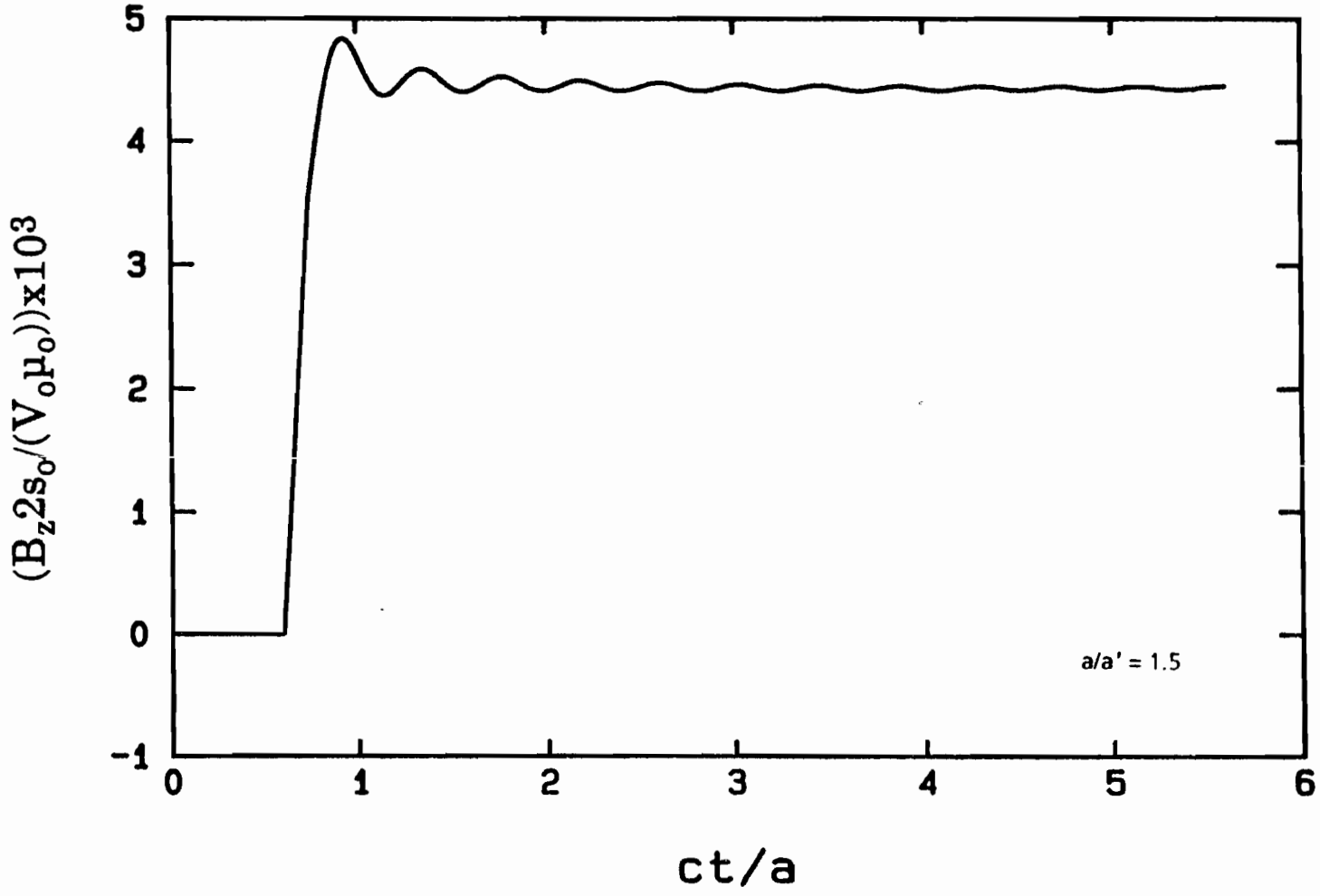

Figure 49. ELLIPTICUS: B_z time domain response to step function excitation at $v = 90°$ plus image at $v = 270°$. Calculation at $x/a = 0$, $y/a' = 0.1$, $z/a = 0$. ELLIPTICUS geometry: $\xi_o = 1.34$, $a/b = 2x10^4$, $R_o = 0.91\ \eta_o \log(a/b)$. Magnetic fields has units of Siemens.

Note: Peak values might not be calculated correctly due to high frequency truncation when performing inverse Fourier transform.

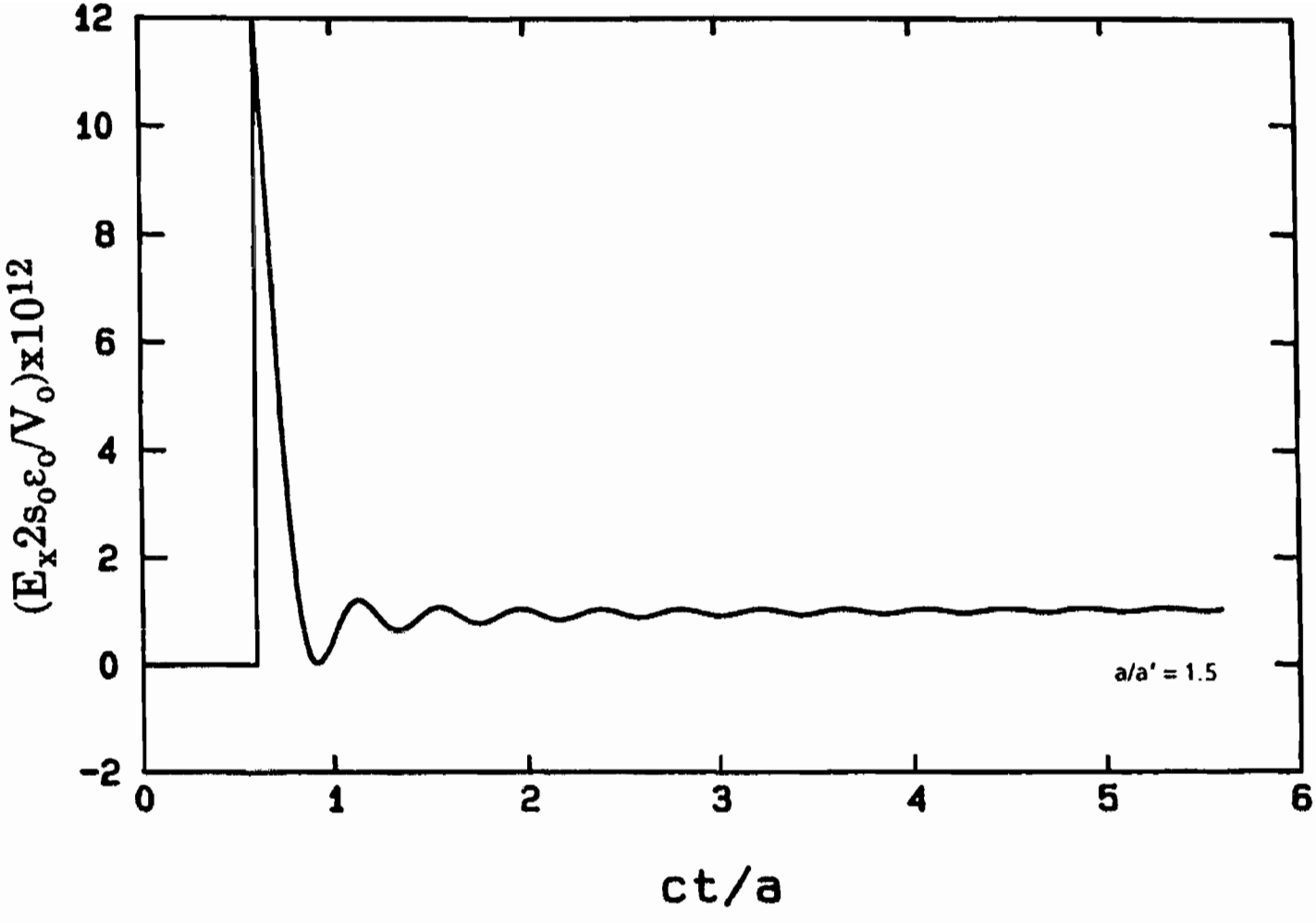

Figure 50. ELLIPTICUS: E_x time domain response to step function excitation at v = 90° plus image at v = 270°. Calculation at x/a = 0, y/a' = 0.1, z/a = 0. ELLIPTICUS geometry: $\xi_o = 1.34$, a/b = $2x10^4$, $R_o = 0.91\ \eta_o \log(a/b)$. Electric field has units of Farad/meter.

Note: Peak values might not be calculated correctly due to high frequency truncation when performing inverse Fourier transform.

$$\bar{B}(t) = -\frac{1}{2\pi}\int_{-\infty}^{+\infty} \bar{B}(ka)\frac{Z_{in}C}{iZ_{in}\omega C - 1} e^{-\omega t} d\omega \qquad (114)$$

where $\bar{E}(ka)$ and $\bar{B}(ka)$ are the fields calculated at some points via Eqs. 70 through 100, with the current specified by Eq. 112. Calculations of Eqs. 113 and 114 were carried out at $x/a = 0$, $y/a' = 0.1$, $z/a = 0$ for the case $\xi_0 = 1.09, 1.34$, with two different values of C: 10^{-7} and 10^{-8} F. The results are presented in Figs. 51 and 52. It is noticed that both fields compared to those of Figs. 47 through 50, are strongly reduced because of the filtering effect, which is more pronounced the smaller the capacitance (i.e. the higher the impedance). For completeness a calculation of the above field response for a TORUS was also performed and the results are illustrated in Fig. 53. Similar features to those of Figs. 51 and 52 are observed.

2.2.2 Two-norm Errors

Two-norm errors for the principal field components were also calculated according to Eqs. 108 and 109 and the results are reported in Figs. 54 and 55. Comparing these curves with those of Fig. 17 obtained for the TORUS one should notice that at very low frequency the 2-norm error for E_x is much larger for the ELLIPTICUS than for the TORUS. In particular, for the case $\xi_0 = 1.09$ the low frequency value is about one order of magnitude higher than that of the TORUS. This is explained by the higher variation of the electric field along x shown by the elliptical geometry over the toroidal one, as illustrated in Fig. 43.

2.3 PARAMETRIC STUDIES FOR ELLIPTICUS DESIGN

In most of the calculations presented so far it was assumed that the uniform loading resistance is $R_0 = G_0 \eta_0 \ln[s_0/2\pi b)]$ with G_0, plotted in Fig. 22, determined in order to achieve $E_y/H_z = 377\Omega$ at the center, at low frequency, for the case of a single δ-gap generator placed at $v = 0^\circ$. To analyze the field behavior as a function of the loading resistance, various values of G_0, other than those of Fig. 22, were considered, and the results are presented in Figs. 56, 57 for the case $\xi_0 = 1.09$, $a/b = 4.7 \times 10^4$ and in Figs. 58, 59 for the case when $\xi_0 = 1.09$, $a/b = 10^2$. In both cases the value $G_0 = 0.78$ is that obtained when Eq. 106 holds. One can notice that, by increasing the loading resistance, the first resonance in both the E and B fields is slightly attenuated, while the first anti-resonance becomes sharper. The higher order resonances tend to decrease also. One question arises regarding the correctness of the asymptotic antenna theory model, since the radiation loss has not been accounted for in our calculations. Such effect, which manifests itself as a frequency-dependent resistance is likely to affect the antenna performance in the neighborhood of the first resonance and anti-

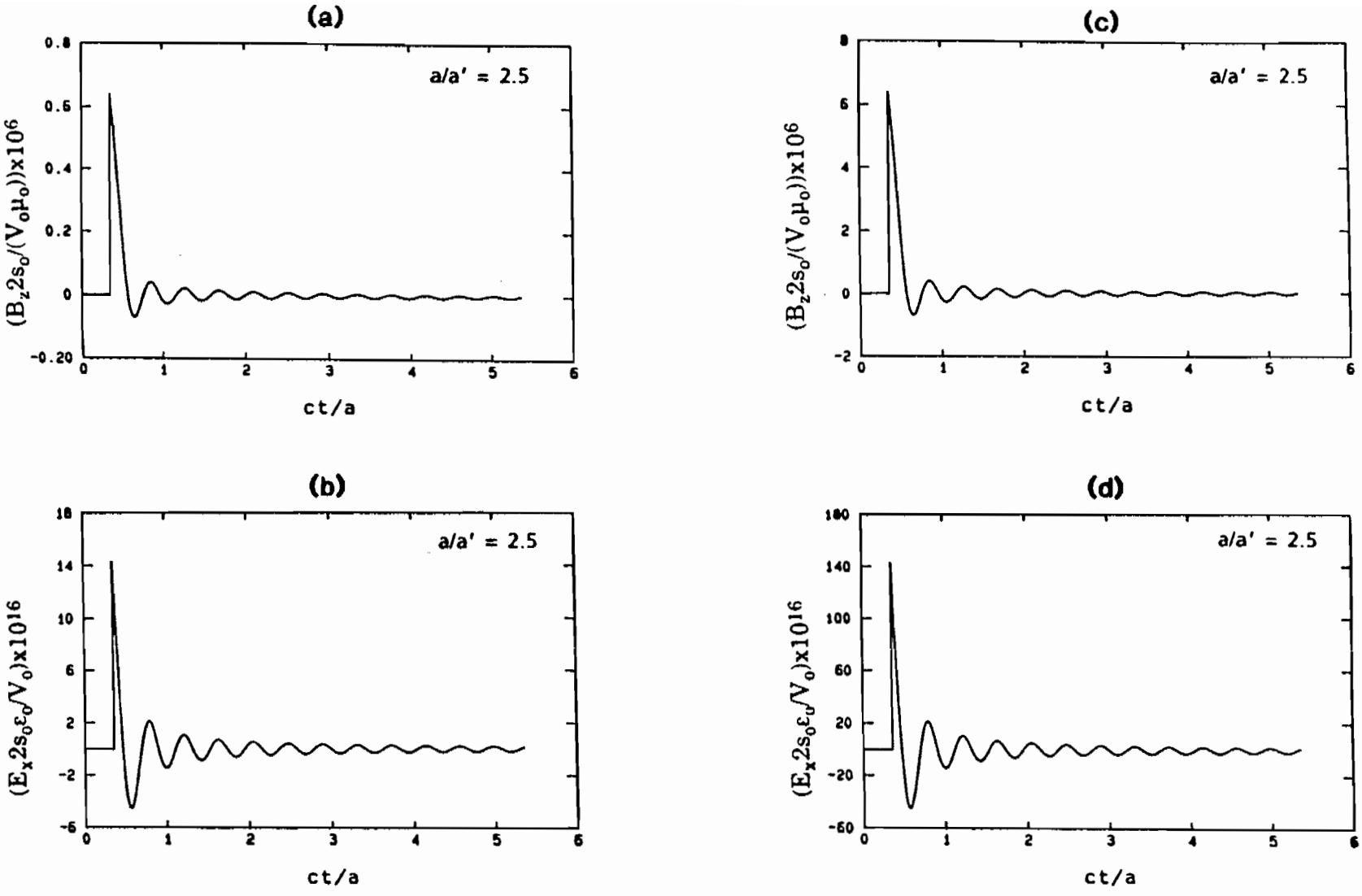

Figure 51. ELLIPTICUS: Time domain response to step function for the case of a source capacitance (a), (b) $C = 10^{-8}$ F; (c), (d) $C = 10^{-7}$ F. Calculation at $x/a = 0$, $y/a' = 0.1$, $z/a = 0$, $\xi_0 = 1.09$, $a/b = 4.7x10^4$, $R_0 = 0.78\eta_0 \ln(a/b)$. Source at $v = 90°$ with image at $v = 270°$. Magnetic field has units of Siemens, electric field has units of Farad/meter.

Note: Peak values might not be calculated correctly due to high frequency truncation when performing inverse Fourier transform.

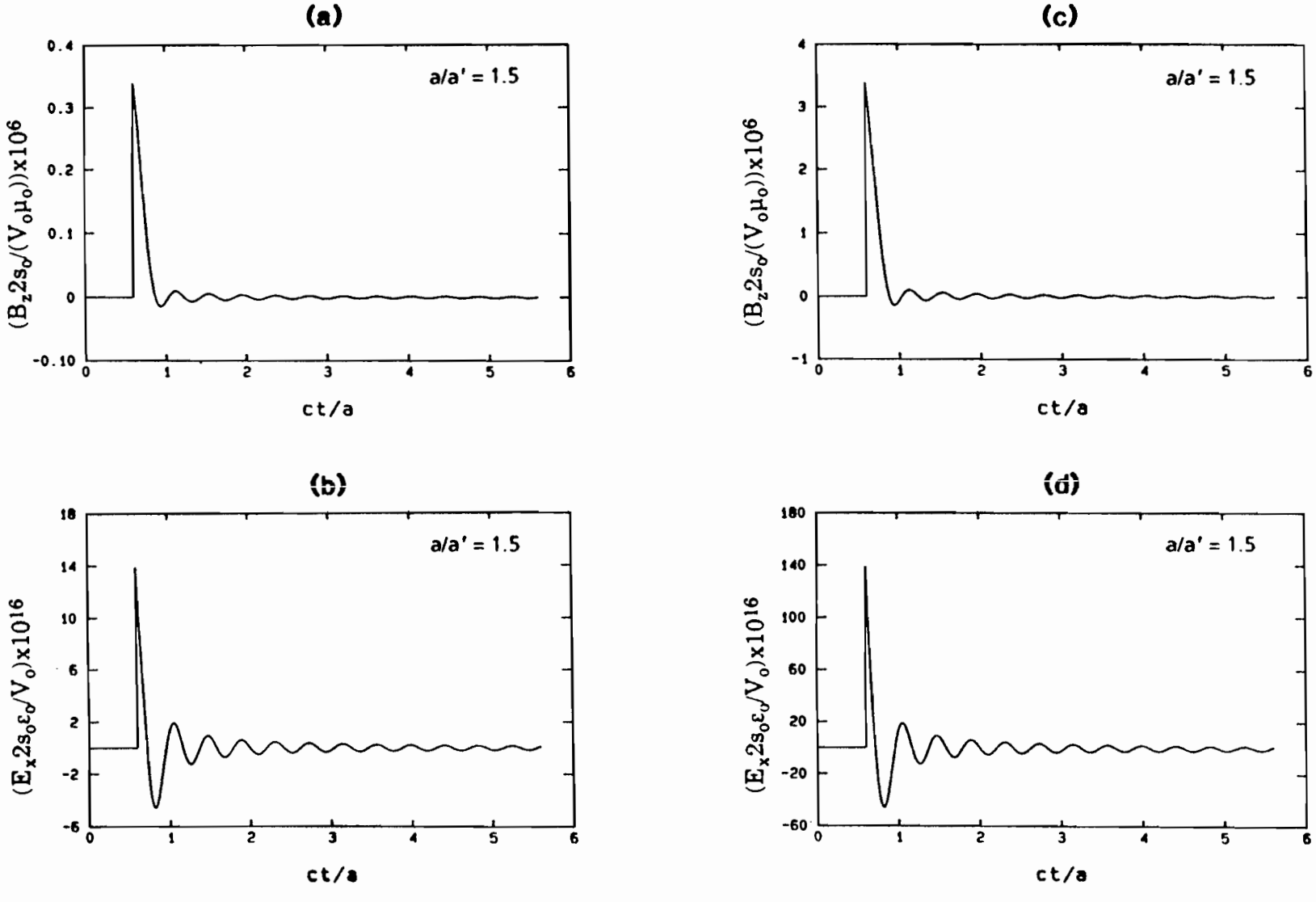

Figure 52. ELLIPTICUS: Time domain response to step function for the case of a source capacitance (a), (b) $C = 10^{-8}$ F; (c), (d) $C = 10^{-7}$ F. Calculation at $x/a = 0$, $y/a' = 0.1$, $z/a = 0$, $\xi_0 = 1.34$, $a/b = 2x10^4$, $R_0 = 0.91\eta_0 \ln(a/b)$. Source at $v = 90°$ with image at $v = 270°$. Magnetic field has units of Siemens, electric field has units of Farad/meter.

Note: Peak values might not be calculated correctly due to high frequency truncation when performing inverse Fourier transform.

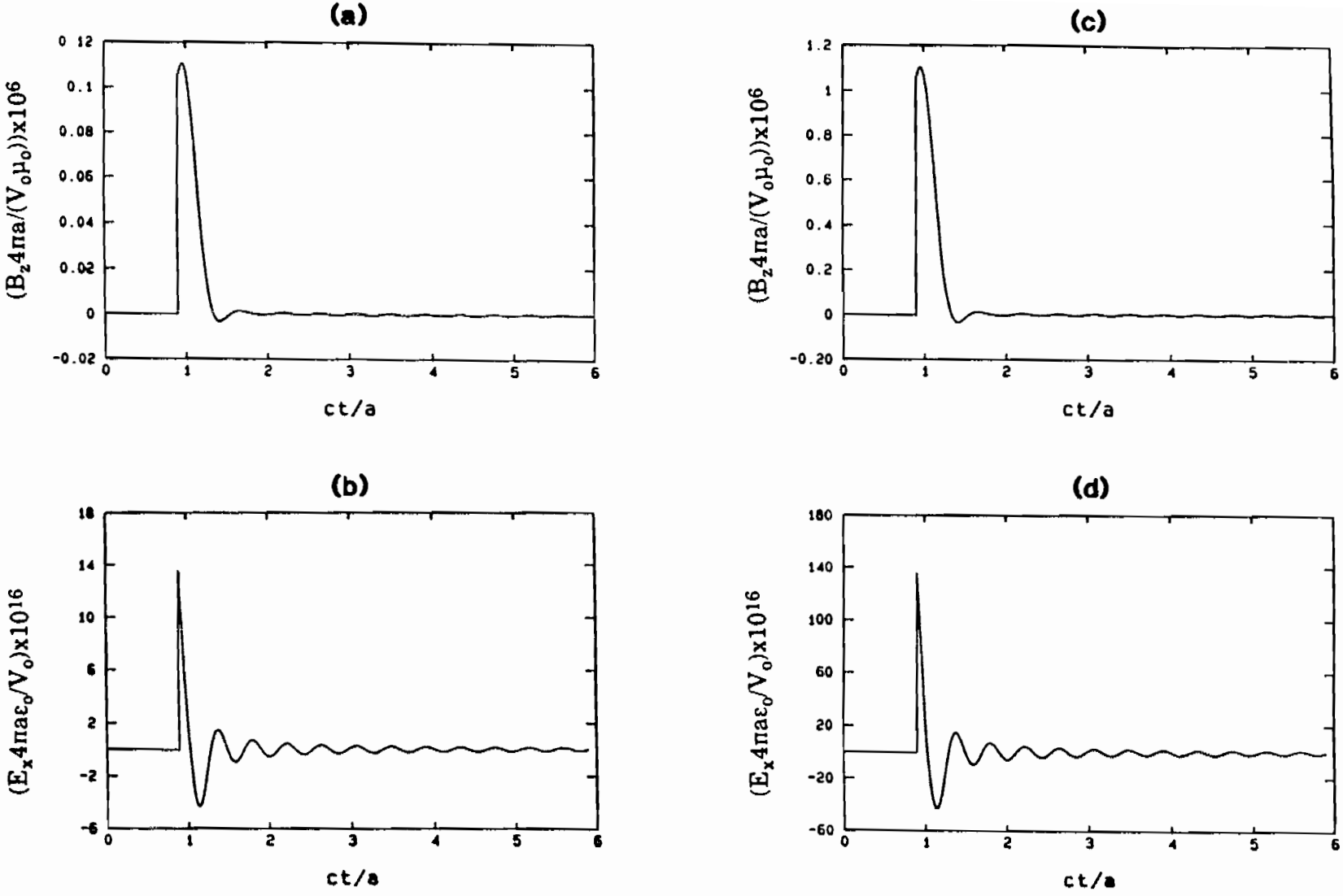

Figure 53. TORUS: Time domain response to step function for the case of a source capacitance (a), (b) $C = 10^{-8}$ F; (c), (d) $C = 10^{-7}$ F. Calculation at $x/a = 0$, $y/a = 0.1$, $z/a = 0$, $a/b = 10^3$, $R_0 = \eta_0 \ln(a/b)$. Source at $\phi = 0°$ with image at $\phi = 270°$. Magnetic field has units of Siemens, electric field has units of Farad/meter.

Note: Peak values might not be calculated correctly due to high frequency truncation when performing inverse Fourier transform.

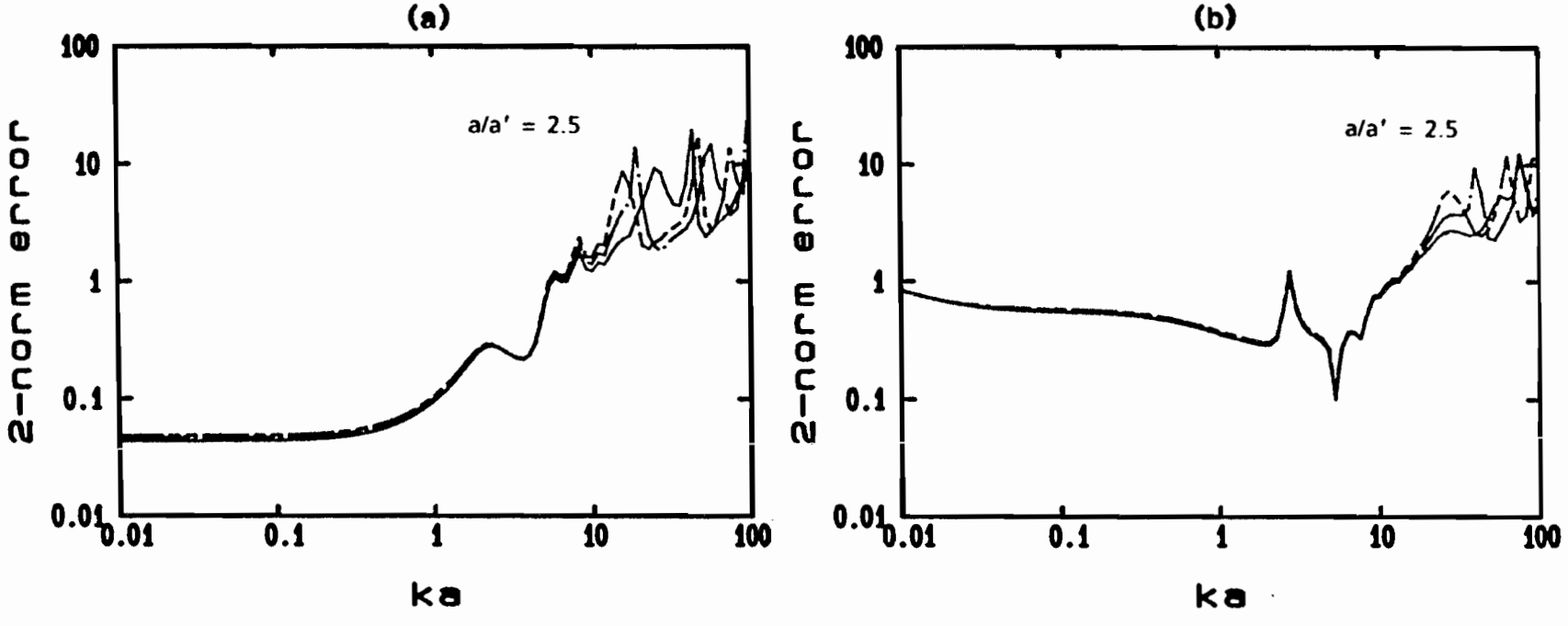

Figure 54. ELLIPTICUS: 2-norm error calculated according to Eq. 108 (a) B_z; (b) E_x. Source is located at v = 90° with image at v = 270°. ELLIPTICUS geometry: $\xi_0 = 1.09$, $a/b = 4.7 \times 10^4$, $R_0 = 0.78\eta_0 \ln[s_0/(2\pi b)]$.

-0.46 < x/a < 0.46 , z/a = 0 and

_____ y/a = 0.1

_____ y/a = 0.2

_____ y/a = 0.25

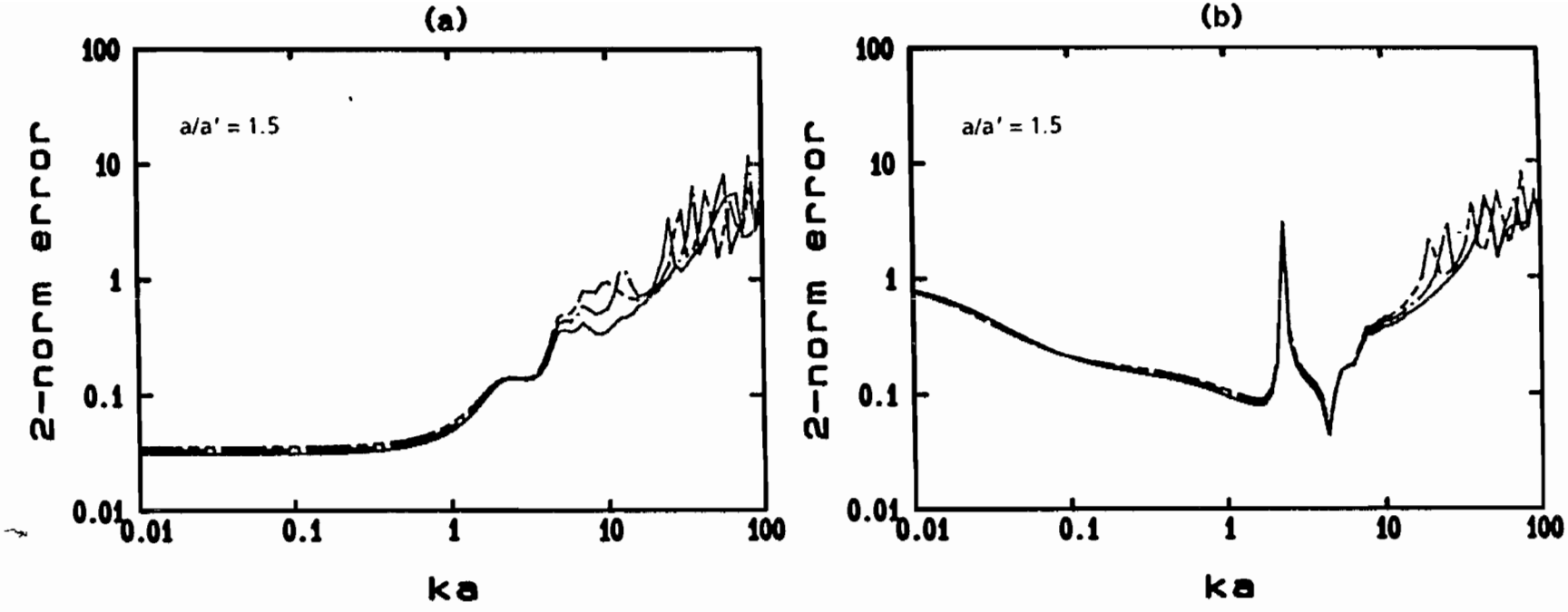

Figure 55. ELLIPTICUS: 2-norm error calculated according to Eq. 108 (a) B_z; (b) E_x. Source is located at $v = 90^\circ$ with image at $v = 270^\circ$. ELLIPTICUS geometry: $\xi_0 = 1.34$, $a/b = 2x10^4$, $R_0 = 0.91\eta_0 \ln[s_0/(2nb)]$.

$-0.37 < x/a < 0.37$, $z/a = 0$ and

_____ $y/a' = 0.1$

_____ $y/a' = 0.2$

_____ $y/a' = 0.25$

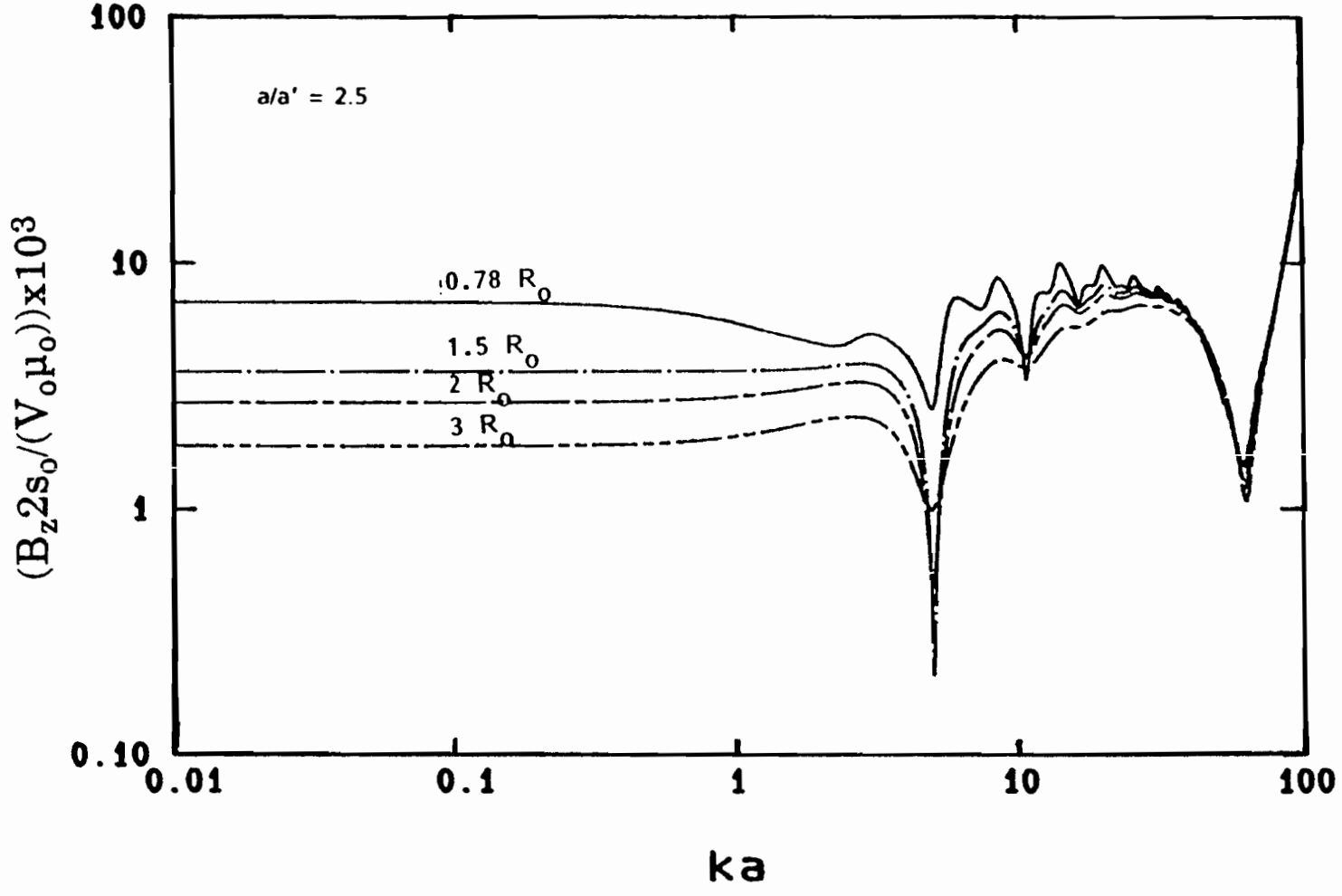

Figure 56. B_z of ELLIPTICUS ($\xi_0 = 1.09$) at x/a = 0.46, y/a' = 0.1, z/a = 0 as a function of the antenna loading resistance. $R_o = \eta_o \ln(s_o/(2\pi b))$. Source at v = 90° with image at v = 270°, a/b = 4.7×10^4. Magnetic field has units of Siemens.

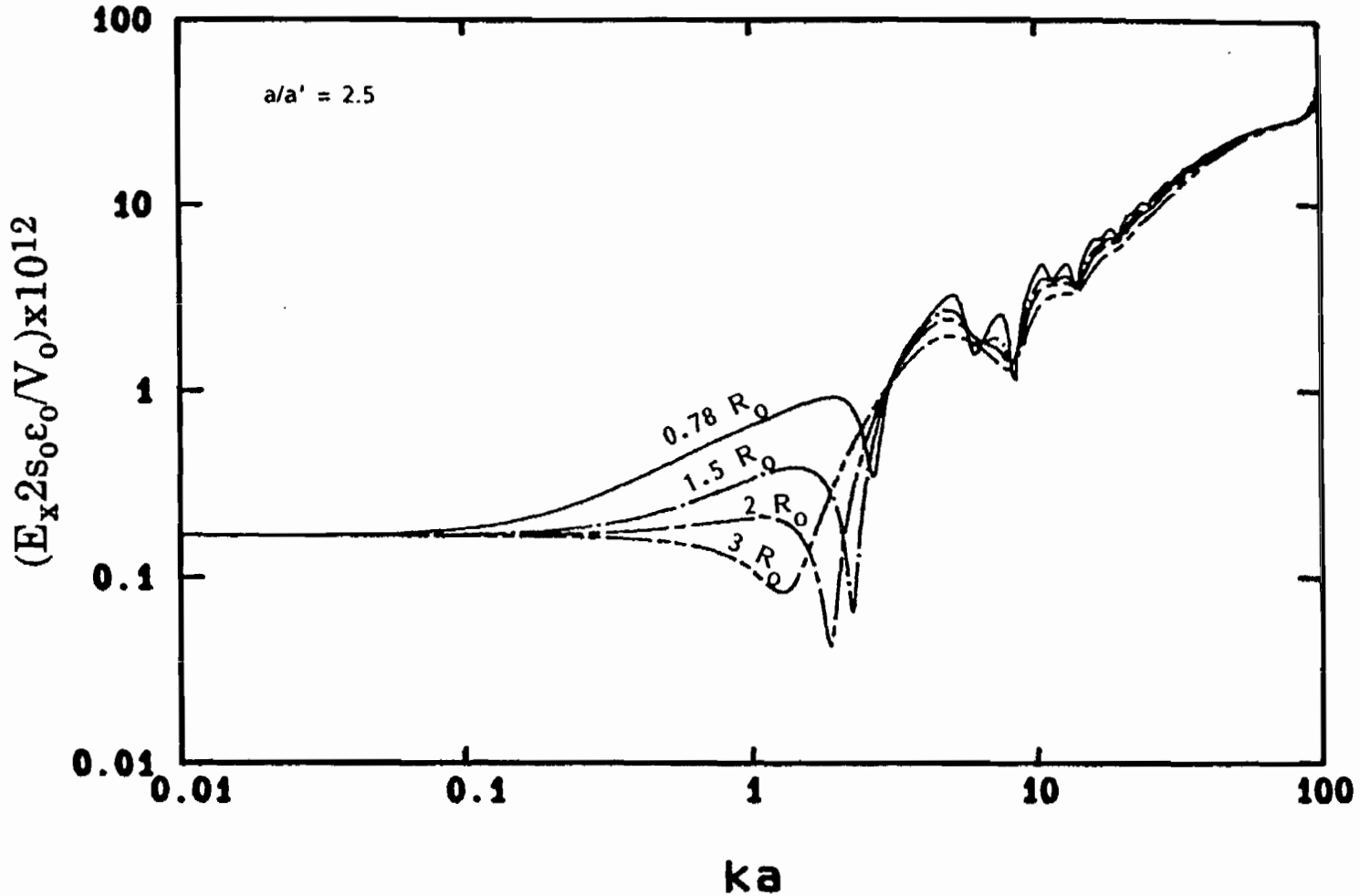

Figure 57. E_x of ELLIPTICUS ($\xi_0 = 1.09$) at $x/a = 0.46$, $y/a' = 0.1$, $z/a = 0$ as a function of the antenna loading resistance. $R_o = \eta_0 \ln(s_o/(2\pi b))$. Source at $v = 90^\circ$ with image at $v = 270^\circ$, $a/b = 4.7 \times 10^4$. Electric field has units of Farad/meter.

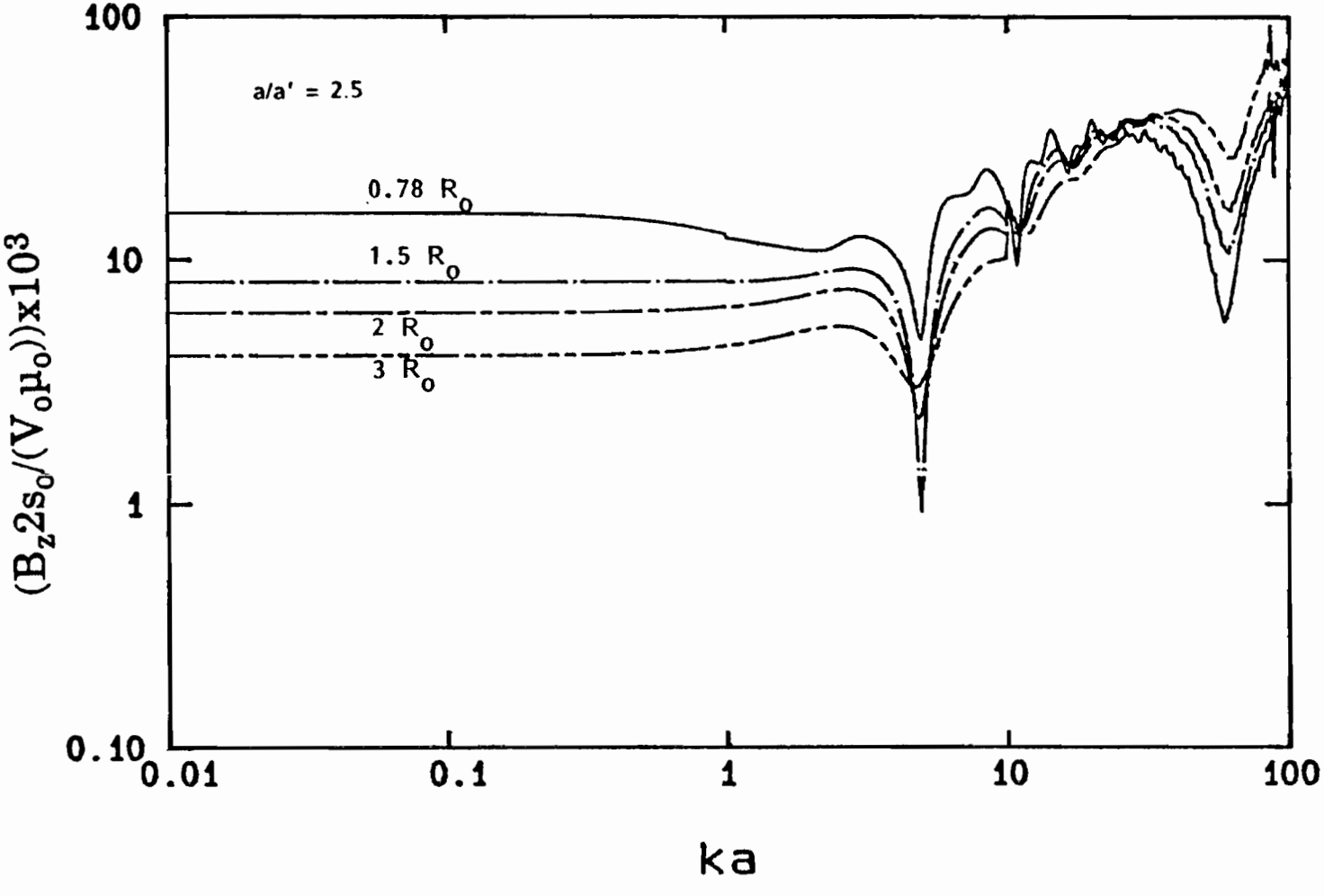

Figure 58. B_z of ELLIPTICUS ($\xi_0 = 1.09$) at $x/a = 0.46$, $y/a' = 0.1$, $z/a = 0$ as a function of the antenna loading resistance. $R_o = \eta_o \ln(s_o/(2\pi b))$. Source at $v = 90°$ with image at $v = 270°$, $a/b = 10^2$. Magnetic field has units of Siemens.

Note: Because $a/b = 10^2$ asymptotic antenna theory breaks down when ka approaches 10.

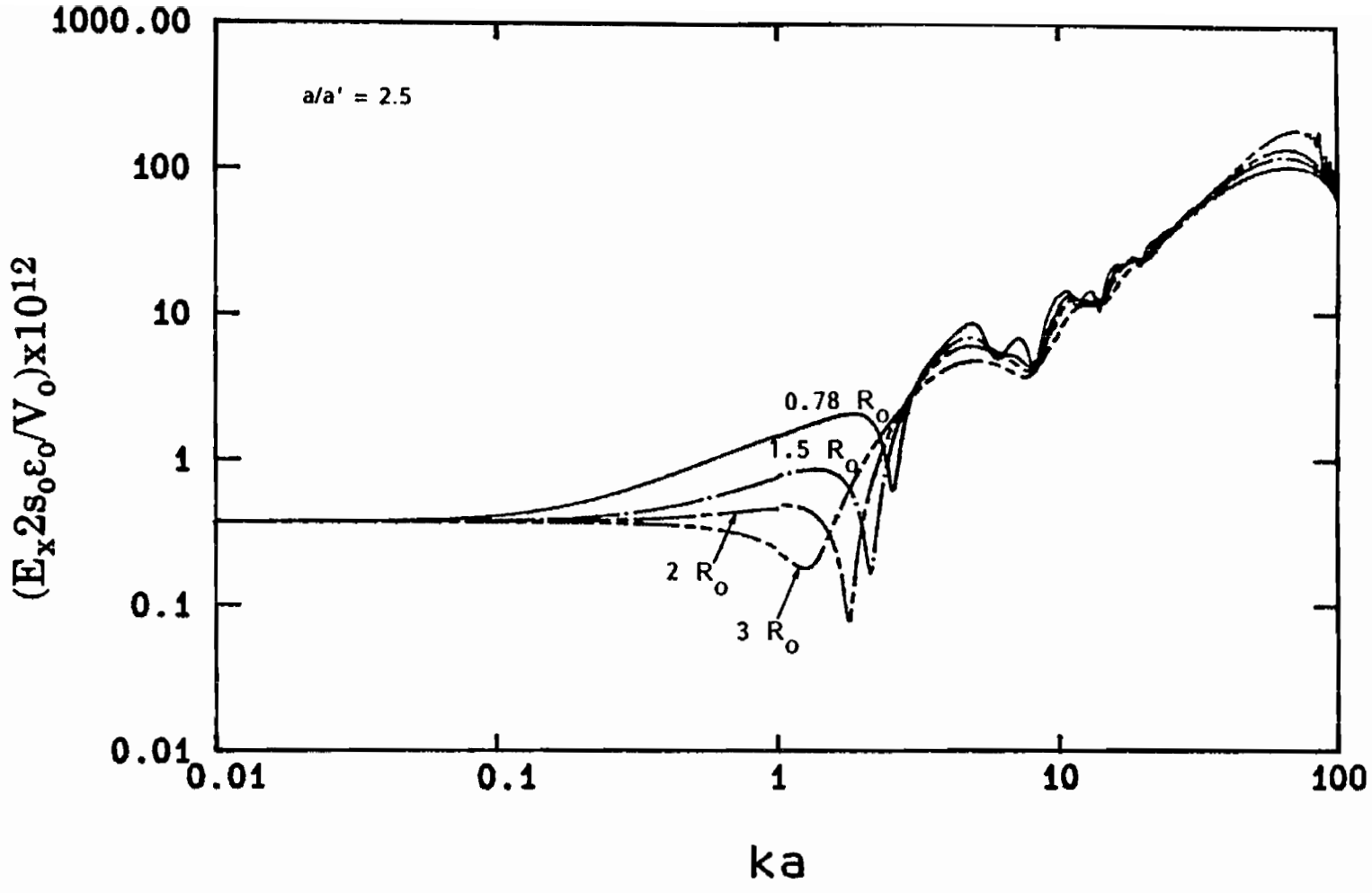

Figure 59. E_x of ELLIPTICUS ($\xi_o = 1.09$) at x/a = 0.46, y/a' = 0.1, z/a = 0 as a function of the antenna loading resistance. $R_o = \eta_o \ln(s_o/(2\pi b))$ Source at v = 90° with image at v = 270°, a/b = 10^2. Electric field has units of Farad/meter.

Note: Because a/b = 10^2 asymptotic antenna theory breaks down when ka approaches 10.

resonance. However, accounting for this effect analytically is very difficult and this effort goes beyond the scope of the present analysis.

Another limitation of the model rests in the assumption of a perfectly conducting ground. In reality the ground has a finite conductivity, typically $\sigma = 10^{-3}$S/m and is also characterized by an electric relative permittivity, $\varepsilon_r = 15$. To account for this effect approximately, at points directly below the source, for instance at $x/a = 0$, $y/a' = 0.1, 0.2, 0.25$, $z/a = 0$, one can find the total field as given by an incident field, calculated assuming the antenna in free-space with a δ-gap source at $v = 90^o$, plus a reflected term. Such term is found by assuming that the incident field at the ground is reflected as though it were a plane wave. Considering the polarization of the fields it is obtained

$$E_x^{tot}(0, y/a', 0) = E_x^{inc}(0, y/a', 0) + R\,E_x^{inc}(0, 0, 0)e^{iky} \tag{115}$$

$$H_x^{tot}(0, y/a', 0) = H_z^{inc}(0, y/a', 0) - R\,H_z^{inc}(0, 0, 0)e^{iky} \tag{116}$$

where E_x^{inc}, H_z^{inc} are calculated using Eqs. 70 through 100 with a δ–gap source located at $v = 90^o$. The Fresnel reflection coefficient R is given by

$$R = \frac{1 - \sqrt{\varepsilon_r(1 - \frac{\sigma}{i\omega\varepsilon})}}{1 + \sqrt{\varepsilon_r(1 - \frac{\sigma}{i\omega\varepsilon})}} \tag{117}$$

Equations 115 and 116 with 117 were calculated for the cases $\xi_0 = 1.09$ and 1.34 and the results are presented in Figs. 60 and 61. R_0 was that of Eq. 107. Therefore one can compare Figs. 60 and 61 to Figs. 37 and 39. It is noted that the effect of the finite ground conductivity results in a smoother field behavior. On the other hand at low frequency this model does not give, at these points, the same results as those obtained for the perfectly conducting ground. The discrepancies might be attributed to the approximation involved in the model described by Eqs. 115, 116 and 117. Nevertheless, it is stressed that the smoother field behavior, particularly at high frequency, is a true indication of the performances of a system on a realistic ground.

To further analyze the effect of the antenna thickness on its performance, Figs. 62 and 63 present the fields calculated at the point $x/a = 0$. $y/a' = 0.1$, $z/a = 0$ for different values of the ratio a/b, for the two elliptical geometries of concern here. It is noted that the field values are higher the lower the

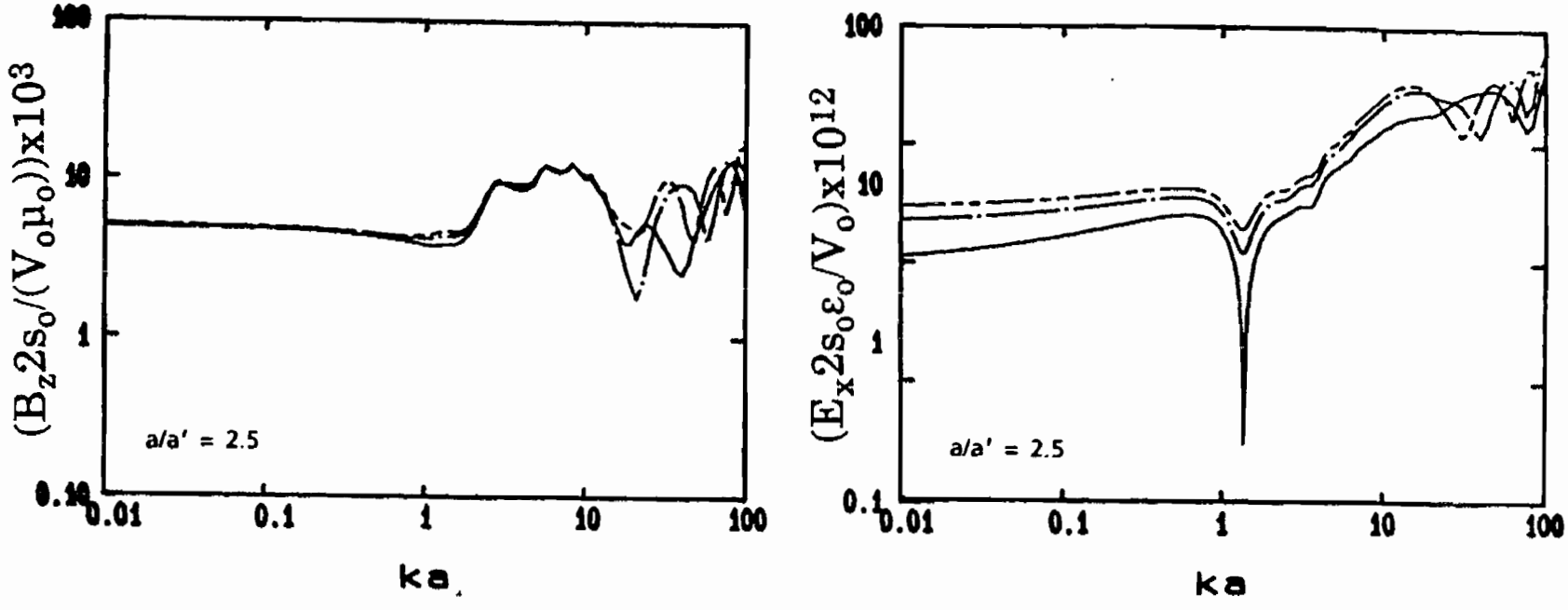

Figure 60. Principal field components of ELLIPTICUS calculated at x/a = 0, z/a = 0 and

_____ y/a' = 0.1

_____ y/a' = 0.2

_____ y/a' = 0.25

Source is at v = 90° and finite conductivity of the soil is accounted for with $\sigma = 10^{-3}$ S/m, $\varepsilon_r = 15$. ELLIPTICUS geometry: $\xi_0 = 1.09$, $a/b = 4.7x10^4$, $R_o = 0.78\ \ln[s_o/(2\pi b)]$. Magnetic field has units of Siemens, electric field has units of Farad/meter.

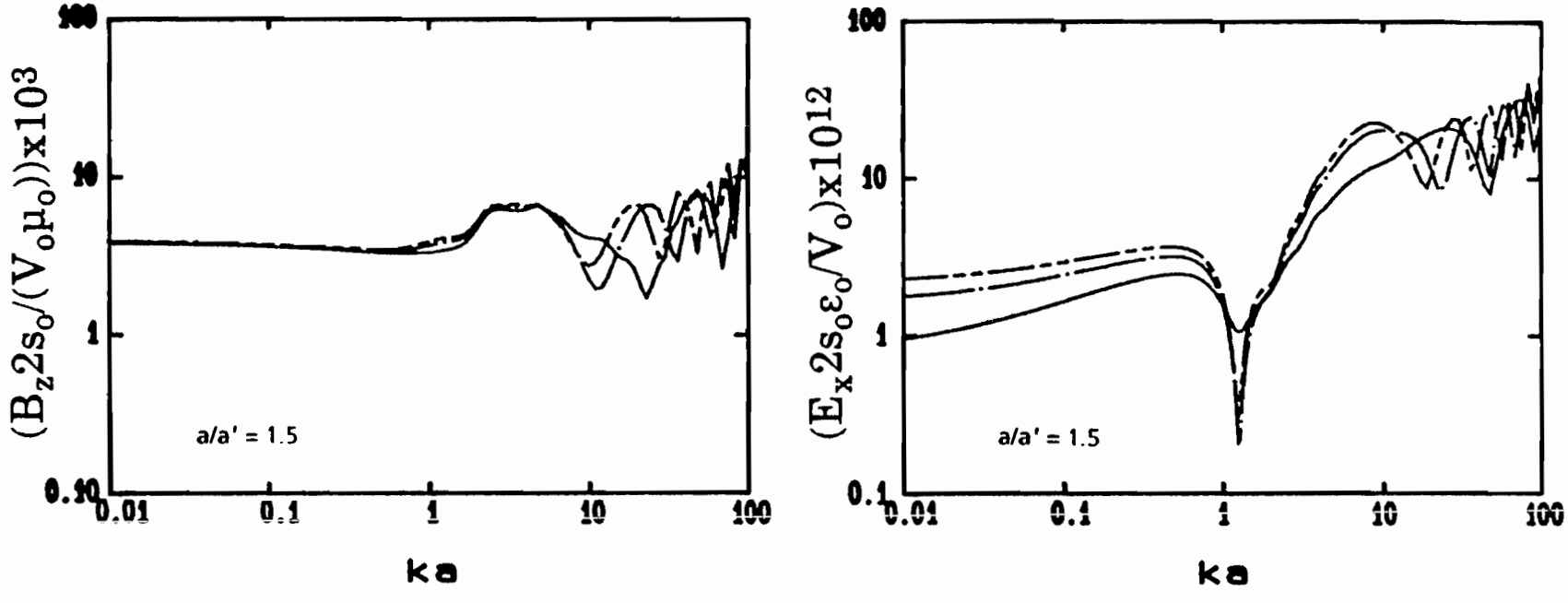

Figure 61. Principal field components of ELLIPTICUS calculated at x/a = 0, z/a = 0 and

_____ y/a' = 0.1

_____ . _____ y/a' = 0.2

_____ _ _ _ _____ y/a' = 0.25

Source is at v = 90° and finite conductivity of the soil is accounted for with $\sigma = 10^{-3}$ S/m, $\varepsilon_r = 15$. ELLIPTICUS geometry: $\xi_o = 1.34$, $a/b = 2x10^4$, $R_0 = 0.91\eta_0 \ln[s_0/(2nb)]$. Magnetic field has units of Siemens, electric field has units of Farad/meter.

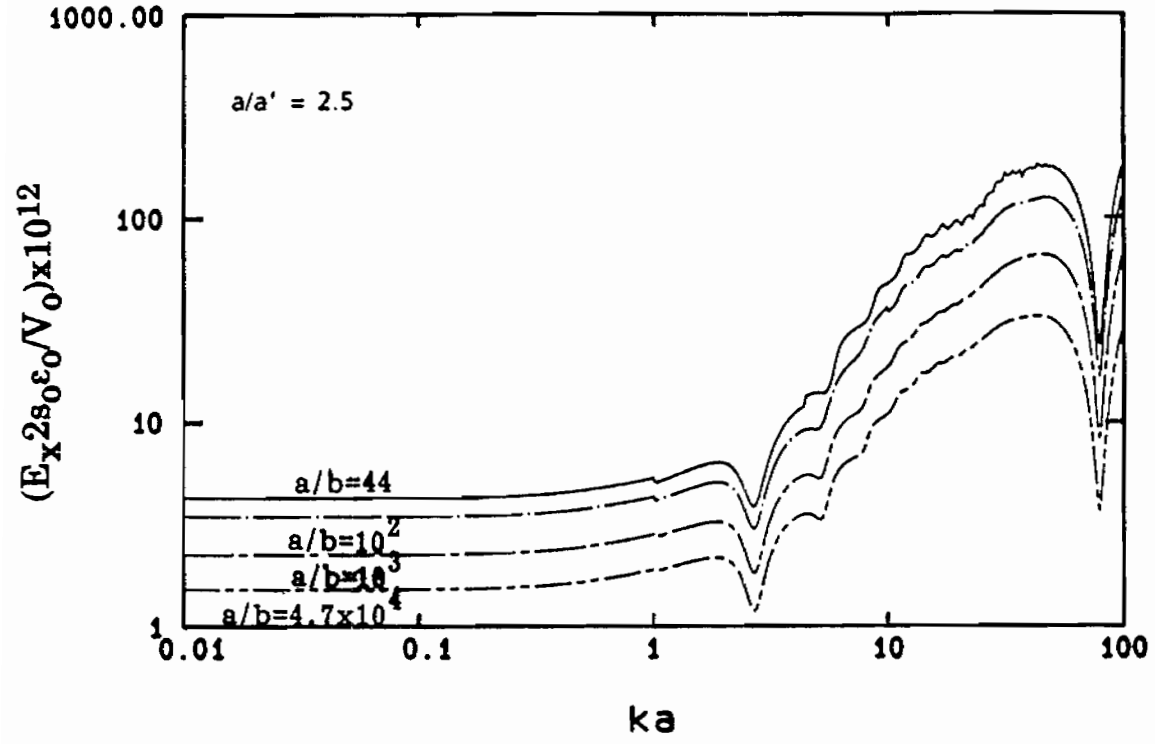

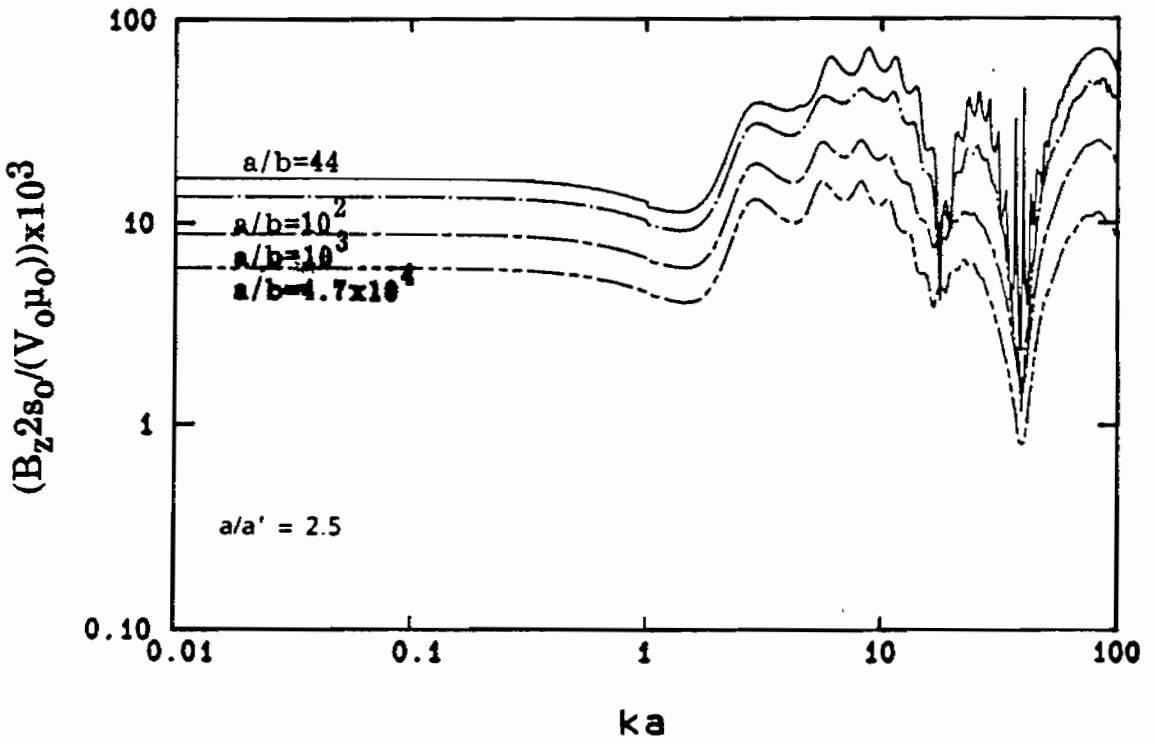

Figure 62. ELLIPTICUS: Field calculations at x/a = 0, y/a' = 0.1, z/a = 0 for different values of a/b. In above curves $\xi_o = 1.09$, $R_o = 0.78\,\eta_o\,\ln(a/b)$. Source is at v = 90° with image at v = 270°. Magnetic field has units of Siemens, electric field has units of Farad/meter.

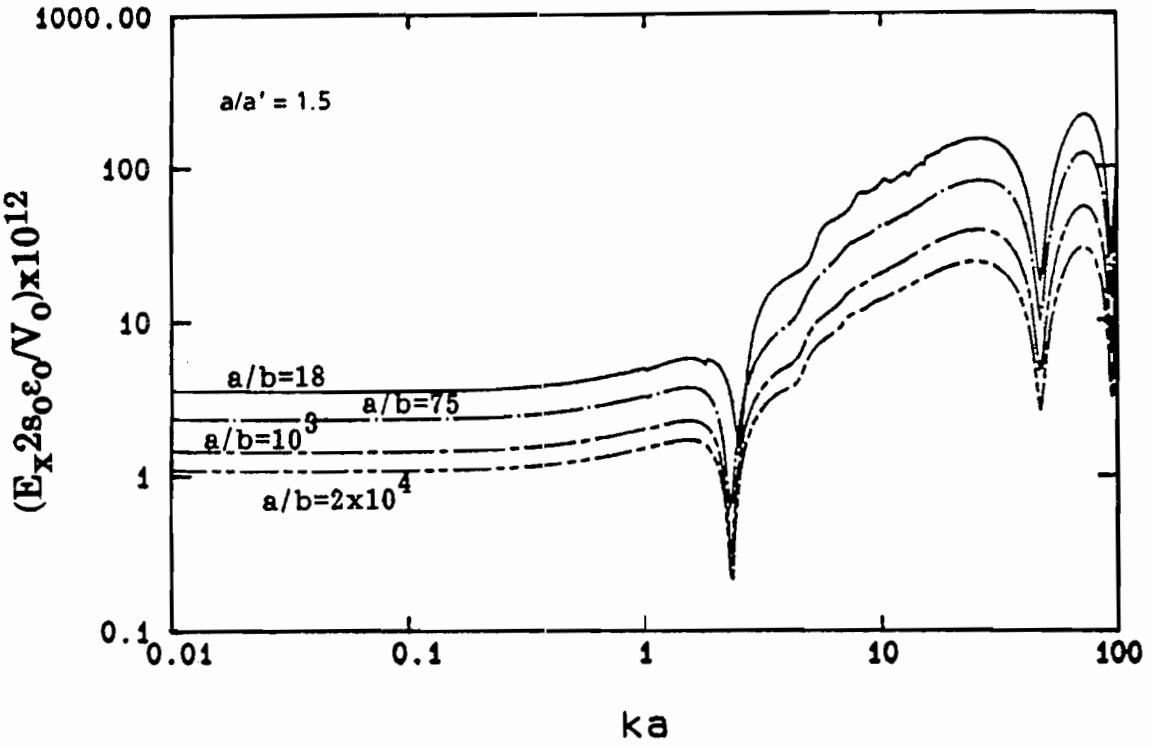

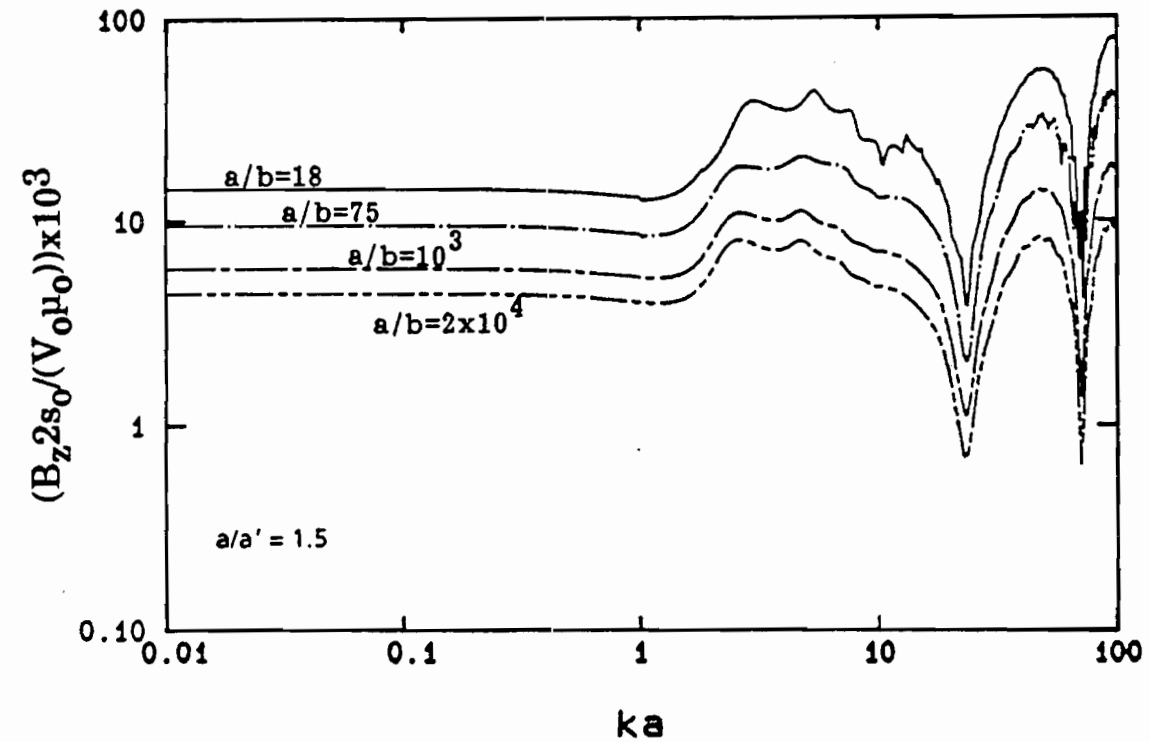

Figure 63. ELLIPTICUS: Field calculations at x/a = 0, y/a' = 0.1, z/a = 0 for different values of a/b. In above curves $\xi_0 = 1.34$, $R_e = 0.91\ \eta_0 \log(s_0/(2\pi b))$. Source is at $v = 90^\circ$ with image at $v = 270^\circ$. Magnetic field has units of Siemens, electric field has units of Farad/meter.

a/b ratio. This is due to the decreasing amplitude of γ and of R_0 which result in a current increase, for a fixed voltage source. Apart from this, the trend of the fields is the same regardless of the a/b ratio. A further investigation was performed on the dependence of the fields on the antenna eccentricity ($1/\xi_0$). Figures 64 and 65 illustrate our findings for seven different values of ξ_0. In both figures the uppermost curve corresponds to a very high eccentricity, whereas the lowermost one corresponds to the case of a nearly circular antenna. The plots clearly show that the fields become smoother the lower the eccentricity, except at high frequency. However, depending on the antenna size, ka = 100 might correspond to frequencies already beyond the range of interest for this antenna's applications.

2.4 DISTRIBUTED SOURCE

Within the approximation of a thin elliptical antenna whose dimensions are much bigger than that of the source region, the issue of the distributed source can be handled in a totally analogous manner to that already discussed for the TORUS. In particular the same results apply to this case also. The reader can thus refer to Fig. 20 which illustrates the variation of the ratio E/H at the center as a function of the source region. Although the effect of the curvature was not taken into account, in any case the resulting variation is contained within a few percent of the value correspondent to the δ-gap generator case. Therefore, we shall not be furtherly concerned with this issue.

2.5 HIGH FREQUENCY CAPABILITIES

Recently people have become concerned with performing tests at increasingly higher frequencies. Therefore, the ability to predict the performances of simulators at frequencies as high as possible is useful both as alternative or in support of testing activities, such as test plan and data interpretation. The following question has been addressed in this note: what is the maximum frequency f_m at which the calculations presented here are still valid? The answer is: f_m less than $c/(2\pi b)$. For thin antennas this limit could be in the hundreds of MHz. Beyond this point the asymptotic antenna theory cannot be applied to this illuminator. Within this limit the theory provides results which are in good agreement with those of Ref. 1 for the TORUS, and also check satisfactorily with available measured data for the ELLIPTICUS. However one should bear in mind that this model rests on the further following assumptions and approximations

- a perfectly conducting ground is used
- radiation loss is not accounted for
- specific source features (i.e. shape, balun) are not considered

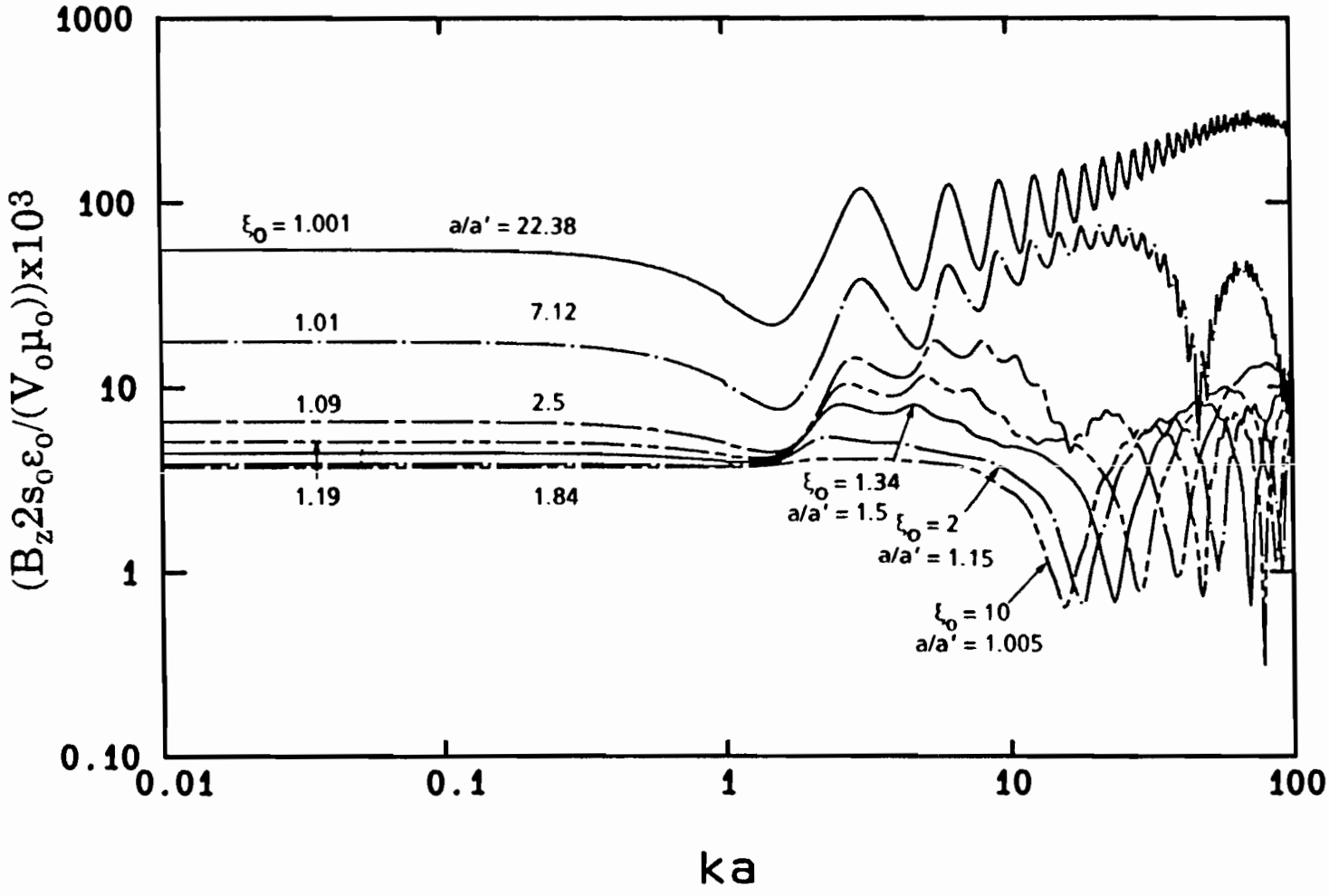

Figure 64. B_z of ELLIPTICUS of different eccentricities at x/a = 0, y/a' = 0.1, z/a = 0. Source at v = 90° with image at v = 270°. R_0 given by curve G_0 in Fig. 22. Magnetic field has units of Siemens.

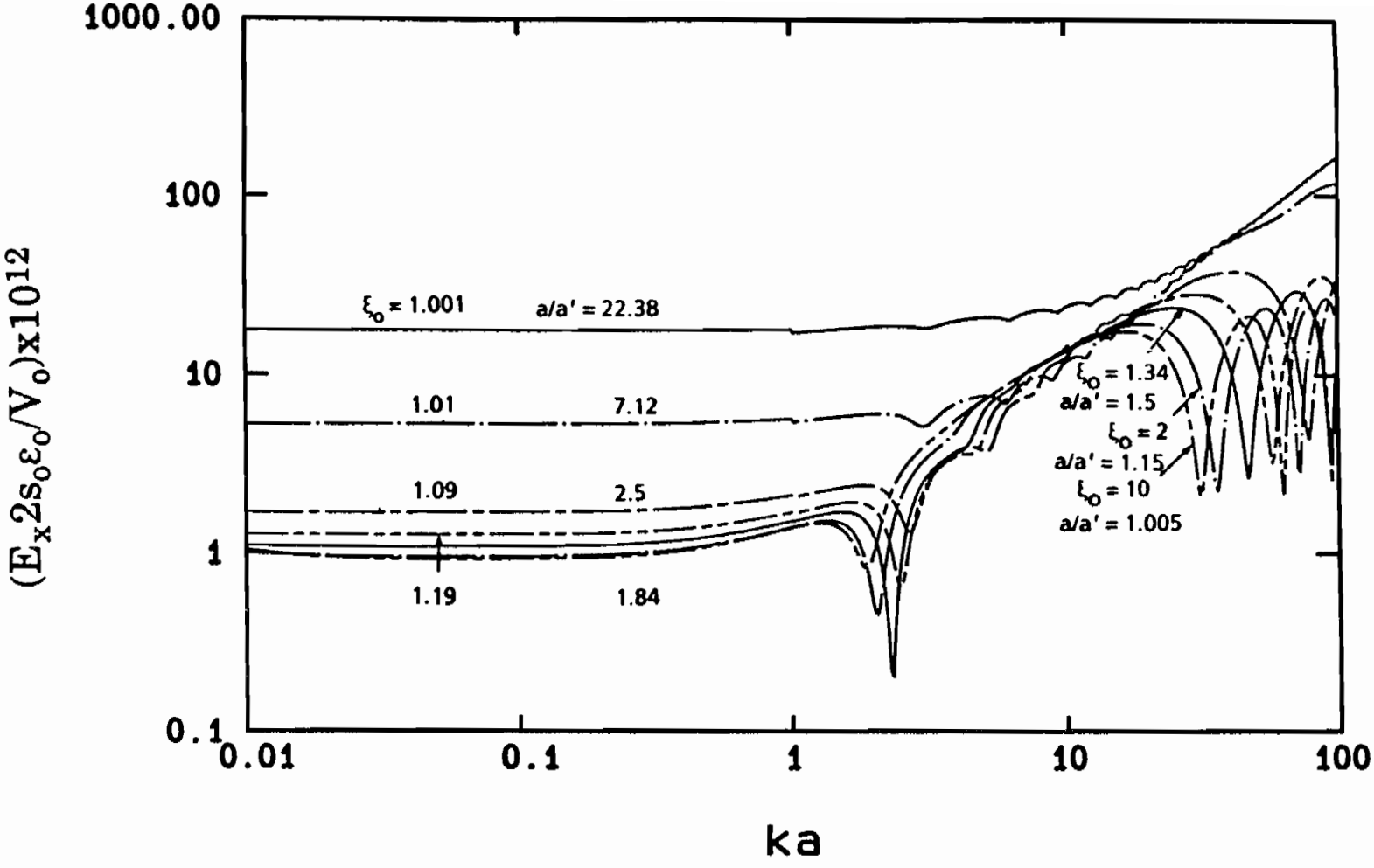

Figure 65. E_x of ELLIPTICUS of different eccentricitiesat x/a = 0, y/a' = 0.1, z/a = 0. Source at v = 90° with image at v = 270°. R_o given by curve G_0 in Fig. 22. Electric field has units of Farad/meter.

Needless to say, it is difficult to quantify how much error these approximations give rise to, with respect to the real situation. The impact of the finite ground conductivity on the fields was addressed in Section 2.3 for a specific case. Once the limitations of applicability of the results obtained in this note are understood, one could still ask the question: can this illuminator work at higher frequencies? Because of the inability of our model to assess its performances at very high frequencies, this is a difficult question to answer within the scope of the present analysis, and could be the subject of further investigations.

3.0 SUMMARY

The asymptotic antenna theory has been applied to the problem of determining the current and the electromagnetic fields produced by thin loop antennas, of circular and elliptical geometries. Part 1 of this Note is concerned with the circular loop antenna. Section 1.1.1 discusses the limits of applicability of the theory and the approximations involved. The current time-domain response to a unit step function is evaluated in Sec. 1.1.2 at three different locations. Section 1.1.3 presents the input impedance and the results are discussed and compared to the theoretical ones associated with a slice generator. Section 1.1.4 discusses the fields at the center of the thin circular loop, for the case when the source is a δ-gap generator. These are compared with the results contained in Ref. 1, assuming the same loading resistance. Both frequency domain calculations as well as time domain field responses to a unit step function excitation are presented. Section 1.1.5 addresses the calculation of the fields anywhere in space. The expressions of all the field components are reported explicitly. In Sec. 1.1.6 the 2-Norm error is defined and illustrated for two particular domains of integration chosen as examples. Section 1.2 deals with the calculation of current and fields in the case when the antenna is a half-TORUS located above a perfectly conducting ground, with a δ-gap source located at $\phi = 90^{\circ}$. Current, fields and 2-Norm error calculations are found in Secs. 1.2.1, 1.2.2 and 1.2.3 respectively. Throughout Sec. 1.2 it was assumed that the loading resistance R_o was half of that used for the case of a complete loop in free space. For this last case a value was determined in Ref. 1 such that the ratio E/H in the low frequency limit, at the center of the antenna, was equal to the free space intrinsic impedance, i.e. 377 Ω. Section 1.3 evaluates the effect of the finite extent of the source region on the ratio E/H at the center of a loop in free space. Since it was found that this effect results in a change of only a couple of percent in the value of such ratio, no further field calculations were carried out for other source locations and/or observation points. Part II deals with the loop of elliptical geometry. Using the same current calculated for the circular loop and adapted to the elliptical geometry (Sections 2.1.1 and 2.1.2) the fields were calculated everywhere in space and the explicit expressions are reported in Sec. 2.1.3. The question of what is the proper loading resistance to achieve a ratio $E/H = 377$ at some specified point and frequency range, depending on the source location and configuration (single or double δ-gap generator) is addressed in Sec. 2.1.4. Assuming a loading resistance obtained for the case of a single δ-gap located at $v = 0^{\circ}$ which makes E_y/H_z or $E_x/H_z = 377$ at the center, the fields at a few points and the 2-Norm errors were calculated for two different elliptical geometries. Comparisons with the corresponding results for the circular loop are discussed also. (Sections 2.1.4, 2.1.5 for single source, Sections 2.2.1, 2.2.2 for double source). Section 2.3 analyzes the dependence of the field behavior on parameters such as the loading resistance, the thickness of the antenna, the eccentricity and the characteristics of the soil. In particular it was found that ellipses of high eccentricity tend to produce smoother fields as a function of frequency.

REFERENCES

1. Baum, C.E. and H. Chang: "Fields at the Center of a Full Circular TORUS and aVertically Oriented TORUS on a Perfectly Conducting Earth," SSN 160, AFWL, Kirtland AFB, December 1972.

2. H. Chang: "Electromagnetic Fields Near the Center of TORUS - Part 1: Fields on the Plane of TORUS," SSN 181, AFWL, KIRTLAND AFB, August 1973.

3. Ramo, S. et al.: "Fields and Waves in Communication Electronics," John Wiley and Sons, 1965.

4. Collin, R.E. and F.J. Zucker: "Antenna Theory - Part 1," McGraw-Hill, 1969, Ch. 9.

5. Wu, T.T. and R.W.P. King: "Driving Point and Input Admittance of Linear Antennas", Journal of Applied Physics, Vol. 30, No. 1, Jan 19589.

6. Marin, L.: "Natural Modes of Certain Thin-wire Structures," IN 186, AFWL, Kirtland AFB, August 1974.

7. King, R.W.P. et al.: "Antennas in Matter," the MIT Press, 1981, Ch. 8.

8. Barnes, P.R., "Pulse Radiation by an Infinitely Long...," SSN 110, AFWL, Kirtland AFB, July 1970.